

THE UNIVERSITY OF TULSA
THE GRADUATE SCHOOL

MODELING SAND TRANSPORTATION IN WELLS
UNDER DIFFERENT MULTIPHASE FLOW CONDITIONS

by
Nursultan Bakyt

A thesis submitted in partial fulfillment of
the requirements for the degree of Master of Science
in the Discipline of Petroleum Engineering

The Graduate School
The University of Tulsa

2021

THE UNIVERSITY OF TULSA
THE GRADUATE SCHOOL

MODELING SAND TRANSPORTATION IN WELLS
UNDER DIFFERENT MULTIPHASE FLOW CONDITIONS

by
Nursultan Bakyt

A THESIS

APPROVED FOR THE DISCIPLINE OF
PETROLEUM ENGINEERING

By Thesis Committee

_____, Chair
Dr. Hong-Quan Zhang

Dr. Ovadia Shoham

Dr. Jun Lu

Dr. Haiwen Zhu

COPYRIGHT STATEMENT

Copyright © 2021 by Nursultan Bakyt

All rights reserved. No part of this publication may be reproduced, stored in a retrieval system, or transmitted, in any form or by any means (electronic, mechanical, photocopying, recording, or otherwise) without the prior written permission of the author.

ABSTRACT

Nursultan Bakyt (Master of Science in Petroleum Engineering)

Modeling Sand Transportation in Wells under Different Multiphase Flow Conditions

Directed by Dr. Hong-Quan Zhang

79 pp., Chapter 6: Conclusions and recommendations

(266 words)

Sand particles can be produced from the reservoirs along with oil, water, and gas in the petroleum industry. Particles can cause serious flow assurance issues, blocking a fluid path and causing fluctuations in oil and gas production and transportation system. Studies have been conducted to identify critical particle transport velocity in horizontal stratified flow. However, very little has been done to identify critical particle transport velocity for different inclination angles and flow patterns in the oil and gas production system. In this study, two mechanistic and three empirical models are selected, modified, developed, and presented for stratified, slug, bubbly, dispersed bubble, and annular flow patterns. A model for particle transport in gas production well is also presented. Zhang et al. (2003) unified gas-liquid pipe flow model is applied to cover all inclination angles to determine flow pattern, liquid holdup, and other flow conditions.

Particle transport in a production system is controlled by many parameters like fluid properties (liquid and gas densities, liquid and gas viscosities), sand particle properties (density, size, concentration, angle of repose, sphericity), well geometry (pipe diameter, roughness and inclination angle), and fluid flow (flow pattern, superficial liquid and gas velocities, liquid

holdup, water cut). The effect of each parameter on the critical particle transport velocity is analyzed to find the most important ones. The evaluations are validated by comparing with the previous work and experiments.

A field case example is analyzed as an application of the models with real field sand particle parameters. Good results are obtained for a large range of sand particle sizes. An angle of repose parameter calculation is demonstrated.

ACKNOWLEDGEMENTS

First of all, I would like to thank Dr. Hong-Quan Zhang for giving me the opportunity to learn from him, and for helping me improve both academically and professionally. Dr. Zhang's professionalism, kindness, and care are irreplaceable. I would also like to thank Dr. Ovadia Shoham, Dr. Jun Lu, and Dr. Haiwen Zhu for participating in my thesis committee and providing me their advices and recommendations to improve my thesis.

This thesis would not be possible without support, patience, and love of my wife, Kalamkas Babagulova, and my sweet children, Assiya Galymzhan and Mansur Galymzhan. They are the reason of my life and they make my every day special and meaningful.

My gratefulness also goes to my parents, grandmother, parents in law, and my siblings for their continuous motivation and encouragement. Thanks to all my TU friends for their support and help in difficult moments of my program.

I would like to express my gratitude to Tulsa University Artificial Lift Projects (TUALP) members. Thanks to all the University of Tulsa professors from whom I learnt a lot. Thanks to Kazakhstani Governmental International Scholarship Bolashak for funding my MSc in Petroleum Engineering program and covering all the expenses.

My family and I will never forget this wonderful part of our life which we spent in the United States.

TABLE OF CONTENTS

COPYRIGHT STATEMENT.....	iii
ABSTRACT.....	iv
ACKNOWLEDGEMENTS.....	vi
TABLE OF CONTENTS.....	vii
LIST OF FIGURES	ix
LIST OF TABLES.....	xii
INTRODUCTION	1
CHAPTER 1: LITERATURE REVIEW	5
1.1 Empirical models of critical particle transport velocity in the particle-liquid flow.....	5
1.2 Empirical models of critical particle transport velocity in the particle-liquid-gas flow.....	9
1.3 Flow pattern classifications and definitions	11
1.3.1 <i>Flow patterns in horizontal and near-horizontal sections.....</i>	<i>12</i>
1.3.2 <i>Flow patterns in vertical and sharply inclined sections</i>	<i>14</i>
CHAPTER 2: ZHANG ET AL. UNIFIED GAS-LIQUID (GAS-OIL-WATER) PIPE FLOW MODELS.....	16
CHAPTER 3: MODELING.....	19
3.1 Mechanistic model 1 - Critical Resuspension Velocity (CRV).....	19
3.1.1 <i>Inputs.....</i>	<i>21</i>
3.1.2 <i>Guessing average liquid velocity.....</i>	<i>22</i>
3.1.3 <i>Hydraulic diameter</i>	<i>22</i>
3.1.4 <i>Near-bed velocity profile</i>	<i>23</i>
3.1.5 <i>Forces acting on a single particle</i>	<i>25</i>
3.1.6 <i>Getting GAMMA</i>	<i>29</i>
3.2 Mechanistic model 2 - Critical Sand Deposition Velocity (CSDV).....	29
3.2.1 <i>Inputs.....</i>	<i>31</i>
3.2.2 <i>Liquid holdup and hydraulic diameter calculation</i>	<i>32</i>
3.2.3 <i>Liquid film velocity calculation</i>	<i>33</i>
3.2.4 <i>Near-bed velocity profile</i>	<i>33</i>

3.2.5	<i>Forces acting on a single particle</i>	35
3.2.6	<i>Torque balance</i>	37
3.3	Empirical model 1 - Critical Gas Core Velocity	38
3.3.1	<i>Inputs</i>	38
3.3.2	<i>V_{gc} calculation</i>	39
3.4	Empirical model 2 - Minimum Particle Pickup Gas Velocity	40
3.4.1	<i>Inputs</i>	40
3.4.2	<i>V_{pu} calculation</i>	41
3.5	Empirical model 3 - Settling Velocity	42
3.6	Model selection and conclusions	42
3.6.1	<i>Conclusions for Critical Resuspension Velocity (CRV) model</i>	42
3.6.2	<i>Conclusions for Critical Sand Deposition Velocity (CSDV) model</i>	43
3.6.3	<i>Conclusions for Critical Gas Core Velocity model</i>	44
3.6.4	<i>Conclusions for Minimum Particle Pickup Gas Velocity model</i> ...	44
3.6.5	<i>Conclusions for Settling Velocity model</i>	44
3.6.6	<i>General conclusions</i>	46
CHAPTER 4:	EXAMPLES, RESULTS, AND DISCUSSIONS	49
4.1	Variables effect on Critical Resuspension Velocity (CRV) and Critical Sand Deposition Velocity (CSDV) models	49
4.1.1	<i>Particle size effect on CRV and CSDV</i>	51
4.1.2	<i>Liquid viscosity effect on CRV and CSDV</i>	54
4.1.3	<i>Inclination angle effect on CRV and CSDV</i>	61
4.1.4	<i>Sand concentration effect on CSDV</i>	64
4.1.5	<i>Multiphase flow and gas parameters effect on CSDV</i>	66
4.1.6	<i>Sphericity effect on CRV and CSDV</i>	68
4.1.7	<i>Pipe diameter, liquid density, and particle density effect on CRV and CSDV</i>	69
4.1.8	<i>Conclusions of all variables effect on CRV and CSDV</i>	72
CHAPTER 5:	FIELD CASE EXAMPLE	74
CHAPTER 6:	CONCLUSIONS AND RECOMMENDATIONS	79
6.1	Conclusions	79
6.2	Recommendations	81
NOMENCLATURE	83
BIBLIOGRAPHY	87
APPENDIX A:	ANGLE OF REPOSE CALCULATION	96

LIST OF FIGURES

1.1	Flow Patterns in Horizontal and Near-Horizontal Pipes (Red Color Represents Gas, Blue Color Represents Liquid).....	13
1.2	Flow Patterns in Vertical and Sharply Inclined Pipes (Red Color Represents Gas, Blue Color Represents Liquid).....	15
2.1	Flow Pattern Map (Air-Mineral Oil, 2 in. ID, -5° inclination) (Taitel and Dukler).....	17
2.2	Flow Pattern Map (Air-Water, p=3, T=20 °C, d= 25.4 mm, Inclination Angle = 90°) (Unified Model).....	17
2.3	Slug Flow Pattern Variables	18
3.1	Algorithm to Calculate Critical Resuspension Velocity.....	20
3.2	Near-bed Velocity Profile Calculation Variables Illustration.....	25
3.3	Forces Acting on a Particle	25
3.4	Algorithm to Calculate Critical Sand Deposition Velocity	31
3.5	Forces Acting on a Half Particle	35
3.6	Experimental Result for Stratified and Slug Flow Patterns (Dabirian, 2016)	48
4.1	FL Parameter as a Function of a Particle Size (Durand and Condolios, 1952).....	52
4.2	CRV versus Particle Diameter	53
4.3	CSDV versus Particle Diameter.....	54
4.4	Liquid Viscosity and Sand Transportation Velocity Behavior for 200 lb/1000 bbl (Zorgani et al., 2017)	56
4.5	Liquid Viscosity and Sand Transportation Velocity Behavior for 200 lb/1000 bbl (Zorgani et al., 2017)	57

4.6	CRV versus Liquid Viscosity	58
4.7	CSDV versus Liquid Viscosity	58
4.8	Comparison of CRV Model, Zorgani et al. (2017) Experimental, and Other Correlation Results	60
4.9	Comparison of CSDV Model, Zorgani et al. (2017) Experimental, and Other Correlation Results	60
4.10	Critical Particle Transport Velocity Change with Inclination Angle (Roco, 1977).....	62
4.11	CRV versus Inclination Angle	63
4.12	CSDV versus Inclination Angle.....	64
4.13	CSDV versus Sand Concentration	65
4.14	CSDV versus Gas Viscosity	67
4.15	CSDV versus Gas Density	67
4.16	CRV versus Sphericity.....	68
4.17	CSDV versus Sphericity	69
4.18	CRV versus Pipe Diameter	70
4.19	CRV versus Liquid Density	71
4.20	CSDV versus Liquid Density.....	71
4.21	CRV versus Particle Density	72
4.22	Impacts of Different Variables on CRV	73
4.23	Impacts of Different Variables on CSDV.....	73
5.1	Particle Distribution and Types of the Well	75
5.2	Particle Types.....	77
5.3	CSDV versus Particle Diameter.....	77
A.1	Sample 1.....	96

A.2	Sample 1.....	97
A.3	Sample 2.....	97
A.4	Sample 2.....	98
A.5	Sample 3.....	98
A.6	Sample 3.....	99

LIST OF TABLES

3.1	General Conclusion.....	46
4.1	Example Input Parameters for CRV Calculation.....	50
4.2	Example Input Parameters for CSDV Calculation	50
4.3	Liquid Viscosity and Sand Transportation Velocity Behavior for 50 lb/1000 bbl (Zorgani et al., 2017)	55
4.4	Liquid Viscosity and Sand Transportation Velocity Behavior for 200 lb/1000 bbl (Zorgani et al., 2017)	56
4.5	Liquid Viscosity and Sand Transportation Velocity Behavior in Selected Correlations for 200 lb/1000 bbl (Zorgani et al., 2017).....	59
5.1	Field Particle Definitions	75
5.2	Field Example Particle Data	75
A.1	Sand Particle Parameters.....	99
A.2	Angle of Repose Result for Three Sand Particle Samples.....	100

INTRODUCTION

The oil and gas production system is very complex due to the gas-liquid multiphase flow and various flow patterns. Flow pattern depends on flow rates, fluid properties, and well geometry. The presence of sand particles adds more complexity and issues. Sand particles can be transported in different flow patterns like stratified, slug, dispersed bubble, bubbly, and annular flows where each flow pattern has its special sand transport mechanism and condition.

One of the main goals in sand control is the prediction of critical sand particle transport velocity. It is vital to prevent sand-bed deposition to maximize oil and gas production and avoid well and pipeline issues because the majority of oil and gas reservoirs are prone to natural sand production. Besides, there are also sand transport issues while well drilling and operations like formation fracturing to increase oil and gas production.

There are some ways to manage sand particles in the wells and pipeline like cleaning operations, downhole sand particle exclusion systems, and operating above critical sand particle transport velocity.

Cleaning operations like pigging can remove sand particles from flowlines. However, pigging itself can cause additional issues if they stuck in the pipeline, arising extra pig removal work and negatively affecting the well flow rate. They are only applicable for low deposition of sand particles.

Downhole sand particle exclusion systems such as gravel packs and screens are very good options. They can be installed from the beginning of the production or at a later date when sand starts to produce with fluid. However, there are some issues related to the installation of

sand exclusion systems. First, as sand production may start at a later time, installing sand exclusion systems can cost a lot because it requires workover operations. Second, exclusion systems can create an additional drawback for well flow performance reducing production and affecting the pressure drop (skin effect). Third, costs are especially high in the offshore environment due to the difficulty of installing exclusion systems and due to the complexity of the overall system where hydrocarbons and sand particles have to be transported from the reservoir through the well, from the wellhead through a long-distance multiphase flowline to the platform and onshore facilities. Fourth, exclusion systems do not fully prevent sand particles (mostly fine particles) from entering the well, requiring transport of the sand particles to the surface.

As a result of the low efficiency of the first two methods, operating above critical sand particle transport velocity, or sand management, is still a preferred option in the petroleum industry. It is a favorable method since it has practical applications and it is commercially beneficial. Sand management is the best way to design and manage the wells with sand production from the beginning or any time during oil and gas production.

Operating at high flow rates together with sand can erode the inner surface of the tubing and pipeline. Erosion due to the high flow rates can cause severe damage resulting in shutting down the entire production, hence disrupting the production plan. It also leads to excessive costs due to the workovers needed to change tubing in the well system. Fluid leakage can occur due to the eroded flowlines which cause severe environmental issues, which again leads to extra risks and costs. On the other hand, operating at low flow rates with sand can reduce production due to the sand particle deposition, therefore blocking the ways of the fluid and increasing the pressure drop in a production system. Sand bed or dune can occur inside the pipelines if the production rate is kept below the critical particle transport velocity. Therefore, finding an optimal flow rate

where average fluid velocity is kept higher or slightly higher than critical particle deposition velocity is crucial for the petroleum industry.

Danielson (2007) perfectly explains the sand transportation mechanism in the near-horizontal section. He states that there are four main regimes depending on the fluid flow rate. Below a critical sand-carrying velocity, sand particles will drop out of the surrounding fluid and form a stable stationary sand bed. As the sand bed builds over time, fluid above the bed is forced into a smaller cross-sectional area, causing the fluid velocity to increase. Then, when velocity reaches a critical value, the sand is transported in a thin layer along the top of the sand bed. A steady-state is reached, and the sand eroded from the top of the bed is replaced by new sand produced from the upstream. On the other hand, at higher fluid velocities, the sand bed begins to break up into a series of slow-moving dunes with the sand particles transported from the upstream to the downstream side of the dune. With the further increase in the fluid velocity, the dunes break up entirely, and sand forms a moving bed along the bottom of the pipe. Finally, at fluid velocities above the critical sand-carrying velocity, sand is fully entrained in the liquid phase and potentially entrained into the gas phase in multiphase flow.

There are many studies related to liquid-sand and gas-sand transportation, but there are few studies covering all three liquid-gas-sand phase transportation in wells and pipelines. In addition, there are many studies where only horizontal and vertical sections of the wells are covered, but only a few studies where all inclination angles are investigated. Also, there are many studies where only stratified flow pattern is studied, but there are few studies where all flow patterns are investigated. All these issues need a comprehensive solution, considering the presence of multiphase flow, all inclination angles, and all flow patterns. In this study, all these aspects will be investigated and solved with an adequate approach.

Overall, this study is divided into 6 Chapters. A literature review is presented in Chapter 1, while in Chapter 2 Zhang et al. (2003) unified gas-liquid and gas-oil-water pipe flow models are introduced. The main parts of this thesis including all mechanistic and empirical models, is presented in Chapter 3. Example results of the previous chapter models are reported in Chapter 4, and an investigation of a field case is presented in Chapter 5. Finally, Chapter 6 summarizes the conclusions and future work recommendations. Also, an angle of repose calculation is explained in Appendix A.

CHAPTER 1

LITERATURE REVIEW

1.1 Empirical models of critical particle transport velocity in the particle-liquid flow

Empirical models are the earliest models that were used to identify critical particle transport velocities. Empirical models are developed based on experimental data, and they are usually very simple to use and do not include complex calculations and iterations. However, they can only be valid for the specific range of data, taken from experimental works. At the earliest time, most of the researches covered only two-phase, particle-liquid flow, due to the complexity of covering gas-liquid-particle flow.

The model developed by Durand (1953) is one of the earliest empirical models used in critical particle transport velocity determination. Durand (1953) did several studies to reach this model

$$V_D = F_1 [2gD(s_d - 1)]^{\frac{1}{2}} \quad (1.1)$$

where V_D is critical deposition velocity, F_1 is an empirical factor accounting for particle size and concentration, g is gravitational acceleration, D is the pipe diameter, and s_d is the ratio of solid density to liquid density.

Condolios and Chapus (1963), who closely worked with Durand to investigate a critical velocity change with particle size, developed another model, based on data for sand concentration less than 0.02 v/v

$$V_C = 3.0C_v^{0.148} \sqrt{gD} \quad (1.2)$$

where, V_C is the critical velocity, C_v is the particle concentration, g is gravitational acceleration, and D is the pipe diameter.

Oroskar and Turian (1980) developed a model which is based on turbulence theory and force balance, and which they described as the minimum fluid velocity which demarcates flows in which the solids form a bed at the bottom of the pipeline from fully suspended flows. Experimental data for particle concentration range from 1% to 50% are compared to the developed model, and 357 published experimental velocities were analyzed. They assumed particle suspension and dispersion by turbulent eddies and considered particle concentration. Particle concentration plays a big role in the model, so correct particle concentration data is vital in using the empirical model. Their model is widely used, very simple, and covers many important parameters

$$\frac{V_C}{\sqrt{gd_p\left(\frac{\rho_p}{\rho_L}-1\right)}} = 1.85C_v^{0.1536}(1 - C_v)^{0.3564}\left(\frac{d_p}{D}\right)^{-0.378} N_{Re}^{0.09}x^{0.3} \quad (1.3)$$

where N_{Re} is a modified Reynolds number

$$N_{Re} = \frac{D\rho_L\sqrt{gd_p\left(\frac{\rho_p}{\rho_L}-1\right)}}{\mu_L} \quad (1.4)$$

V_C is the critical velocity, g is gravitational acceleration, d_p is the particle diameter, ρ_p is the particle density, ρ_L is the liquid density, C_v is the particle concentration, D is the pipe diameter, x is the fraction of eddies with instantaneous velocities equal to or greater than the terminal velocity of the particle and it is close to unity.

Davies (1987) also developed a minimum mean particle transport velocity model based on turbulence theory. The author explains that his model is developed to fully suspend all the particles existing in a horizontal section of a pipeline. The sedimentation behavior of the particle

was investigated with the lifting velocities of different sizes of eddies. Compared to Durand and Condolios model and Oroskar and Turian model, Davies's model is an improvement:

$$V_C = 1.08C_v v^{-0.09} d_p^{0.18} \left(\frac{2g(\rho_p - \rho_L)}{\rho_L} \right)^{0.54} D^{0.46} \quad (1.5)$$

where V_C is the critical velocity, C_v is the particle concentration, v is the liquid kinematic viscosity, d_p is the particle diameter, g is gravitational acceleration, ρ_p is the particle density, ρ_L is the liquid density, and D is the pipe diameter.

Kokpinar and Gogus (2001) developed a critical particle transport velocity model where below the critical velocity particles will deposit, and above no particle deposition will occur. They analyzed various data from the previous experimental works, combining them with their experimental data, developed the next empirical model:

$$\frac{V_C}{\sqrt{gD}} = 0.055 \left(\frac{d_p}{D} \right)^{-0.6} C_v^{0.27} (s_d - 1)^{0.07} \left(\frac{\rho_L u_t d_p}{\mu_L} \right)^{0.30} \quad (1.6)$$

where V_C is the critical velocity, g is gravitational acceleration, D is the pipe diameter, d_p is the particle diameter, C_v is the particle concentration, s_d is the ratio of solid density to liquid density, ρ_L is the liquid density, u_t is the particle settling velocity in mixture flow, and μ_L is the liquid dynamic viscosity.

Al-Mutahar (2006) adopted the horizontal two-phase flow model developed by Oroskar and Turian (1980), and developed a new mechanistic model based on force balance and turbulent theory. He extended an initial approach to low concentration slurries, inclined flow, and multiphase flow, and then developed a new approach for two-phase and multiphase flows. Finally, a new critical deposition velocity model for two-phase flow is reached

$$V_D = 5.66 \left[f(c) \sqrt{d_p g (s_f - 1)} \right]^{\frac{8}{7}} \left(\frac{D \rho_L}{\mu_L} \right)^{\frac{1}{7}} \left(\frac{1}{\Omega} \right)^{\frac{8}{7}} \quad (1.7)$$

where V_D is critical deposition velocity, $f(c)$ is a function of concentration, d_p is the particle diameter, g is gravitational acceleration, D is the pipe diameter, ρ_L is the liquid density, and μ_L is the liquid dynamic viscosity. To account for turbulent dissipation (Ω), and if particle concentration is equal or above 1 %, a function suggested by Davies (1987) is used, which is

$$\Omega = \frac{1}{1+3.64C} \quad (1.8)$$

However, if particle concentration is lower than 1%, Al-Mutahar (2006) believes that Davies (1987) function does not give an accurate result. Therefore, a new function is developed and used

$$\Omega = \frac{1}{0.5(1+3.64C)} \quad (1.9)$$

Danielson (2007) developed a liquid-particle model for the minimum velocity to prevent sand bed formation at the bottom of the pipe. First, he used data from SINTEF STRONG JIP to develop a correlation for the particle transportation model, where he obtained a good fit for both sand bed height and pressure drop. He assumed that there is a critical slip velocity between particle and liquid, which remains relatively constant over a wide range of fluid flow velocities. The author identified that inclination does not affect particle transport velocity in particle-liquid flow, while particle transportation in multiphase flow (particle-liquid-gas) can be a strong function of inclination angle. A feature of this model is that critical slip between particle and liquid is not affected by the presence of surrounding gas. Then, using particle diameter to augment the surface roughness, the following correlation is developed based on the particle, fluid, and pipe parameters

$$V_C = 0.23v^{-\frac{1}{9}}d_p^{\frac{1}{9}}(gD(s_d - 1))^{\frac{5}{9}} \quad (1.10)$$

where V_c is the critical velocity, ν is the liquid kinematic viscosity, d_p is the particle diameter, g is gravitational acceleration, D is the pipe diameter, s_d is the ratio of solid density to liquid density.

Some of the important ranges used by Danielson to experiment are inclination angles from -1.35 to +4.00 degree, a total length of the loop of 215 m, length of the test section of 15 m, the pipe diameter of 0.069 m, the median particle diameter of 280 and 550 microns.

In addition, the Danielson (2007) drift-flux model can predict particle holdup, particle carrying velocity, gravitational, and frictional pressure gradients. The author developed a map showing the border between particle bed formation and no particle bed formation for air-water-particle flow.

1.2 Empirical models of critical particle transport velocity in the particle-liquid-gas flow

After more or less covering two-phase particle-liquid flow, many researchers started to investigate critical particle transport velocity for three-phase particle-liquid-gas flow. Due to the complexity of considering all phases, there is still no perfect empirical or mechanistic model which could be used to calculate the critical particle transport velocity for all inclination angles, flow patterns, and many other parameters and phenomena existing in the drilling and production system.

One of the widely used models which still relevant in determining critical particle velocity is Salama's (2000) empirical model. Based on Wicks (1971), Oroskar and Turian (1980), and Davies (1987) studies, Salama (2000) developed a correlation which is described as the minimum velocity needed to suspend all particles in a system. He has conducted an experiment using a 12 m long duplex stainless steel pipe with an internal diameter of 108.2 mm

to get data for the model development. He used 100, 280, and 500-micrometer particle sizes. As a surrounding fluid, he used water, gas (CO₂, N₂, air), and oil. Varying superficial gas velocity, he selected 0.03, 0.1, 0.2, 0.3, 0.4 m/s superficial liquid velocities for his experiments. He believes that using his model, the minimum fluid velocity can be calculated below which particle bed will occur at the bottom of a horizontal pipeline, and above which all particles will be transported out. However, one of the drawbacks of Salama (2000) model is that it does not have a particle concentration factor. Salama (2000) correlation for horizontal multiphase flow is

$$V_{MC} = \left(\frac{V_{SL}}{V_m}\right)^{0.53} d_p^{0.17} \left(\frac{\mu_L}{\rho_L}\right)^{-0.09} \left(\frac{\rho_p}{\rho_L} - 1\right)^{0.55} D^{0.47} \quad (1.11)$$

where V_{MC} is the critical sand deposition mixture velocity, V_{SL} is the superficial liquid velocity, V_m is the mixture velocity, d_p is the particle diameter, ρ_L is the liquid density, μ_L is the liquid dynamic viscosity, ρ_p is the particle density, and D is the pipe diameter.

Ibarra (2014) did extensive work on developing a correlation to predict critical sand deposition mixture velocity for horizontal stratified flow. Combining experimental and theoretical works, he studied the hydrodynamic flow behavior of gas-liquid-particle flow at low particle concentrations. The data from his experiments include superficial gas and liquid velocities, particle concentration, and liquid holdup. The developed model can predict a transition between moving and stationary beds for various particle concentrations. He took Oroskar and Turian (1980) model as a base and combined it with other equations to develop a new correlation. Ibarra (2014) experimentally confirmed that critical particle transport velocity increases with the increase of particle concentration. His empirical model has a very good agreement and very low relative error compared with the experimental data:

$$\frac{V_{MC}}{\sqrt{g d_p \left(\frac{\rho_p}{\rho_L} - 1\right)}} = 1.3277 \left(\frac{V_{SL}}{V_{MC}}\right)^{-0.285} (1 - C_v)^{-35.490} \left(\frac{d_p}{D}\right)^{-0.378} N_{Re}^{0.09} \quad (1.12)$$

where the modified Reynolds number to incorporate the effect of the gas density is

$$N_{Re} = \frac{D \rho_L \sqrt{g d_p \left(\frac{\rho_L}{\rho_g} - 1 \right)}}{\mu_L} \quad (1.13)$$

V_{MC} is the critical sand deposition mixture velocity, g is gravitational acceleration, d_p is the particle diameter, ρ_p is the particle density, ρ_L is the liquid density, ρ_g is the gas density, V_{SL} is the superficial liquid velocity, C_v is the particle concentration, D is the pipe diameter, and μ_L is the liquid dynamic viscosity.

Ibarra (2017) modified his previous model and reported another correlation

$$\frac{V_{MC}}{\sqrt{g d_p \left(\frac{\rho_p}{\rho_L} - 1 \right)}} = 1.651 \left(\frac{V_{SL}}{V_{MC}} \right)^{-0.236} (1 - C_v)^{-33.8} \left(\frac{d_p}{D} \right)^{-0.378} N_{Re}^{0.09} \quad (1.14)$$

1.3 Flow pattern classifications and definitions

The term flow pattern refers to the geometrical configuration of the gas and liquid phases in a pipe. When gas and liquid flows simultaneously in a pipe, the two phases can distribute themselves in a variety of flow configurations (Shoham, 2006). Flow patterns change with the change of variables like inclination angle, superficial gas and liquid velocities, fluid density and viscosity, pipe diameter, and so on. Interfacial forces between existing gas and liquid phases develop different flow configurations. Due to the difference in flow pattern behaviors, critical particle transport velocity will also be different in multiphase flow.

Although many investigations are trying to classify each flow pattern into even more parts, Shoham (2006) simply and perfectly explains all the flow patterns existing in multiphase flow in all inclination angles. Flow patterns observed during his experimental work in horizontal and near-horizontal multiphase flow are Stratified flow (Stratified-Smooth and Stratified-Wavy),

Intermittent flow (Slug and Elongated-Bubble flows), Annular flow, and Dispersed Bubble flow patterns. Flow patterns existing in vertical and sharply inclined multiphase flow are Slug flow, Churn flow, Annular flow, Bubbly flow, and Dispersed Bubble flow. The following two sections include Shoham's (2006) explanation of each flow pattern.

1.3.1 Flow patterns in horizontal and near-horizontal sections

a) Stratified flow pattern occurs in relatively low gas and liquid flow rates. The two phases are separated by gravity, where the liquid phase lies at the bottom of the pipe, and the gas phase is on the top of the liquid phase. Shoham subdivided Stratified flow into **Stratified-Smooth** (Figure 1.1), where the gas-liquid interface is smooth, and **Stratified-Wavy** (Figure 1.1), where the gas rate is relatively higher than a critical velocity causing liquid waves on the interface.

b) Intermittent flow pattern is characterized by an alternate flow of liquid and gas (Shoham, 2006), it occurs in a wide range of gas and liquid flow rates. The intermittent flow is divided into **Slug flow** (Figure 1.1), where the gas flow rate is higher and the flow at the front of the slug is in the form of an eddy with entrained bubbles, and **Elongated-Bubble flow** (Figure 1.1), where gas and liquid flow rates are relatively lower and calmer respectively, and the liquid slug is free of entrained bubbles. This flow pattern is very complex due to its unique flow behavior with the mechanism where the fast-moving liquid slug overrides the slow-moving liquid film ahead of it. The liquid in the slug body may be aerated by small bubbles, which are concentrated toward the front of the slug and at the top of the pipe (Shoham, 2006).

c) Annular flow pattern (Figure 1.1) occurs at very high gas flow rates. The liquid phase flows as a thin film around the pipe, which is usually thicker at the bottom of the pipe

compared to the top of the pipe, while the gas phase flows in a core of high velocity, which may contain entrained liquid droplets and sand particles. Shoham also added a subgroup for Annular flow called **Wavy-Annular flow** (Figure 1.1), where the liquid moves forward uphill with frothy waves superimposed on the film, and the waves move much slower than the gas phase.

d) Dispersed Bubble flow (Figure 1.1) occurs at very high liquid flow rates. The liquid is the continuous phase, and the gas phase is dispersed as discrete bubbles in the liquid phase in the entire cross-sectional pipe area. Under this flow pattern, liquid and gas phases move at the same velocity, the mixture velocity.

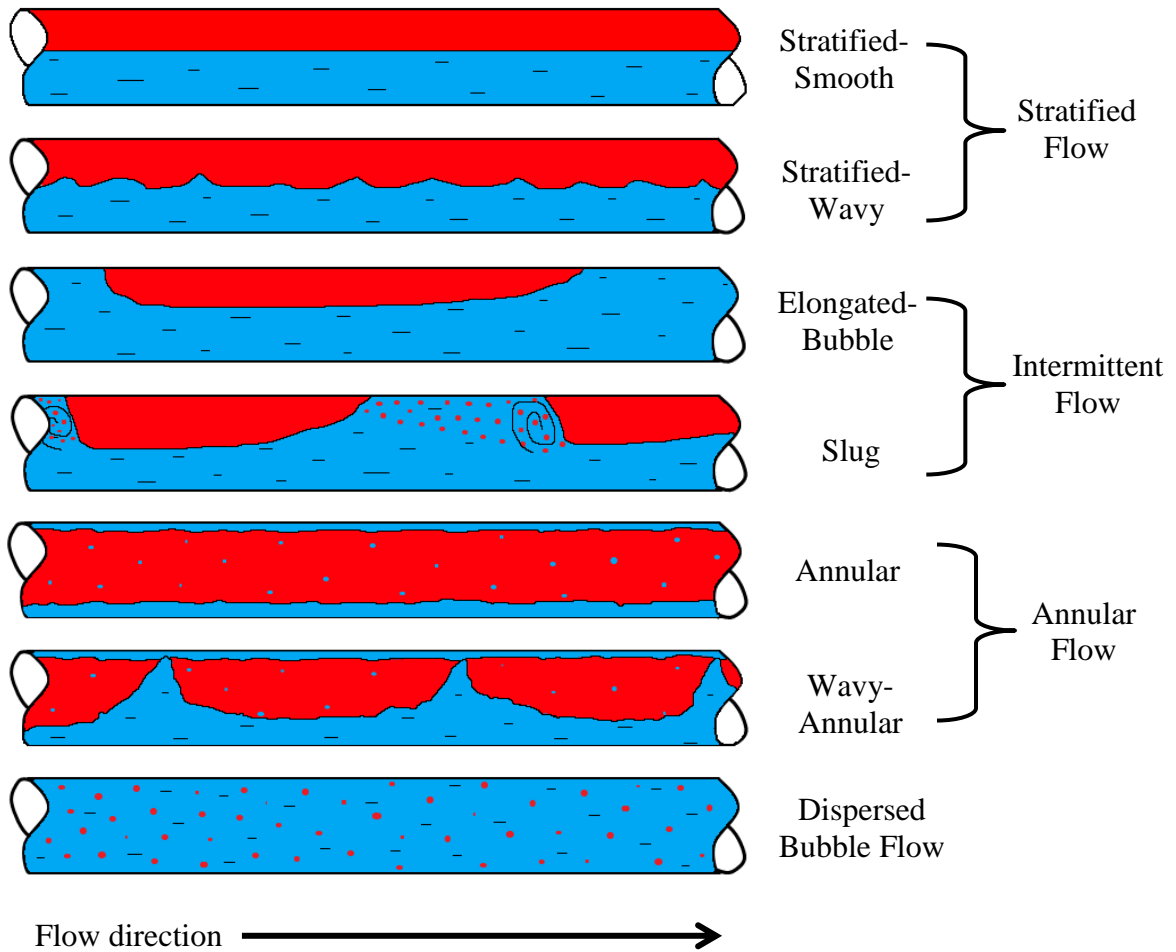


Figure 1.1 Flow Patterns in Horizontal and Near-Horizontal Pipes (Red Color Represents Gas, Blue Color Represents Liquid)

1.3.2 Flow patterns in vertical and sharply inclined section

a) Slug flow pattern (Figure 1.2) is symmetric around the pipe axis in the vertical section. Most of the gas phase is located in a large bullet-shaped gas pocket called “Taylor-bubble” with a diameter almost equal to the pipe diameter. In this flow pattern, a thin liquid film falls downward between the pipe wall and the Taylor-bubble (Shoham, 2006). There is a mixing zone aerated with small gas bubbles between Taylor-bubbles, which looks like a bubbly flow pattern.

b) Churn flow (Figure 1.2) is characterized by an oscillatory movement of the liquid phase and occurs at higher gas flow rates, where the liquid slugs bridging the pipe become shorter and frothy (Shoham, 2006). Churn flow looks more chaotic comparing to slug flow, with no clear boundaries between the two phases. This flow pattern is specific only for vertical flow.

c) Annular flow (Figure 1.2) in vertical flow, like in a horizontal flow, occurs at very high gas flow rates, where liquid droplets and sand particles are entrained in the gas core. The liquid film thickness around the pipe is slow-moving and approximately uniform.

d) Bubbly flow (Figure 1.2) in the vertical section occurs at relatively low liquid rates, with low turbulence, and characterized by slippage between gas and liquid phases, resulting in large values of liquid holdup (Shoham, 2006). In this flow pattern, the gas phase moves upward in a continuous liquid phase in a zigzag motion.

e) Dispersed Bubble flow (Figure 1.2) in vertical flow like in horizontal flow occurs at relatively high liquid flow rates, where the gas phase is dispersed as discrete bubbles in a continuous liquid phase.

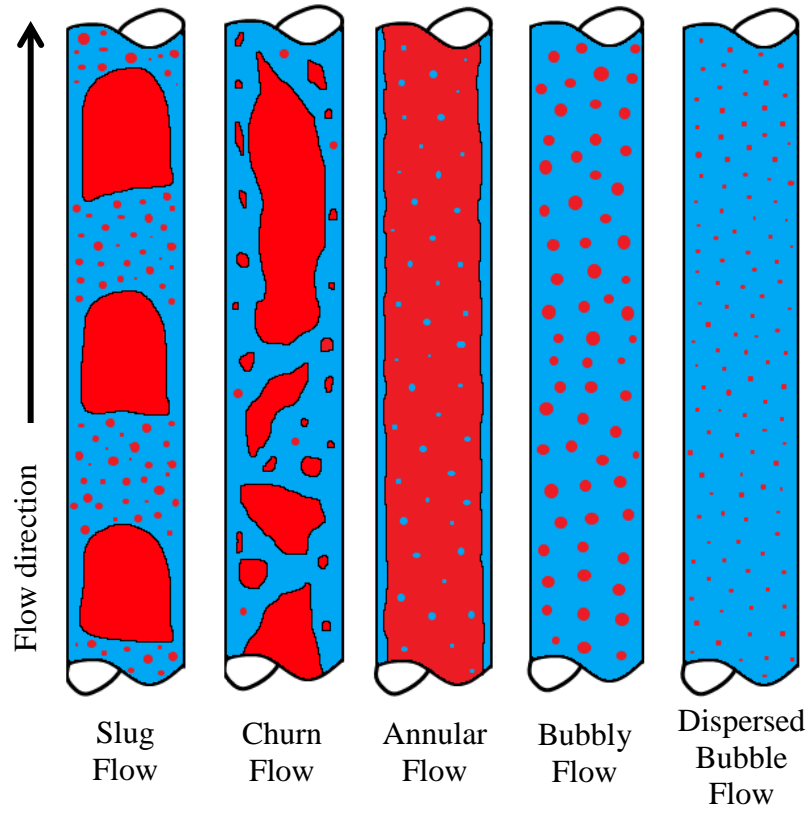


Figure 1.2 Flow Patterns in Vertical and Sharply Inclined Pipes (Red Color Represents Gas, Blue Color Represents Liquid)

CHAPTER 2

ZHANG ET AL. UNIFIED GAS-LIQUID (GAS-OIL-WATER) PIPE FLOW MODELS

Mechanistic models for gas-liquid pipe flows have been developed since the middle of the 1970's (Zhang et al., 2003). Comparing to the empirical models, the mechanistic models are considered cover more physics and to be more accurate. This is because most of the empirical models are developed only for special flow conditions and pipe, particle parameters, therefore they do not give accurate results if used for different parameters than the original experimental work. Xiao (1990) developed a mechanistic model for near-horizontal pipelines, Kaya (1998) developed a model for vertical and deviated wells, and Gomez et al. (1999) developed a model for inclination angles from horizontal to vertical. Barnea (1987), combining different flow conditions, and existing mechanistic and empirical models, proposed a unified model of flow pattern prediction for the whole range of inclination angles.

The main goal of Zhang et al. unified gas-liquid pipe flow model is to predict flow pattern transitions, pressure gradient, liquid holdup, and slug characteristics. Unified means the model covers all inclination angles from -90 degree to +90 degree. The model is based on dynamics of slug characteristics, which is at the center of the flow pattern map, and sharing transition boundaries with all other flow patterns (Figures 2.1 and 2.2). Zhang et al. (2003) developed the momentum and continuity equations for slug flow by considering the entire liquid film region as the control volume (Figure 2.3). Therefore, the momentum exchange between the slug body and the film zone is introduced into the combined momentum equation. The existence

condition for slug flow is embodied in the equations, therefore the transition from slug flow to other flow patterns can be predicted (Zhang et al., 2003).

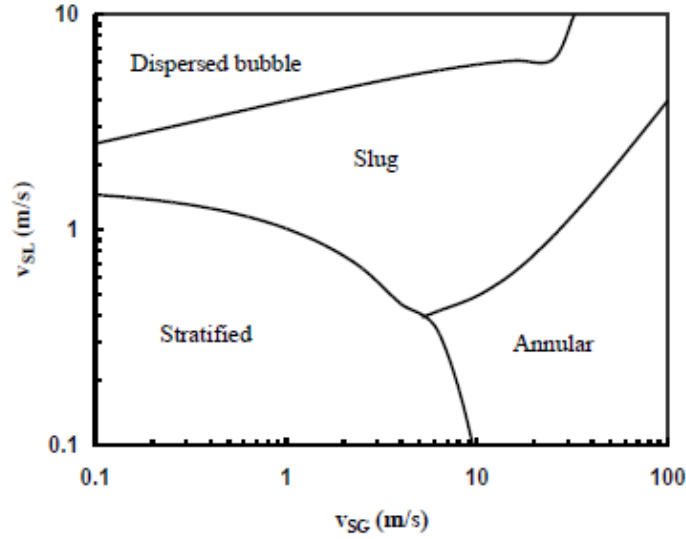
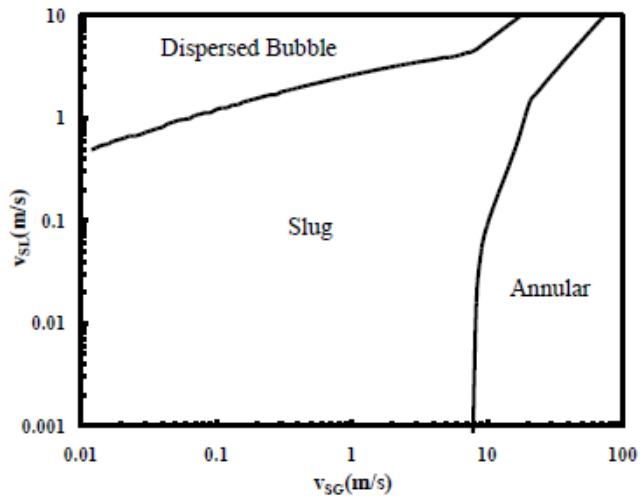


Figure 2.1 Flow Pattern Map (Air-Mineral Oil, 2 in. ID, -5° inclination) (Taitel and Dukler)



Flow Pattern Map (Air-Water, $p = 3$ atm, $T = 20$ °C, $d = 25.4$ mm, $\phi = 90^\circ$)
(Unified Model)

Figure 2.2 Flow Pattern Map (Air-Water, $d = 25.4$ mm, Inclination Angle = 90°) (Unified Model)

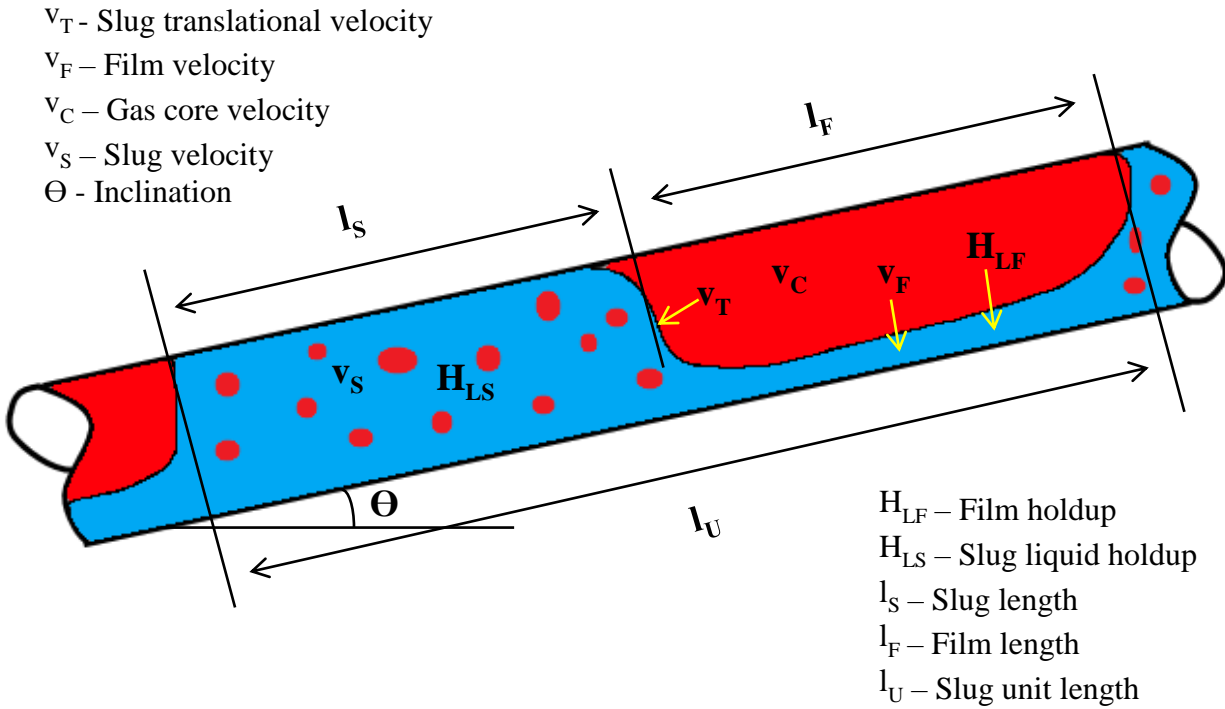


Figure 2.3 Slug Flow Pattern Variables

Zhang also developed a three-phase unified model to predict flow behaviors during the production and transportation of oil, gas, and water through wellbores and pipelines.

In the current study, Zhang et al. (2003) unified gas-liquid pipe flow mechanistic model is used to predict required parameters for critical particle transport velocity models. However, Zhang's three-phase gas-oil-water unified model can also be used to treat water separately. The main variables and data needed in the critical particle transport velocity model from the Zhang et al. (2003) unified gas-liquid pipe flow model are:

H_L - liquid holdup	v_s - slug velocity
D_h - hydraulic diameter	v_f - film velocity
V_L - liquid velocity	V_m - mixture velocity
V_{GCV} - gas core velocity	Flow patterns

CHAPTER 3

MODELING

3.1. Mechanistic model 1 - Critical Resuspension Velocity (CRV)

The Critical Resuspension Velocity (CRV) is defined as the minimum average fluid velocity at which the first layer of the particle on a stationary particle bed starts to be entrained into the fluid flow (Duan, 2005). Mechanistic model 1, developed by Duan (2005), is mainly for drilling cutting transportation purposes. However, with proper changes in variables and equations, the model can also be used in propping-agent transport in hydraulic fracturing, gravel-pack-displacement operation, and sand control in production operations. Therefore, some changes have been made to use the model in oil and gas production and transportation.

Duan (2005) noticed that a protruding particle on a particle bed is entrained into the suspension layer of a fluid by two dominant mechanisms that depend on the relationship between solids angle of repose and well inclination angle. At lower borehole angles, which are smaller angles than the particle angle of repose, the particle tends to be lifted from the particle bed to resuspend. When the borehole angle is greater than the angle of repose, rolling along the particle bed is the dominant resuspension mechanism (Duan, 2005). Therefore, Duan developed the CRV model based on the rolling mechanism. The focus of his study was on horizontal and high angle boreholes, where the borehole angle is greater than the particle angle of repose. So, when particles on the particle surface bed begin to roll, the particle bed height starts to decrease. With the higher fluid velocity, the particle bed can totally be transported to the surface.

In this model, Zhang et al. (2003) unified gas-liquid pipe flow model is applied to identify flow pattern.

Duan (2005) made the following assumptions to simplify the model development: (1) stationary-solids bed with a uniform thickness, (2) particles with the same diameter, (3) steady-state incompressible fluid, and (4) Newtonian fluid flow.

One of the important steps in the CRV model calculation is identifying flow pattern, which can be obtained using Zhang et al. (2003) unified gas-liquid pipe flow model.

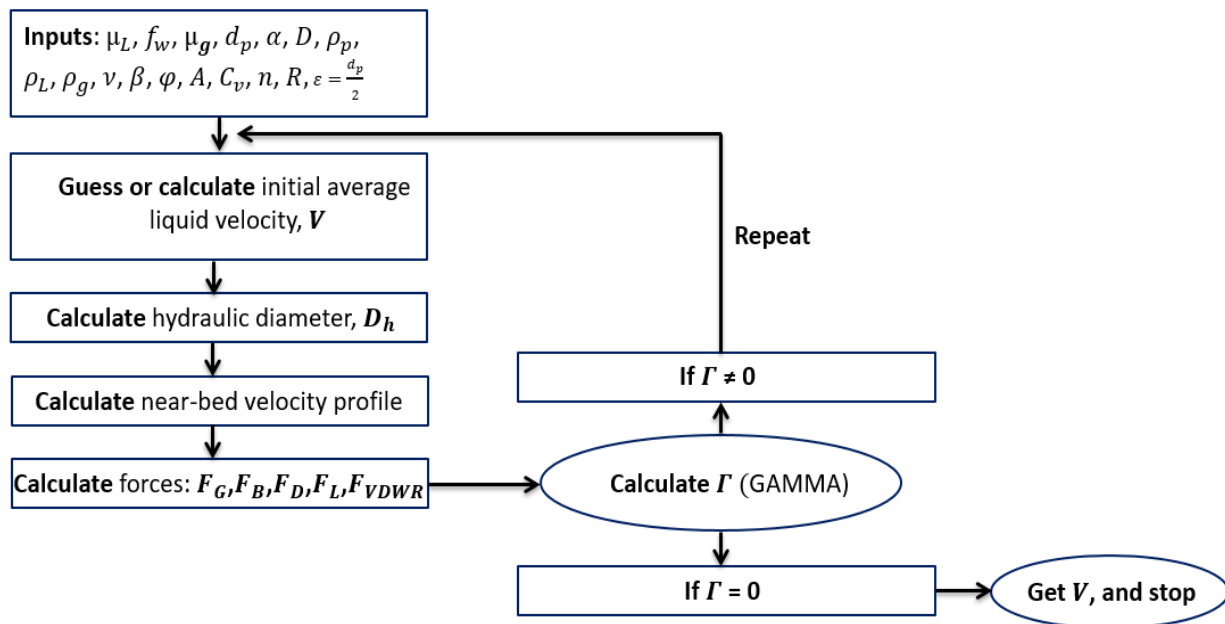


Figure 3.1 Algorithm to Calculate Critical Resuspension Velocity

Figure 3.1 shows the steps to calculate CRV. Further, all the calculation steps will be explained separately.

3.1.1 Inputs

For the mechanistic model 1, the required inputs are:

1. μ_L = liquid dynamic viscosity
2. μ_g = gas dynamic viscosity
3. f_w = water fraction
4. d_p = particle diameter
5. α = well inclination angle
6. D = pipe diameter
7. ρ_p = particle density
8. ρ_L = liquid density
9. ρ_g = gas density
10. ν = liquid kinematic viscosity
11. β = angle of repose
12. φ = particle sphericity
13. A = pipe cross-sectional area
14. C_v = particle concentration
15. n = fluid behavior index (Assuming Newtonian fluid, n is equal to 1)
16. K = fluid-consistency index, which can be assumed as equal to μ_L
17. R = pipe radius
18. $\varepsilon = \frac{d_p}{2}$ = pipe roughness

Understanding the angle of repose term is very important in this study, which is the maximum angle, measured in degrees from horizontal, at which particles or other solid materials remain in a place without sliding. It is an essential input for the mechanistic model, so it should

be measured very carefully corresponding to the reservoir sand samples before running a computer tool. The higher the angle of repose, the greater will be a friction between the particles resisting to free flow. The angle of repose calculation is presented in APPENDIX A, as one of the steps of CRV model calculation. If there is no sand sample, an approximate value should be taken from the literature.

3.1.2 Guessing average liquid velocity

Average liquid velocity, V , at the end of all calculations, is the Critical Resuspension Velocity, which is found by iterating all the existing equations. Initial V value is needed to start mechanistic model 1 calculation. The average liquid velocity value can be estimated itself or knowing the pipe area, calculated by estimating liquid flow rate.

3.1.3 Hydraulic diameter

Hydraulic pipe diameter is calculated as the following:

$$D_h = \frac{4A_f}{S_w + S_b} \quad (3.1)$$

$$A_f = R^2 \arccos\left(\frac{h-R}{R}\right) + (R-h)\sqrt{R^2 - (R-h)^2} \quad (3.2)$$

$$S_b = 2\sqrt{R^2 - (R-h)^2} \quad (3.3)$$

$$S_w = 2R \arccos\left(\frac{h-R}{R}\right) \quad (3.4)$$

$$h = 337.8d_p(C_v^{0.5} - 0.001) \quad (3.5)$$

where D_h is the hydraulic diameter, A_f is the fluid flow area above the particle bed, h is the moving particle bed height, S_w and S_b are the wetted perimeters of the well and particle bed respectively. However, it is noted that the hydraulic diameter value does not highly impact on the

final CRV result, but it is still an important variable. The moving bed height equation can be improved if a best fit stationary bed height correlation is developed for the production system.

3.1.4 Near-bed velocity profile

Obtaining a near-bed velocity profile is crucial for drag and lift force calculation. Variables like local liquid velocity, V_{LL} , particle Reynolds number, R_{ep} , and dimensionless shear rate, η , are needed to calculate drag and lift coefficients.

Duan (2005) studied that the velocity profile determined by Schlichting (1955) can be used for the viscous sublayer which is closest to the particle bed. If the particle protrudes into the buffer zone or the logarithmic layer above the viscous sublayer, in this situation, the velocity profile developed by Kallio and Reeks (1989) can be picked. So the near-bed velocity profile calculation is as follows:

if $y^+ \leq 5$, then

$$V_{LL} = y \left(\frac{\tau_{bed}}{K} \right)^{\frac{1}{n}} \quad (3.6)$$

$$\frac{dV_{LL}}{dy} = \left(\frac{\tau_{bed}}{K} \right)^{\frac{1}{n}} \quad (3.7)$$

$$V_{LL}^+ = \frac{V_{LL}}{V_f} \quad (3.8)$$

if $5 < y^+ \leq 30$, then

$$V_{LL}^+ = -1.076 + 1.445(y^+) + 0.04885(y^+)^2 + 0.0005813(y^+)^3 \quad (3.9)$$

$$V_{LL} = V_f V_{LL}^+ \quad (3.10)$$

$$\frac{dV_{LL}}{dy} = \frac{V_{LL}}{y} \quad (3.11)$$

if $y^+ > 30$, then

$$V_{LL}^+ = 2.5 \ln(y^+) + 5.5 \quad (3.12)$$

$$V_{LL} = V_f V_{LL}^+ \quad (3.13)$$

$$\frac{dV_{LL}}{dy} = \frac{V_{LL}}{y} \quad (3.14)$$

where, V_{LL} is the local liquid velocity, $\frac{dV_{LL}}{dy}$ is the local liquid velocity gradient, V_{LL}^+ is the dimensionless local liquid velocity, fluid-consistency index is assumed as $K = \mu_L$, dimensionless

distance from the mean bed surface is $y^+ = yV_f^{\frac{2-n}{n}} \left(\frac{\rho_L}{K}\right)^{\frac{1}{n}}$, distance from mean bed surface to the

particle center assumed as $y = \frac{d_p}{2}$, bed friction velocity is $V_f = \left(\frac{\tau_{bed}}{\rho_L}\right)^{0.5}$, average bed shear

stress is $\tau_{bed} = f_{bed} \frac{\rho_L V^2}{2}$, bed friction factor for laminar flow is $f_{bed} = \frac{16}{Re}$, bed friction factor for

turbulent flow modified from the equation for non-Newtonian turbulent flow in a rough pipe

obtained by Reed and Pilehvari (1993) is $\frac{1}{\sqrt{f_{bed}}} = -4 \log \left(\frac{0.27 \varepsilon_{bed}}{D_h} + \frac{1.26 n^{-1.2}}{\left(Re f_{bed} \left(1 - \frac{n}{2}\right)\right)^{n-0.75}} \right)$, mean

bed roughness is $\varepsilon_{bed} = \frac{d_p}{2} (1 + \sin \beta)$, and finally Reynolds number is calculated as $Re =$

$\frac{D_h^n \rho_L V^{2-n}}{8^{n-1} K}$. The average liquid velocity, V , is used in the τ_{bed} and Re equations. Figure 3.2 shows

some near-bed velocity calculation variables.

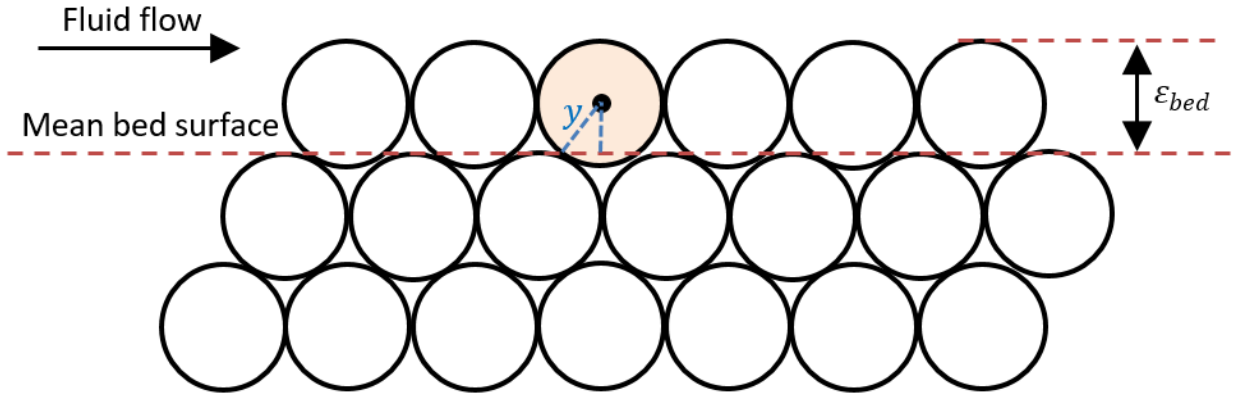


Figure 3.2 Near-bed Velocity Profile Calculation Variables Illustration

3.1.5 Forces acting on a single particle

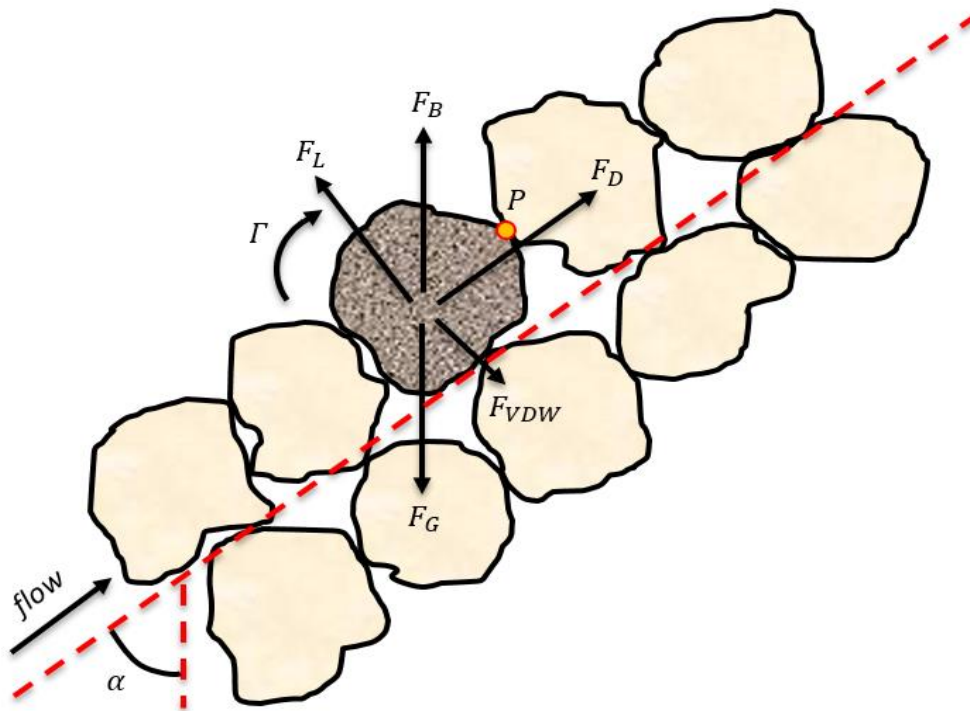


Figure 3.3 Forces Acting on a Particle

Duan (2005) investigated forces acting on one particle at the surface of the particle bed. Five different forces are shown in Figure 3.3. Gravity force, F_G , is a downward force, which is acting on a particle because of gravity, while buoyancy force, F_B , is an upward force, which is

acting on a particle because of the weight of the surrounding fluid. Lift force, F_L , and drag force, F_D , are hydrodynamic forces caused by a fluid flow, where the first is created because of near particle velocity gradient, and the second mainly depends on surrounding fluid velocity and exists between particles and fluid. Van der Waals force, F_{VDWR} , is an attractive force existing between neighboring particles, which becomes dominant when the diameter of the closely contacted particles is less than 0.1 mm (fine particles). Small diameter particles tend to stick to each other creating more difficulty in their transportation.

The above forces generate a momentum rate, Γ , with respect to the contact point, P . When Γ is greater than zero, one particle will roll along with the next neighboring particles. The critical state is when Γ equals to zero, and an average fluid velocity at which Γ equals zero is the CRV (Duan, 2005).

Returning to the forces calculation, gravity and buoyancy forces are expressed as the following:

$$F_G = \frac{\pi d_p^3}{6} \rho_p g \quad (3.15)$$

$$F_B = \frac{\pi d_p^3}{6} \rho_L g \quad (3.16)$$

Duan (2005) believes that for very small particles CRV can be very high and can show a very special behavior due to the van der Waals force, which tends to bind particles together and resist particle rearrangement. He reports that with the increase of particle size, these attractive forces become less important, and then gravity becomes the main force to restrict particle movement, while drag and lift are the main forces to initiate particle movement. The van der Waals force is calculated as

$$F_{VDWR} = 6F_{VDW} \sin \beta \quad (3.17)$$

$$F_{VDW} = -\frac{A_H d_p}{24s^2} \quad (3.18)$$

$$A_H = 4.14 \times 10^{-20} \quad (3.19)$$

$$s = 1.78 \times 10^{-5} d_p^{0.77} \quad (3.20)$$

where F_{VDWR} is the resultant van der Waals force, F_{VDW} is the reduced van der Waals force proposed by Schenkel and Kitchener (1960), A_H and s are, respectively, the Hamaker constant and the particle-separation distance given by Yu et al. (2003). The coefficient 6 in F_{VDWR} equation was selected because Duan (2005) experimentally proved that one particle will have 6 neighboring particles.

The drag force is expressed as

$$F_D = 0.5C_D \rho_L V_{LL}^2 A_p \quad (3.21)$$

$$A_p = 0.25\varphi\pi d_p^2 \quad (3.22)$$

$$C_D = 0.8C_{DU}[1 + (5 \times 10^{-4}R_{ep} + 0.0179)\eta] \quad (3.23)$$

$$R_{ep} = \frac{\rho_L V_{LL}^{2-n} d_p^n}{K} \quad (3.24)$$

$$\eta = \left(\frac{dV_{LL}}{dy}\right) \frac{y}{V_{LL}} \quad (3.25)$$

where C_D is the drag coefficient, A_p is the characteristic area of the particle, C_{DU} is the drag coefficient in a uniform flow, R_{ep} is the particle Reynolds number, K is the fluid-consistency index, η is the dimensionless shear rate. V_{LL} , $\frac{dV_{LL}}{dy}$, and y variables can be taken from the near-bed velocity profile calculation result. The drag coefficient is a function of particle Reynolds number. Using the drag coefficient result of Graham and Jones (1994) for a finite Reynolds number and the drag coefficient for low particle Reynolds number, the final drag coefficient of a sphere in a power-law fluid expressed as:

$$\text{if } R_{ep} < (0.2)2^n, \text{ then } C_{DU} = \frac{24}{R_{ep}}(2 - n) \quad (3.26)$$

$$\text{if } (0.2)2^n \leq R_{ep} < (24)2^n, \text{ then } C_{DU} = \frac{35.2}{\left(\frac{R_{ep}}{2^n}\right)^{1.03}} + n \left(1 - \frac{20.9}{\left(\frac{R_{ep}}{2^n}\right)^{1.11}}\right) \quad (3.27)$$

$$\text{if } (24)2^n \leq R_{ep} \leq (100)2^n, \text{ then } C_{DU} = \frac{37}{\left(\frac{R_{ep}}{2^n}\right)^{1.1}} + 0.25 + 0.36n \quad (3.28)$$

The last force to be defined is the lift force, which is expressed as

$$F_L = 0.5C_L\rho_L V_{LL}^2 A_p \quad (3.29)$$

where A_p is the characteristic area of the particle, C_L is the lift coefficient. Two lift coefficient expressions are used in this model. The first one is the lift coefficient for a small sphere in a slow shear flow defined by Saffman (1965), which is

$$\text{if } R_{ep} < 1, \text{ then } C_L = 2.47 \sqrt{\frac{d_p}{R_{ep}V_{LL}} \left(\frac{dV_{LL}}{dy}\right)} \quad (3.30)$$

and the second is the lift coefficient as a function of particle Reynolds number and dimensionless shear rate given by Kurose and Komori (1999), which is

$$\text{if } R_{ep} \geq 1, \text{ then } C_L = K_0\eta^{0.9} + K_1\eta^{1.1} \quad (3.31)$$

where,

$$\text{if } 1 \leq R_{ep} \leq 5, \text{ then } K_0 = -0.3161R_{ep} + 0.7976 \quad (3.32)$$

$$\text{if } 5 < R_{ep} \leq 10, \text{ then } K_0 = 0.1378R_{ep} - 1.4719 \quad (3.33)$$

$$\text{if } 10 < R_{ep} \leq 300, \text{ then } K_0 = -1.53 \times 10^{-5}R_{ep}^2 + 1.362 \times 10^{-3}R_{ep} - 0.1293 \quad (3.34)$$

$$\text{if } 300 < R_{ep} \leq 500, \text{ then } K_0 = 9.6 \times 10^{-6}R_{ep}^2 - 5.583 \times 10^{-3}R_{ep} - 0.3011 \quad (3.35)$$

and

$$\text{if } 1 \leq R_{ep} \leq 10, \text{ then } K_1 = -0.3739R_{ep} + 3.8318 \quad (3.36)$$

$$\text{if } 10 < R_{ep} \leq 300, \text{ then } K_1 = 8.77 \times 10^{-8}R_{ep}^3 - 1.64 \times 10^{-5}R_{ep}^2 + 8.12 \times 10^{-5}R_{ep} + 0.1866 \quad (3.37)$$

$$\text{if } 300 < R_{ep} \leq 500, \text{ then } K_1 = -1.0925 \times 10^{-5}R_{ep}^2 + 5.888 \times 10^{-3}R_{ep} + 0.318 \quad (3.38)$$

where K_0 and K_1 coefficients are functions of particle Reynolds number.

3.1.6 Getting GAMMA

The last step in the CRV model is calculating the momentum rate applied to a particle on a particle bed, Γ ,

$$\Gamma = \frac{d_p}{2}(F_L \cos \beta + F_D \sin \beta - F_G \sin(\alpha + \beta) - (F_B + F_{VDWR}) \cos \beta) \quad (3.39)$$

where α is the well inclination angle, and β is the angle of repose. Based on the particle rolling mechanism for horizontal and highly inclined wellbores, the critical state for a particle's movement on a particle bed is when the resultant momentum rate with respect to the contact point P, equals zero (Duan, 2005). Note that GAMMA equation from Duan's original paper and thesis is different compared to the abovementioned GAMMA equation. Finally, the average liquid velocity, V , when $\Gamma = 0$ is exactly Critical Resuspension Velocity.

3.2. Mechanistic model 2 - Critical Sand Deposition Velocity (CSDV)

Critical sand deposition velocity is defined as the minimum velocity that keeps all particles moving at all time, above which either the dune or bed is sliding, whereas below it either one is stationary (Dabirian, 2016). The mechanistic model developed by Dabirian (2016) is for stratified flow, meaning that it is applicable for horizontal and near-horizontal sections.

Dabirian (2016) developed two mechanistic models to predict critical sand deposition velocity for stationary dunes and stationary beds. Unlike Duan (2005), where he analyzed the whole particle, Dabirian (2016) analyzed only half of the particle. In a mechanistic model for stationary dune, he analyzed a particle located on top of the dune, while in a mechanistic model for stationary bed, the analyzed particle is located at the bottom of the moving bed layer, or on a stationary mono-layer particles. In the study, saltation and rolling are the main mechanisms to transport sand particles. Saltation means that particles existing on the top of the bed are picked up and bounce downstream on the bed. As the saltation process continues, it causes some sand particles to be collected behind larger particles that move at slower velocities (Dabirian, 2016).

In the current study, the CSDV model is modified by applying Zhang et al. (2003) unified gas-liquid pipe flow model, mean bed roughness, average bed shear stress, fluid behavior index, particle sphericity, and by changing near-bed velocity profile, friction factor, particle characteristic area, particle Reynolds number calculation equations. Dabirian's (2016) mechanistic model covers many important flow variables needed to calculate the critical particle transport velocity, but with the modification, the CSDV model takes into account even more of them.

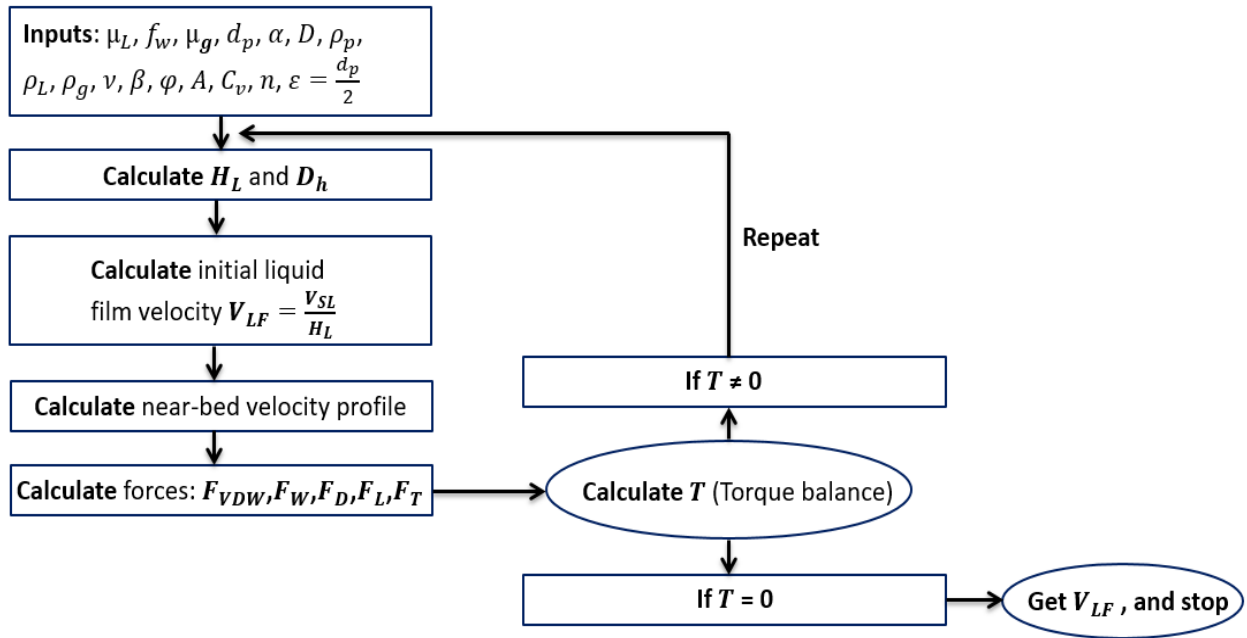


Figure 3.4 Algorithm to Calculate Critical Sand Deposition Velocity

Figure 3.4 provides the steps to calculate CSDV. It is important to note that CRV and CSDV models may have similar inputs, approaches, and equations. In order not to be confused, even if two mechanistic models may have similar approach, all the equations for CSDV model will be shown alternately and explained separately.

3.2.1 Inputs

Followings are the inputs needed for the calculation of the CSDV model:

1. μ_L = liquid dynamic viscosity
2. μ_g = gas dynamic viscosity
3. f_w = water fraction
4. d_p = particle diameter
5. α = well inclination angle
6. D = pipe diameter

7. ρ_p = particle density
8. ρ_L = liquid density
9. ρ_g = gas density
10. ν = liquid kinematic viscosity
11. β = angle of repose
12. φ = particle sphericity
13. A = pipe cross-sectional area
14. C_v = particle concentration
15. n = fluid behavior index. Assuming Newtonian fluid, n is equal to 1
18. $\varepsilon = \frac{d_p}{2}$ = pipe roughness

3.2.2 Liquid holdup and hydraulic diameter calculation

Application of Zhang et al. (2003) unified gas-liquid pipe flow model is crucial to get liquid holdup, H_L , and hydraulic diameter, D_h values. Generally, the main variables and data needed for critical sand deposition velocity from Zhang et al. (2003) unified gas-liquid pipe flow model are liquid holdup, H_L , hydraulic diameter, D_h , liquid velocity, V_L , slug velocity, v_s , film velocity, v_f , and flow patterns. However, getting H_L and D_h variables, and determining flow pattern are enough for CSDV model calculation.

Liquid holdup and hydraulic diameter values should be used in this model if only the flow pattern is stratified flow. If the flow pattern is different than stratified, using H_L and D_h values of other flow patterns will give an incorrect result.

So, making sure that flow pattern is stratified flow, then giving specific superficial liquid velocity, V_{SL} , and superficial gas velocity, V_{SG} , liquid holdup and hydraulic diameter values can be calculated from Zhang et al. (2003) unified gas-liquid pipe flow model.

3.2.3 Liquid film velocity calculation

Liquid film velocity, V_{LF} , at the end of all calculations, is the Critical Sand Deposition Velocity, which is found by iterating all the existing equations. Knowing superficial liquid velocity, V_{SL} , and liquid holdup, H_L , initial liquid film velocity can be calculated as

$$V_{LF} = \frac{V_{SL}}{H_L} \quad (3.40)$$

3.2.4 Near-bed velocity profile

The near-bed velocity profile for the CSDV model is the same as for the CRV model, except the mean bed roughness, ε_{bed} , the distance taken from the center of the analyzed particle, y_p , and Reynolds number, Re . However, Reynolds number result is the same as for CRV if assume fluid behavior index, n , as 1. Dabirian (2016) analyzed only half of the particle, because of that, distance taken from the center of the analyzed particle is assumed as $y_p = \frac{d_p}{4}$.

The velocity profile determined by Schlichting (1955) can be used for the viscous sublayer which is closest to the particle bed. If the particle protrudes into the buffer zone or the logarithmic layer above the viscous sublayer, the velocity profile developed by Kallio and Reeks (1989) can be picked. So the near-bed velocity profile calculation is as follows:

if $y^+ \leq 5$, then

$$V_{LL} = y_p \left(\frac{\tau_{bed}}{K} \right)^{\frac{1}{n}} \quad (3.41)$$

$$\frac{dV_{LL}}{dy_p} = \left(\frac{\tau_{bed}}{K}\right)^{\frac{1}{n}} \quad (3.42)$$

$$V_{LL}^+ = \frac{V_{LL}}{V_f} \quad (3.43)$$

if $5 < y^+ \leq 30$, then

$$V_{LL}^+ = -1.076 + 1.445(y^+) + 0.04885(y^+)^2 + 0.0005813(y^+)^3 \quad (3.44)$$

$$V_{LL} = V_f V_{LL}^+ \quad (3.45)$$

$$\frac{dV_{LL}}{dy_p} = \frac{V_{LL}}{y_p} \quad (3.46)$$

if $y^+ > 30$, then

$$V_{LL}^+ = 2.5 \ln(y^+) + 5.5 \quad (3.47)$$

$$V_{LL} = V_f V_{LL}^+ \quad (3.48)$$

$$\frac{dV_{LL}}{dy_p} = \frac{V_{LL}}{y_p} \quad (3.49)$$

where V_{LL} is the local liquid velocity, $\frac{dV_{LL}}{dy_p}$ is the local liquid velocity gradient, V_{LL}^+ is the

dimensionless local liquid velocity, fluid-consistency index is assumed as $K = \mu_L$, dimensionless

distance from the mean bed surface is $y^+ = y_p V_f^{\frac{2-n}{n}} \left(\frac{\rho_L}{K}\right)^{\frac{1}{n}}$, distance taken from the center of the

analyzed particle is assumed as $y_p = \frac{d_p}{4}$, bed friction velocity is $V_f = \left(\frac{\tau_{bed}}{\rho_L}\right)^{0.5}$, average bed shear

stress is $\tau_{bed} = f_{bed} \frac{\rho_L V_{LF}^2}{2}$, bed friction factor for laminar flow is $f_{bed} = \frac{16}{Re}$, bed friction factor

for turbulent flow modified from the equation for non-Newtonian turbulent flow in a rough pipe

obtained by Reed and Pilehvari (1993) is $\frac{1}{\sqrt{f_{bed}}} = -4 \log \left(\frac{0.27 \varepsilon_{bed}}{D_h} + \frac{1.26 n^{-1.2}}{\left(Re f_{bed} \left(1 - \frac{n}{2}\right)\right)^{n-0.75}} \right)$, mean

bed roughness is $\varepsilon_{bed} = \frac{d_p}{2}$, and finally Reynolds number is calculated as $Re = \frac{\rho_L V_{LF} D_h}{\mu_L}$. The

liquid film velocity variable, V_{LF} , is used in the τ_{bed} and R_e equations. Calculating near-bed velocity profile is important for the drag and lift force determination.

3.2.5 Forces acting on a single particle

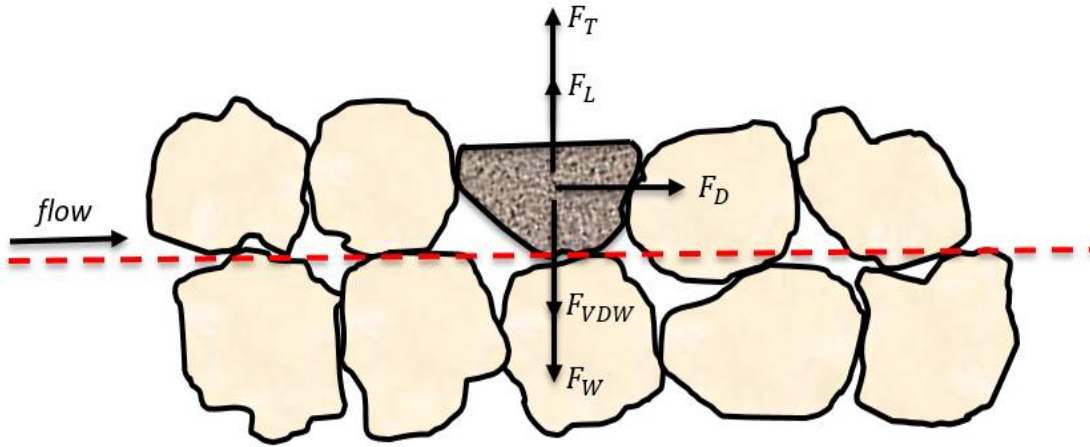


Figure 3.5 Forces Acting on a Half Particle

Dabirian (2016) investigated forces acting on half of a particle. Five different forces are shown in Figure 3.5. Apparent weight force, F_W , which is the difference between gravity and buoyancy forces, turbulent force, F_T , which is caused by the turbulence of the fluid flow. The other ones are drag force, F_D , lift force, F_L , and van der Waals force, F_{VDW} , which have the same definition as for the CRV model.

Apparent weight force is calculated as

$$F_W = \frac{\pi d_p^3}{6} g(\rho_p - \rho_L) \quad (3.50)$$

The van der Waals force is defined as:

$$F_{VDW} = \frac{A_H d_p}{12s^2} \quad (3.51)$$

$$A_H = 6.5 \times 10^{-20} \quad (3.52)$$

$$s = 6.2 \times 10^{-9} \quad (3.53)$$

where F_{VDW} is the van der Waals force, A_H is the Hamaker constant, and s is the particle-separation distance.

The drag force is expressed as

$$F_D = 0.5C_D\rho_L V_{LL}^2 A_p \quad (3.54)$$

$$A_p = 0.25\phi\pi d_p^2 \quad (3.55)$$

$$C_D = \frac{24}{Re_p} + \frac{6}{1+Re_p^2} + 0.4 \quad (3.56)$$

$$Re_p = \frac{\rho_L V_{LL} d_p}{\mu_L} \quad (3.57)$$

where C_D is the drag coefficient, A_p is the characteristic area of the particle, and Re_p is the particle Reynolds number. The local liquid velocity, V_{LL} , is explained in the near-bed velocity profile calculation.

Modified Saffman's equation by Wang et al. (1996) based on Hall (1988) experimental results is used to determine the lift force:

$$\text{if } 1.8 < r^+ < 100, \text{ then } F_L = 1.615 \frac{\mu_L V_{LL} d_p^2}{\nu^{0.5}} \left(\frac{dV_{LL}}{dy_p} \right)^{0.5} F(r^+) \quad (3.58)$$

$$F(r^+) = \frac{20.9(r^+)^{2.31}}{10^{(1.962 \log(r^+) + 1.412)}} \quad (3.59)$$

$$r^+ = \frac{d_p}{2} \left(\frac{\nu}{\frac{dV_{LL}}{dy_p}} \right)^{-0.5} \quad (3.60)$$

$$\text{else, } F_L = 1.615 \frac{\mu_L V_{LL} d_p^2}{\nu^{0.5}} \left(\frac{dV_{LL}}{dy_p} \right)^{0.5} \quad (3.61)$$

where local liquid velocity, V_{LL} , and local liquid velocity gradient, $\frac{dV_{LL}}{dy_p}$, are shown in the near-bed velocity profile calculation.

Turbulent force is negligible if the flow is laminar and if the particle size is less than the viscous sublayer, δ . Otherwise, Dabirian (2016) believes that the turbulent force is calculated

based on the fraction of the turbulent energy that is available to suspend a particle in the liquid phase. In this mechanistic model, he assumed that part of the turbulent energy is dissipated as heat, which will not contribute to suspend particles. Therefore, the turbulent portion that causes particle suspension is reduced by a factor of w . Overall, the turbulent force equation is given as:

if $R_e < 2100$ or $d_p < \delta$, then $F_T = 0$

$$\delta = 5 \frac{v}{V_f} \quad (3.62)$$

else, $F_T = 0.25\rho_L V_f^2 d_p^2 \left(\frac{\pi}{4}\right) w$ (3.63)

$$w = \frac{4}{\pi} \lambda \exp\left(-\frac{4\lambda^2}{\pi}\right) + \left(\frac{\sqrt{\pi}}{2}\right) \left(1 - \operatorname{erf}\left(\frac{j}{2}\sqrt{\pi}\right)\right) \quad (3.64)$$

$$j = \frac{2\lambda}{\sqrt{\pi}} \quad (3.65)$$

$$\lambda = \frac{V_{set}(1-C_v)^2}{V_{LF}} \quad (3.66)$$

$$V_{set} = \frac{g d_p^2 (\rho_p - \rho_L)}{18\mu_L} \quad (3.67)$$

where V_f is the bed friction velocity, calculated in near-bed velocity profile, erf is the error function in python programming language, and V_{set} is the settling velocity.

3.2.6 Torque balance

The last step in the CSDV model is the torque balance for the stationary bed, T , which is calculated as

$$T = \left(\frac{d_p}{2} F_D \sin \beta\right) + \left(\frac{d_p}{2} (F_T + F_L - F_{VDW}) \cos \beta\right) + \left(\frac{d_p}{2} (-F_W) N \cos(\alpha - \beta)\right) \quad (3.68)$$

$$N = C_{MB} \left(\frac{y_{MB}}{d_p}\right) + (1 - C_{MB}) \quad (3.69)$$

$$\frac{y_{MB}}{d_p} = 337.8 (C_v^{0.5} - 0.001) \quad (3.70)$$

$$C_{MB} = 0.74$$

where α is the well inclination angle, and β is the angle of repose, N is the dimensionless weight of the analyzed particle and other particles on top of the moving bed layer, C_{MB} is the maximum particle packing, y_{MB} is the moving bed layer height, and $\frac{y_{MB}}{d_p}$ is the dimensionless moving bed. Similar to the CRV model, liquid film velocity, V_{LF} , when $T = 0$ is exactly the Critical Sand Deposition Velocity.

3.3 Empirical model 1 - Critical Gas Core Velocity

Critical Gas Core Velocity model, V_{gc} , is based on Ibarra (2017) work, where he investigated critical sand deposition velocity in horizontal stratified flow. Ibarra modified and combined Oroskar and Turian (1980) and Salama (2000) models to develop a new model. To get liquid holdup value, he used Chisholm (1967) model.

In this study, the same Ibarra's model will be used. However, Zhang et al. (2003) unified gas-liquid pipe flow model will be used to determine liquid holdup value and flow pattern. Ibarra (2017) used his model for stratified horizontal flow, although in this study, the model is used for the gas core of annular flow.

One of the important steps in the model calculation is identifying the flow pattern, which can be obtained using Zhang et al. (2003) unified gas-liquid pipe flow model. The model will be correct if only the flow pattern is Annular, so the superficial gas velocity should be high enough to reach annular flow.

3.3.1 Inputs

Followings are the inputs needed for the calculation of critical gas velocity:

1. μ_L = liquid dynamic viscosity

2. d_p = particle diameter
3. D = pipe diameter
4. ρ_p = particle density
5. ρ_L = liquid density
6. ρ_g = gas density
7. C_v = particle concentration
8. V_{SL} = superficial liquid velocity
9. V_{SG} = superficial gas velocity

3.3.2 V_{gc} calculation

Giving input parameters, then, applying Zhang et al. (2003) unified gas-liquid pipe flow model, superficial liquid velocity, V_{SL} , superficial gas velocity, V_{SG} , liquid holdup, H_L , can be calculated. From Zhang et al. (2003) unified gas-liquid pipe flow model, the annular flow pattern should be obtained. Then, modified Reynolds number incorporating gas density effect, N_{Re} , is calculated as

$$N_{Re} = \frac{D \rho_L \sqrt{g d_p \left(\frac{\rho_L}{\rho_g} - 1 \right)}}{\mu_L} \quad (3.71)$$

The following is a calculation of critical mixture velocity, V_{MC} ,

$$\frac{V_{MC}}{\sqrt{g d_p \left(\frac{\rho_p}{\rho_L} - 1 \right)}} = 1.651 \left(\frac{V_{SL}}{V_{MC}} \right)^{-0.236} (1 - C_v)^{-33.8} \left(\frac{d_p}{D} \right)^{-0.378} N_{Re}^{0.09} \quad (3.72)$$

Finally, critical gas core velocity, V_{gc} , is calculated as:

$$V_{gc} = \frac{V_{SGC}}{(1 - H_L)} \quad (3.73)$$

$$V_{SGC} = V_{MC} - V_{SL} \quad (3.74)$$

where V_{SGC} is critical superficial gas velocity.

3.4 Empirical model 2 - Minimum Particle Pickup Gas Velocity

Minimum Particle Pickup Gas Velocity model, V_{pu} , is defined as the minimum velocity required to re-suspend a particle that is initially at rest at the bottom of the pipe. Another definition is that it is the minimum velocity required to initiate rolling, sliding, and suspension of particles. Minimum particle pickup gas velocity is very important in gas production and transportation system. High gas velocity may cause pipe erosion and high energy cost because of the increased pressure drop in a pipeline system, which negatively impacts the economics. A low gas flow rate may cause an accumulation of sand particles in a system, which may cause flow assurance and other issues.

The minimum particle pickup gas velocity model includes two different models. One is Cabrejos and Klinzing (1994) model, and the second is Hayden (2003) model. The usage of each model depends on the particle size. In this model, Zhang et al. (2003) unified gas-liquid pipe flow model is used to calculate liquid holdup. This is a new approach because Zhang et al. (2003) unified gas-liquid pipe flow model was not considered in the original models of Cabrejos and Klinzing (1994), and Hayden (2003). Further, all the equations and calculations will be explained step by step.

3.4.1 Inputs

Following are the inputs needed for the calculation of minimum particle pickup gas velocity:

1. μ_L = liquid dynamic viscosity
2. μ_g = gas dynamic viscosity
3. d_p = particle diameter
4. D = pipe diameter
5. ρ_p = particle density
6. ρ_L = liquid density
7. ρ_g = gas density
8. $\nu_{gas} = \frac{\mu_g}{\rho_g}$, gas kinematic viscosity

3.4.2 V_{pu} calculation

Giving input parameters, specific superficial liquid, V_{SL} , and superficial gas velocities, V_{SG} , liquid holdup, H_L , parameter needs to be calculated by applying Zhang et al. (2003) unified gas-liquid pipe flow model. However, liquid holdup can be assumed as 0 if there is no liquid phase. After getting liquid holdup, average gas velocity, V_G , and particle Reynolds number, R_{ep} , can be determined as follows:

$$V_G = \frac{V_{SG}}{(1-H_L)} \quad (3.75)$$

$$R_{ep} = \frac{d_p \rho_g V_G}{\mu_g} \quad (3.76)$$

Finally, minimum particle pickup gas velocity, V_{pu} , is calculated as

$$\text{if } d_p < 0.0001, \text{ then } V_{pu} = \frac{2.62 \nu_{gas}^{\frac{13}{21}} D^{\frac{3}{21}}}{\mu_g^{\frac{8}{21}}} \left(\frac{\pi}{6} g (\rho_p - \rho_g) + \frac{1.302 \times 10^{-6}}{d_p^2} \right)^{\frac{8}{21}} \quad (3.77)$$

$$\text{if } d_p \geq 0.0001, \text{ then } \frac{V_{pu}}{\sqrt{g d_p}} = 0.0428 R_{ep}^{0.175} \left(\frac{D}{d_p} \right)^{0.25} \left(\frac{\rho_p}{\rho_g} \right)^{0.75} \quad (3.78)$$

where in case when particle diameter is less than 0.0001 meters, Cabrejos and Klinzing (1994) model is used, while when particle diameter is equal or more than 0.0001 meters, Hayden (2003) model is used.

3.5 Empirical model 3 - Settling velocity

Chien (1994) developed a new correlation to predict the settling velocity of irregularly shaped particles in both Newtonian and non-Newtonian fluids. The settling velocity model can be used in many spheres of petroleum engineering. The main assumption is that liquid holdup is 1. The main usage of the model in this study is vertical oil production wells. Chien's model presented by Salama (2000) is:

$$V_{set} = 1.2 \left(\frac{v}{D} \right) \left[-1 + \sqrt{1 + 0.073 \left(\frac{\Delta\rho}{\rho_L} \right) \left(\frac{D}{v} \right)^2} \right] \quad (3.79)$$

where V_{set} is the settling velocity, v is the liquid kinematic viscosity, D is the pipe diameter, $\Delta\rho$ is the difference between particle density and liquid density, and ρ_L is the liquid density.

A new mechanistic model could be developed for the vertical wells. However, due to the lack of experimental facility, and as a result impossibility of the model validation, it was decided to leave the development of the mechanistic model as future work, and use Chien's settling velocity model for the vertical wells.

3.6 Model selection and conclusions

3.6.1 Conclusions for Critical Resuspension Velocity (CRV) model

1. The model is best for Dispersed Bubble (D-B), Bubbly (BUB), and slug section of Slug flow patterns.

2. The model is applicable for all inclination angles except vertical, near-vertical, and downward sections.
3. Conditions to avoid sand deposition for D-B and BUB flow patterns is when mixture velocity is higher than average liquid velocity, $V_m > V$. Condition to avoid sand deposition for the slug section of slug flow is when slug velocity is higher than average liquid velocity, $v_s > V$. Mixture and slug velocities are calculated from Zhang et al. (2003) unified gas-liquid pipe flow model.
4. Minimum liquid flow rate can also be calculated using the CRV model.

3.6.2 Conclusions for Critical Sand Deposition Velocity (CSDV) model

1. The model is best for Stratified flow, and for the film section of Slug flow.
2. If the flow pattern is Stratified, the model is only applicable for horizontal and near-horizontal sections. However, if the flow pattern is Slug, including horizontal section, the model can also be applicable to even higher inclination angles, with the condition at which Slug flow pattern form (flow conditions) kept the same as for horizontal and near-horizontal sections.
3. Applying Zhang et al. (2003) unified gas-liquid pipe flow model into CSDV model, gas-liquid-solid three-phase flow model can be developed. Moreover, applying Zhang et al. (2006) unified gas-oil-water pipe flow model into CSDV model, where oil and water are considered and studied separately, even a gas-oil-water-solid four-phase model can be developed.

4. Conditions for both Stratified flow pattern and film section of slug flow pattern to avoid sand deposition is when film velocity is higher than liquid film velocity, $v_f > V_{LF}$. Film velocity can be calculated from Zhang et al. (2003) unified gas-liquid pipe flow model.
5. The model is selected because it is developed specifically for stratified flow based on experiments.
6. Minimum liquid and gas flow rates can also be calculated using the CSDV model.

3.6.3 Conclusions for Critical Gas Core Velocity model

1. The model is applicable for gas core of Annular flow pattern.
2. Applicable for horizontal and near-horizontal sections.
3. Condition to avoid sand deposition, is when gas core velocity is higher than critical gas core velocity, $V_{GCV} > V_{gc}$.

3.6.4 Conclusions for Minimum Particle Pickup Gas Velocity model

1. The model can be applicable for gas production wells.
2. Zhang et al. (2003) unified gas-liquid pipe flow model is applied in case of insignificant liquid phase presence. Otherwise liquid holdup is assumed as 0.
3. Condition to avoid sand deposition is average gas velocity higher than minimum pickup gas velocity, $V_G > V_{pu}$.

3.6.5 Conclusions for Settling Velocity model

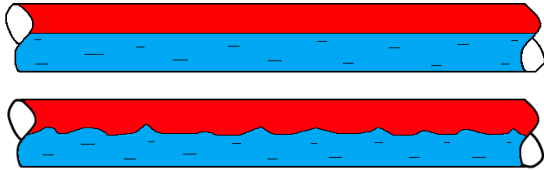
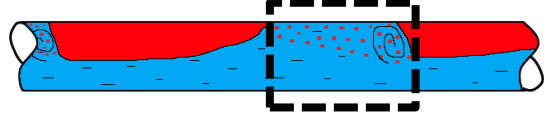
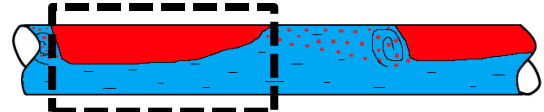
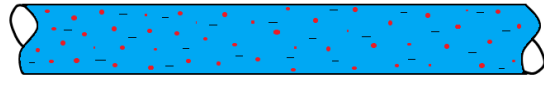
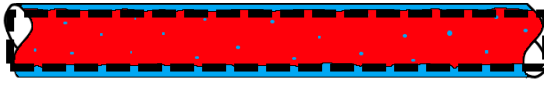
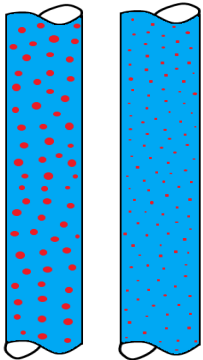

1. The model can be applicable for Dispersed Bubble (D-B) and Bubbly (BUB) flow patterns.

2. The model is applicable only for vertical wells.
3. The main assumption is that liquid holdup is 1.
4. Condition to avoid sand deposition is mixture velocity higher than the settling velocity,

$$V_m > V_{set}.$$

3.6.6 General conclusions

Table 3.1 General Conclusion

		Flow Pattern	Applicable Model
Stratified Flow			Mechanistic Model 2 (Critical Sand Deposition Velocity Model)
Slug Flow	Slug section		Mechanistic Model 1 (Critical Resuspension Velocity Model)
	Film section		Mechanistic Model 2 (Critical Sand Deposition Velocity Model)
Dispersed Bubble Flows (Horizontal)			Mechanistic Model 1 (Critical Resuspension Velocity Model)
Annular Flow (Gas Core)			Empirical Model 1 (Critical Gas Core Velocity Model).
Dispersed Bubble and Bubbly Flows (Vertical)			Empirical Model 3 (Settling Velocity Model).
Gas Production Wells			Empirical Model 2 (Minimum Particle Pickup Gas Velocity Model).

According to Angelsen et al. (1989), stratified flow is the most-critical flow regime for sand deposition. It is mainly because of the low liquid velocity which is common for stratified flow. One other reason is an inclination angle. Stratified flow only exists in horizontal and near-horizontal sections, at which sand deposition can be severe and may cause serious flow assurance issues.

Slug flow is very complex when the task is the determination of the critical sand transportation velocity. Therefore, to simplify the critical particle transport velocity calculation for slug flow, the slug flow pattern is considered separately, dividing it into two sections as slug section and film section. Then, using Critical Resuspension Velocity Model and Critical Sand Deposition Velocity Model, critical liquid velocities of both slug and film sections are determined. However, Figure 3.6 shows Dabirian's (2016) experimental result where he proves that there is no sand deposition in slug flow patterns. Sand deposition can occur in a film section of slug flow. However, slug velocity is mostly higher than sand deposition velocity and can transport all sand particles in both slug and film sections.

In most cases, due to the high mixture velocity, the sand deposition may not be an issue if the flow pattern is Dispersed Bubble flow, while Bubbly flow needs more investigation.

Sand transportation in annular flow is a very complex study, where all liquid, gas, and droplet velocities should be taken into account. In annular flow, sand may be transported in the liquid film and gas core. The mechanism that causes liquid droplets to be entrained can also make sand particles to be entrained in the gas core. Because of the high fluid velocity and particle existence, erosion issues will be more important in annular flow rather than the sand deposition.

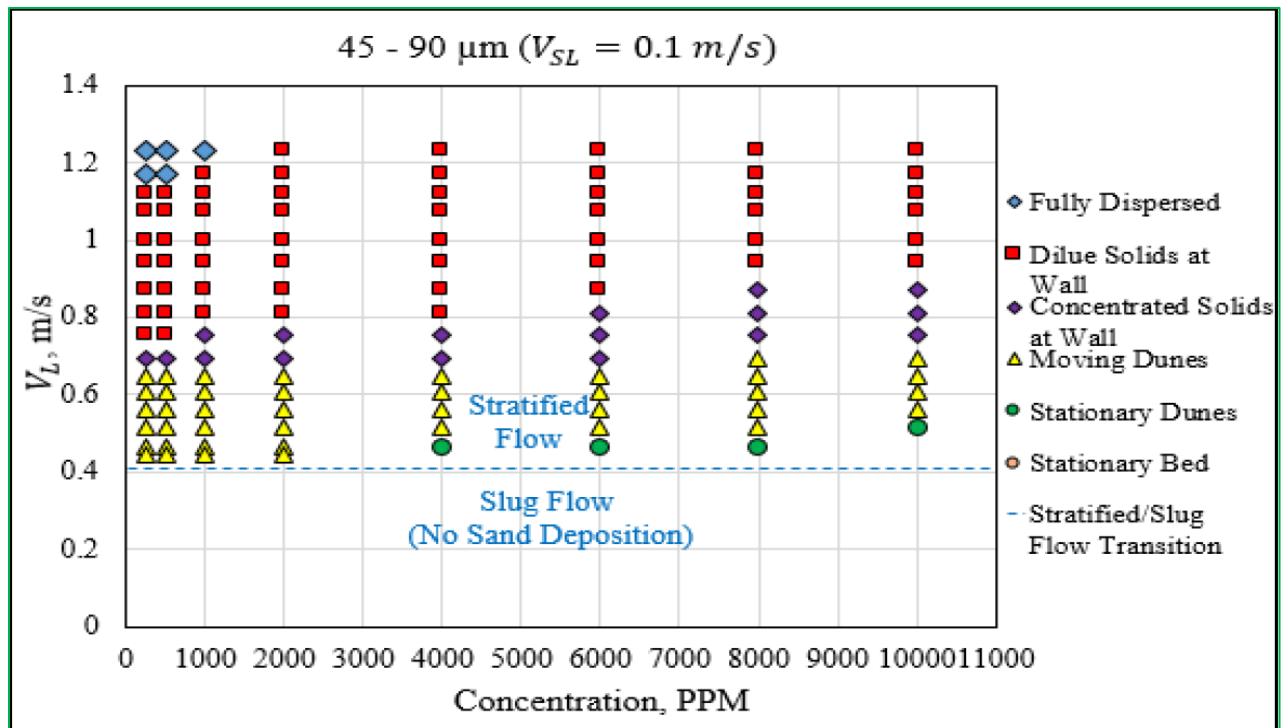


Figure 3.6 Experimental Result for Stratified and Slug Flow Patterns (Dabirian, 2016)

CHAPTER 4

EXAMPLES, RESULTS, AND DISCUSSIONS

One of the reasons sand transportation is very complex is because of many affecting variables. Fluid, particle, well, and flow parameters cause complexity in determining critical particle transport velocity. It is very important to use the correct input variables as they will significantly affect the final result.

4.1 Variables effect on Critical Resuspension Velocity (CRV) and Critical Sand Deposition Velocity (CSDV) models

Following input parameters are used in an example of CRV model:

Table 4.1 Example Input Parameters for CRV Calculation

Variables	Values
Liquid density, kg/m ³	892.5
Liquid viscosity, Pa·s	0.0046002
Sand size, m	0.0002
Pipe diameter, m	0.1
Inclination angle (from vertical), degrees. 90 degree means horizontal	90
Angle of repose, degrees	35
Sphericity	1
<i>n</i> , fluid behavior index	1
Sand density, kg/m ³	2500
Gas viscosity, Pa·s	1.8E-05
Gas density, kg/m ³	18
Water fraction	0.1
Flow pattern	Dispersed Bubble Flow

Following input parameters are used in an example of CSDV model:

Table 4.2 Example Input Parameters for CSDV Calculation

Variables	Values
Liquid density, kg/m ³	892.5
Liquid viscosity, Pa·s	0.0046002
Sand size, m	0.0002
Pipe diameter, m	0.1
Inclination angle (from horizontal)	0

Angle of repose, degrees	60
Sphericity	1
n , fluid behavior index	1
Sand density, kg/m ³	2500
Gas viscosity, Pa·s	1.8E-05
Gas density, kg/m ³	18
Water fraction	0.1
Flow pattern	Stratified

4.1.1 Particle size effect on CRV and CSDV

Sand particle size is one of the main parameters that affect sand transportation velocity in both production and drilling systems. Taking into account sand particle size does not give straightforward results. Particle size is a parameter that causes complexity in critical particle transport velocity calculation. Depending on the size and other important conditions, critical particle transport velocity value may fluctuate. According to Duan (2005), when tested with water in a horizontal section, a volumetric concentration of smaller particles is higher compared to the larger particles, hence transportation of smaller particles is more difficult. It is difficult to reduce cutting bed thickness when small particles are dominant. However, the results may differ under different conditions. Particles around 0.5 mm in diameter are the most difficult size to be transported out (Walker and Li, 2000).

Previously, the graph generated by Durand and Condolios (1952) is used to determine required critical sand transportation velocity. In this study, the graph is used to compare and validate the results of the CRV and the CSDV models.

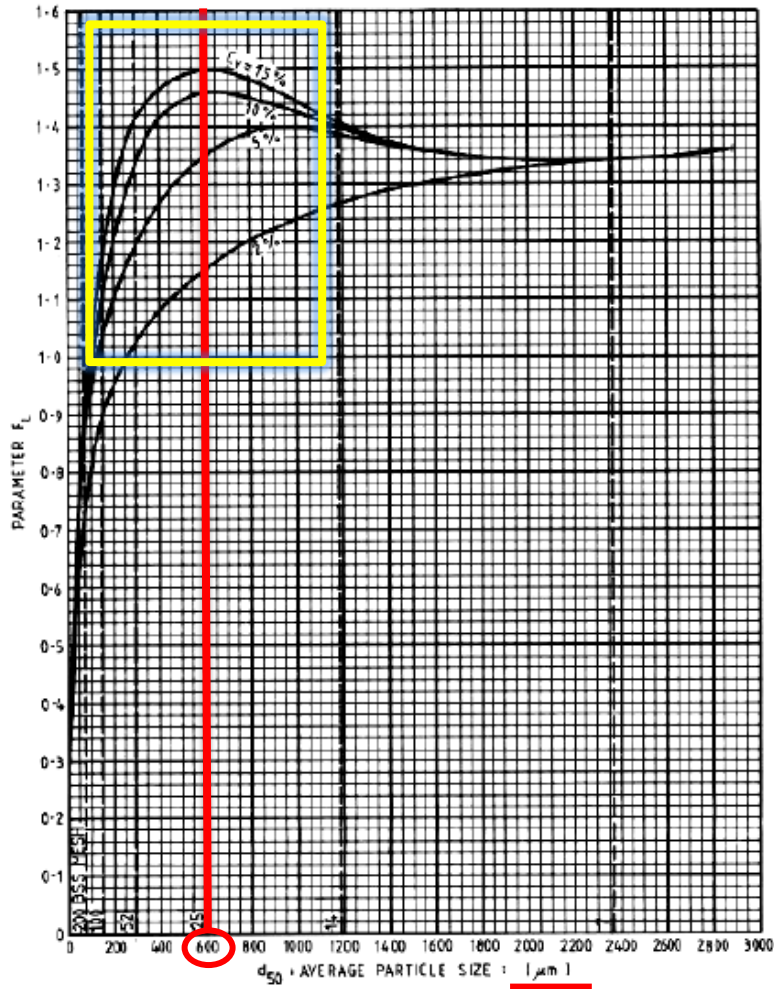


Figure 4.1 F_L Parameter as a Function of Particle Size (Durand and Condolios, 1952)

Durand and Condolios determined that the critical particle transport velocity increases with the increase of particle size until 600 microns. However, the result also depends on the particle volumetric concentration. Figure 4.1 shows that the critical particle transport velocity first increases and then decreases when the particle volumetric concentration range is between 0.05 and 0.15 v/v, whereas the critical particle transport velocity only increases when the volumetric concentration is 0.02 v/v. Critical particle transport velocity slightly increases for all particle concentrations when the particle size is higher than 2200 microns, although this size is not common in oil and gas production system.

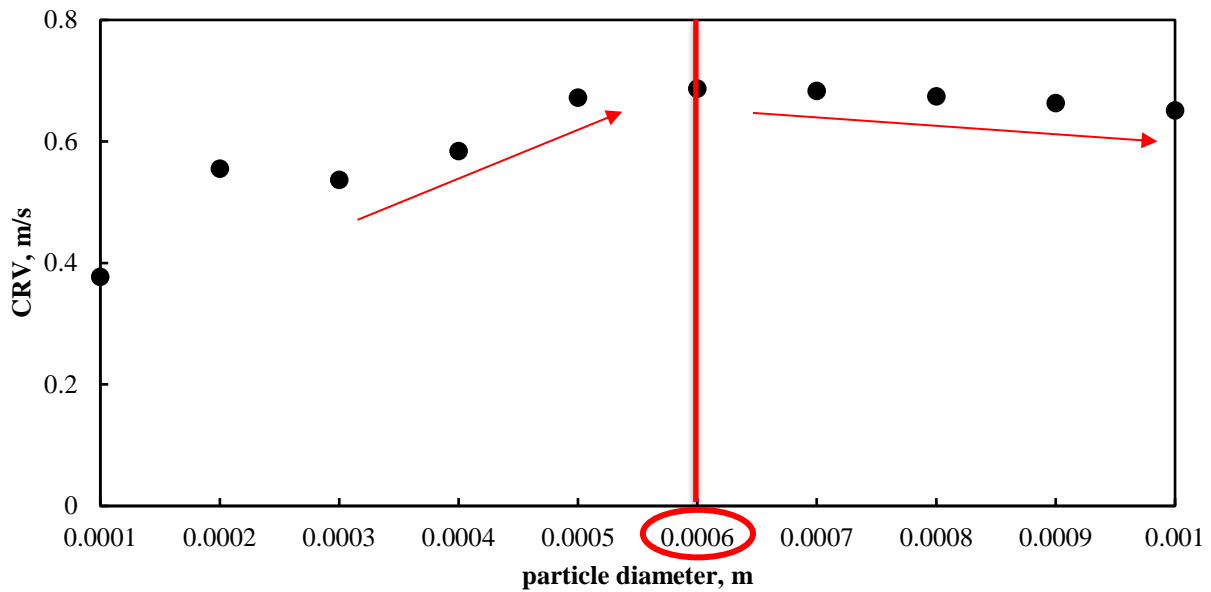


Figure 4.2 CRV versus Particle Diameter

Comparing Figure 4.2 and the Durand and Condolios graph, the same phenomena can be observed, where critical particle transport velocity increases until 0.0006 m, which is 600 microns and then slightly decreases. The figure also matches with Walker and Li (2000) study, where they identify that 0.0005 m particles are the most difficult to clean out. In general, the CRV model correctly identifies all the behavior related to particle size changes.

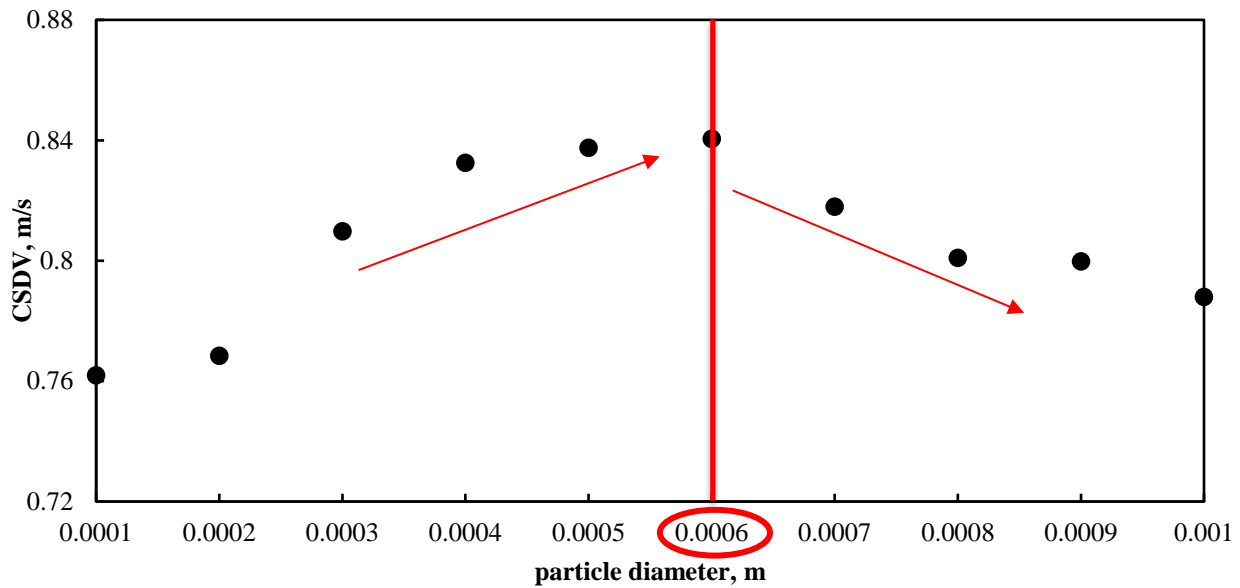


Figure 4.3 CSDV versus Particle Diameter

The same behavior for the CSDV can be observed in Figure 4.3. Similarly, comparing the CSDV with Durand and Condolios graph, CSDV value increases until 0.0006 m, and then starts to decrease.

Concluding, the CRV and the CSDV models correctly demonstrate all the behavior related to particle size changes.

4.1.2 Liquid viscosity effect on CRV and CSDV

Liquid viscosity is one of the factors that affect particle transport in both single and multiphase flows. Every sand transportation model, mechanistic or empirical includes liquid viscosity parameters. The solutions of these models are conflicting, not all the authors carried out experimental study while developing their correlations. Some of the researchers claim that critical particle transport velocity decreases with the increase of liquid viscosity, while others claim that it fluctuates. Najmi et al. (2015) studied sand particle transport with 3 cP and 10 cP

liquid viscosity values. From his experiment, he concluded that sand transport velocity increases with the increase of liquid viscosity.

There are other experimental works done to find critical particle transport velocity for specific values of liquid viscosity, but not all of them cover a wide range of liquid viscosity values. However, there is an experimental work published by both Yan (2010) and Zorgani et al. (2017), where they cover a wide range of liquid viscosity value, from 0.001 kg/m·s to 0.340 kg/m·s. To be specific, 0.001 kg/m·s, 0.007 kg/m·s, 0.02 kg/m·s, 0.105 kg/m·s, 0.200 kg/m·s, and 0.340 kg/m·s were used in the experimental work. The conclusion is critical particle transport velocity increases as the liquid viscosity increases in a turbulent flow, at a high Reynolds number. In laminar flow, when liquid viscosity increases, Reynolds number decreases, and the critical particle transport velocity decreases too. Yan (2010) explains this phenomena that shear force acting on the particles from the surrounding liquid increases and high viscous liquid tends to decrease the sand particles settling velocity value. Experimental results for 50 lb/1000 bbl and 200 lb/1000 bbl are shown in Tables 4.3, 4.4, and Figures 4.4, 4.5.

Table 4.3 Liquid Viscosity and Sand Transportation Velocity Behavior for 50 lb/1000 bbl (Zorgani et al., 2017)

Fluids	Liquid viscosity cP (kg/ms)	Transport velocity (m/s)	Pipe diameter (m)	Reynolds number	Sand/oil flow regimes
Water	0.001	0.5	0.1	50000	Sand dunes
CMC solution (7 cP)	0.007	0.7	0.1	10000	Sand dunes
CMC solution (20 cP)	0.02	0.75	0.1	3750	Connected sand dunes
Oil 105 cP	0.105	0.35	0.0776	226.33	Sliding sand bed
Oil 200 cP	0.200	0.25	0.0776	85.36	Sliding sand bed
Oil 340 cP	0.340	0.07	0.0776	14.11	Sliding sand bed

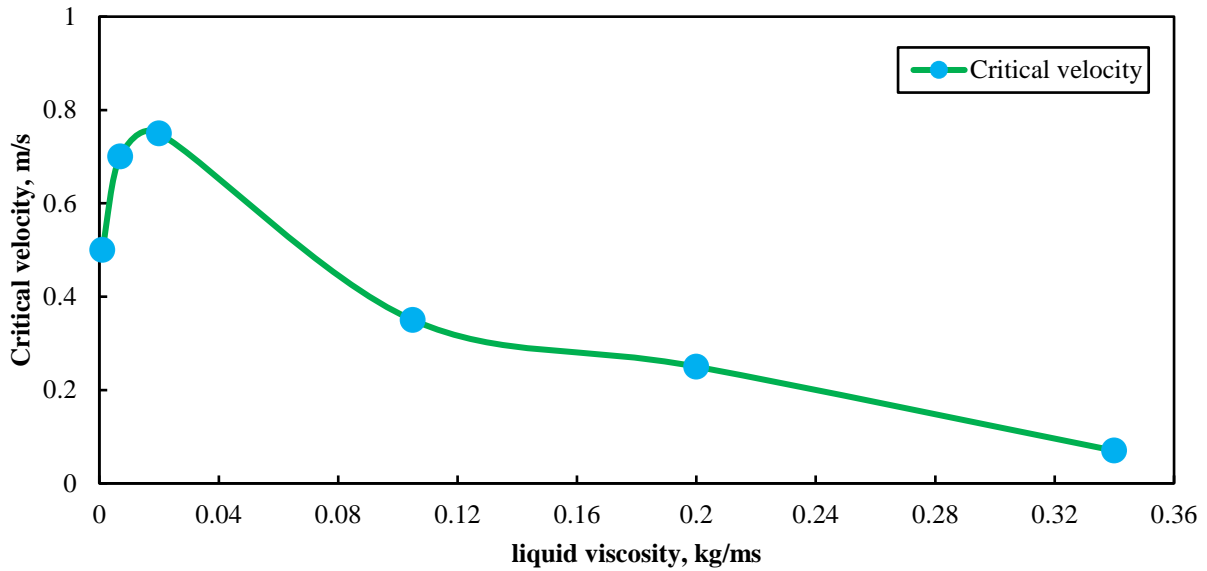


Figure 4.4 Liquid Viscosity and Sand Transportation Velocity Behavior for 50 lb/ 1000 bbl (Zorgani et al., 2017).

Table 4.4 Liquid Viscosity and Sand Transportation Velocity Behavior for 200 lb/1000 bbl (Zorgani et al., 2017)

Fluids	Liquid viscosity cP (kg/ms)	Transport velocity (m/s)	Pipe diameter (m)	Reynolds number	Sand/oil flow regimes
Water	0.001	0.7	0.1	70000	Sand dunes
CMC solution (7 cP)	0.007	0.75	0.1	10714.2	Sand dunes
CMC solution (20 cP)	0.02	0.8	0.1	4000	Connected sand dunes
Oil 105 cP	0.105	0.4	0.0776	291	Sliding sand bed
Oil 200 cP	0.200	0.3	0.0776	102.4	Sliding sand bed
Oil 340 cP	0.340	0.2	0.0776	40.31	Sliding sand bed

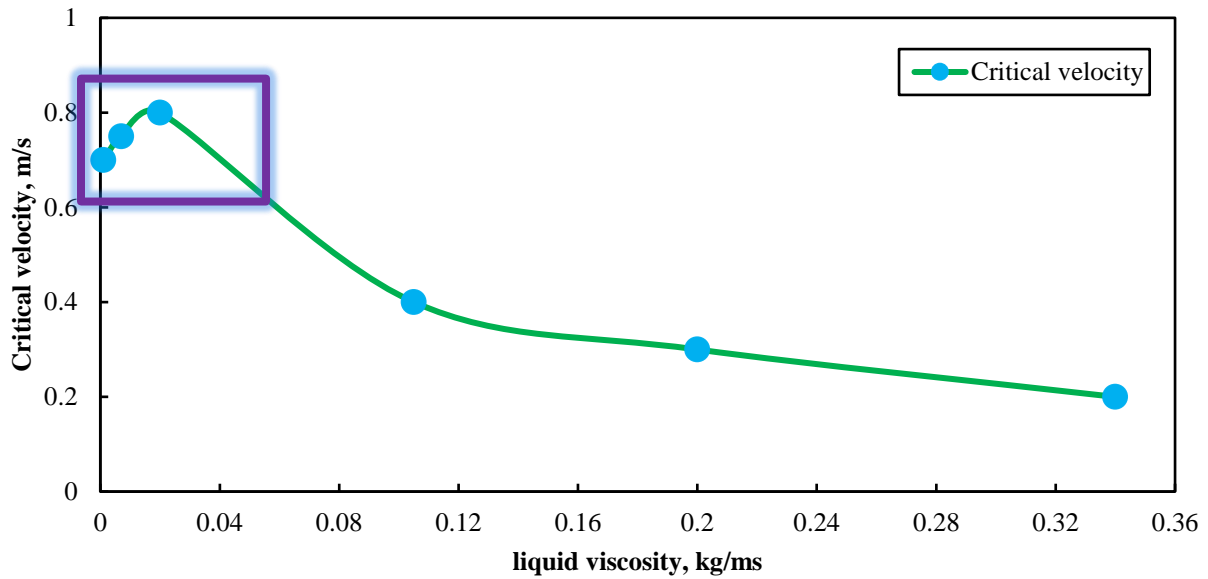


Figure 4.5 Liquid Viscosity and Sand Transportation Velocity Behavior for 200 lb/1000 bbl (Zorgani et al., 2017)

To validate the CRV model, the result of the CRV model is compared with Zorgani et al. (2017) experimental results. In Figure 4.6, it can be seen that critical particle transport velocity behaves similarly as the change of liquid viscosity, first increases, and then decreases.

Similarly, Zorgani et al. (2017) experimental result is compared with the CSDV model, and the same behavior is shown in Figures 4.7, where with the increase of liquid viscosity, the CSDV first increases, and then decreases.

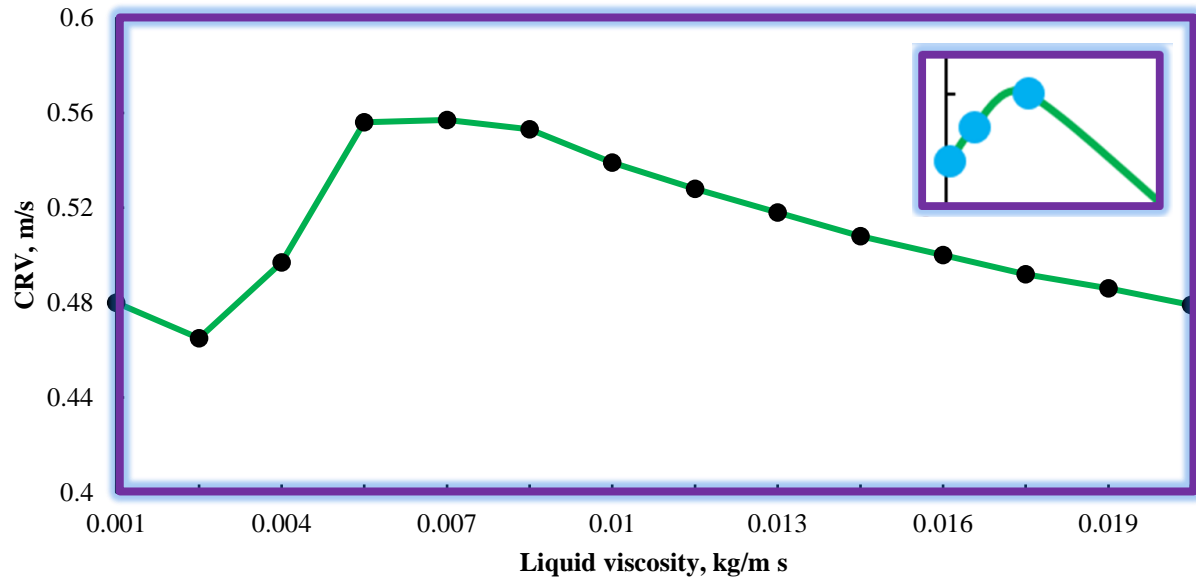


Figure 4.6 CRV versus Liquid Viscosity

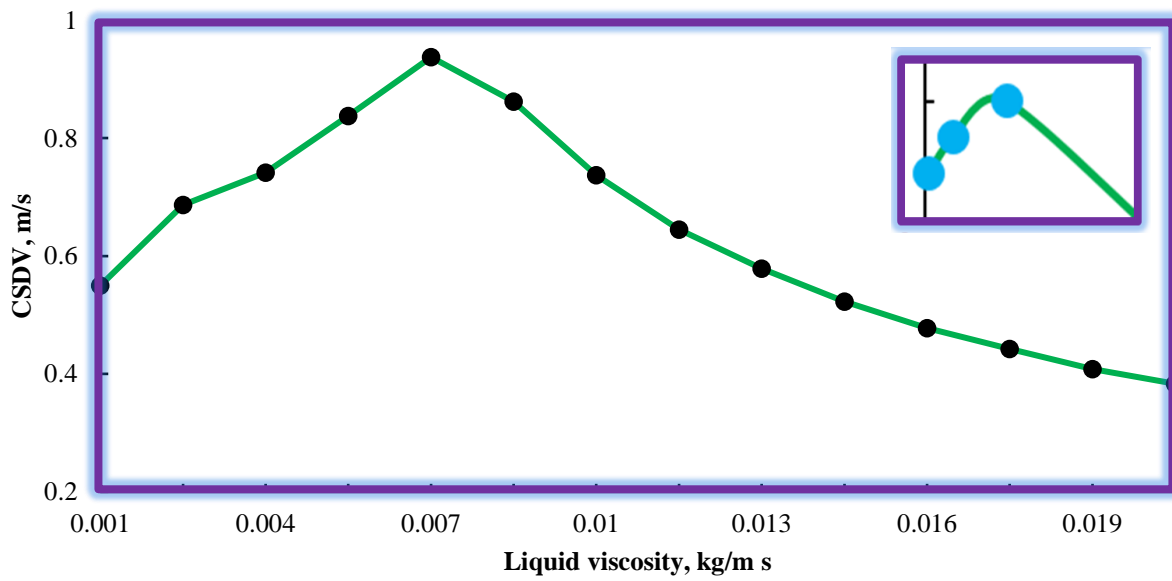



Figure 4.7 CSDV versus Liquid Viscosity

Zorgani et al. (2017) also compared his experimental work results with other existing empirical correlations. As shown in Table 4.5 all empirical correlations show critical particle

transportation velocity decrease with increase of liquid viscosity, while his experimental work proves otherwise. Giving the same parameters, Salama and Kokpinar et al. correlations significantly under-predicts the critical particle transport velocity, while Wicks correlation over-predicts. Most of the correlations under-predict critical particle transport velocity when liquid viscosity is at 0.007 kg/m·s and 0.02 kg/m·s. Oroskar and Turian, Al-Mutahar, and Danielson correlations predict well when the liquid viscosity is at 0.2 kg/m·s, although they over-predict the result when the liquid viscosity is at 0.34 kg/m·s. So, this comparison indicates that with the change in liquid viscosity, empirical models may not always give accurate results.

Table 4.5 Liquid Viscosity and Sand Transportation Velocity Behavior in Selected Correlations for 200 lb/1000 bbl (Zorgani et al., 2017)

Liquid viscosity (cP)	Minimum transport velocity, MTC (m/s)							
	Experiment	Oroskar and Turian	Salama (2000)	Turian et al. (1987)	Kokpinar et al. (2001)	Al-Mutahar	Wicks (1970)	Danielson
1	0.7 ↑	0.65 ↓	0.36 ↓	0.87 ↓	0.43 ↓	0.51 ↓	0.92 ↓	0.54 ↓
7	0.75 ↑	0.54 ↓	0.31 ↓	0.87 ↓	0.13 ↓	0.39 ↓	0.90 ↓	0.44 ↓
20	0.8 ↑	0.49 ↓	0.28 ↓	0.87 ↓	0.07 ↓	0.33 ↓	0.88 ↓	0.39 ↓
105	0.4 ↓	0.42 ↓	0.24 ↓	0.86 ↓	0.02 ↓	0.28 ↓	0.87 ↓	0.31 ↓
200	0.3 ↓	0.39 ↓	0.22 ↓	0.86 ↓	0.01 ↓	0.25 ↓	0.86 ↓	0.29 ↓
340	0.2 ↓	0.37 ↓	0.21 ↓	0.85 ↓	0.01 ↓	0.23 ↓	0.85 ↓	0.27 ↓



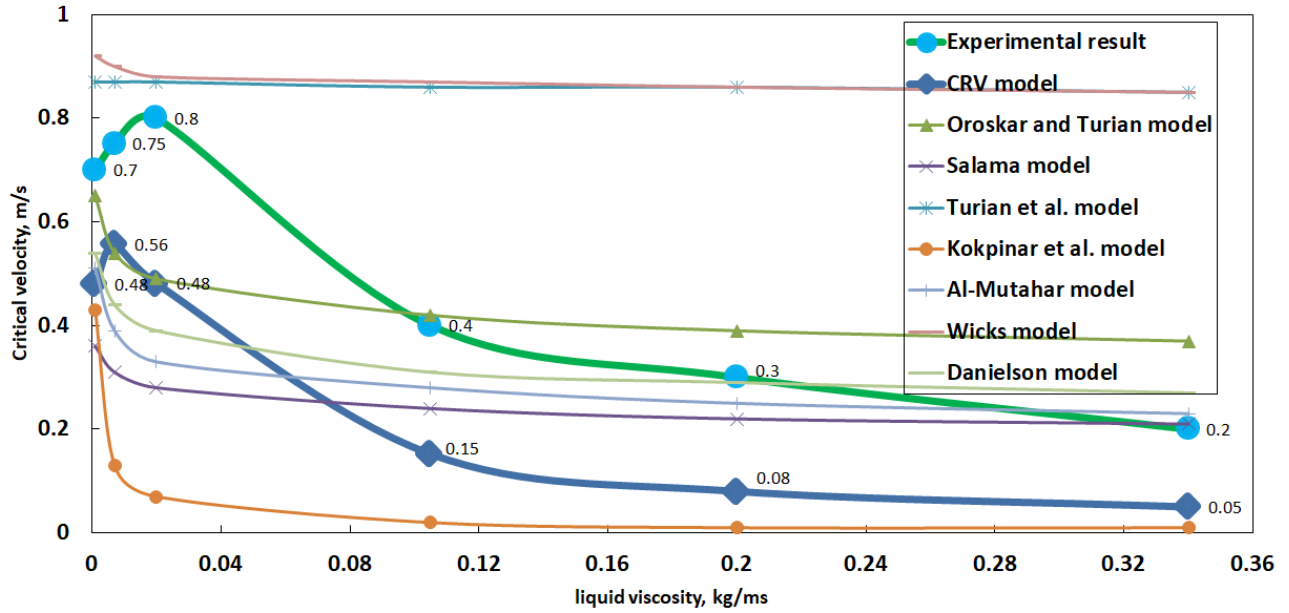


Figure 4.8 Comparison of CRV Model, Zorgani et al. (2017) Experimental, and Other Correlation Results

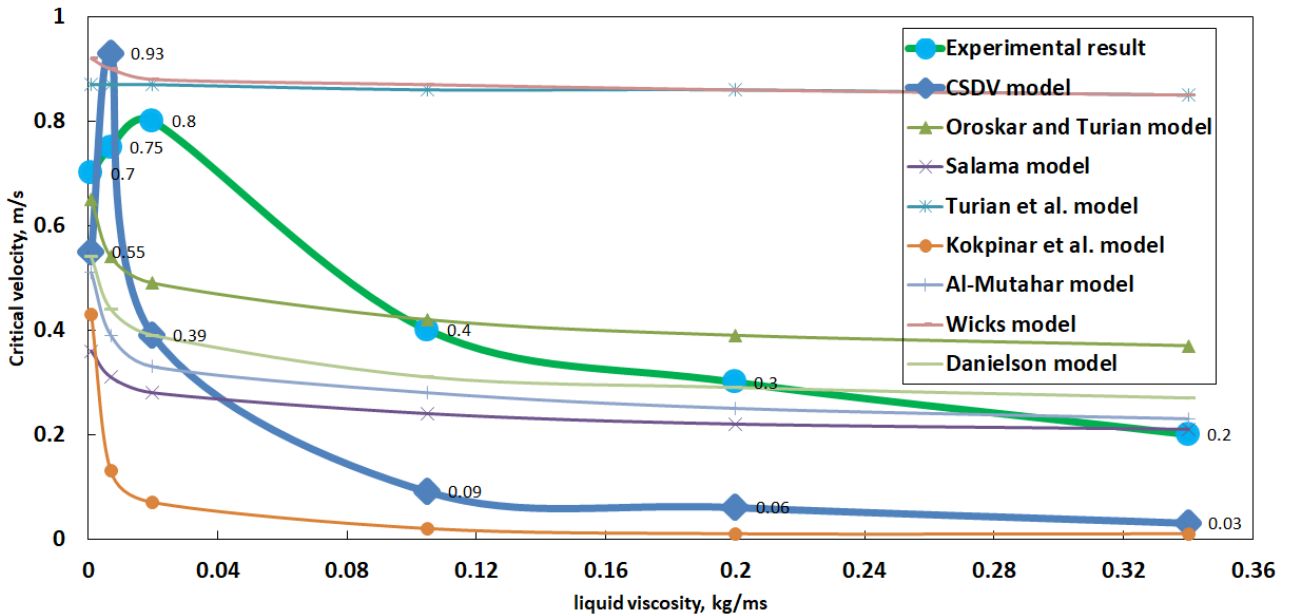


Figure 4.9 Comparison of CSDV Model, Zorgani et al. (2017) Experimental, and Other Correlation Results

The same viscosity values were selected to compare the CRV and CSDV results with Zorgani et al. (2017) experimental results and with other empirical correlations (Figure 4.8 and

4.9). Different input values were given for the model calculation due to the unknown input data from Zorgani et al. (2017). Due to the difference in fluid, pipe, sand, and other input parameters, the CRV and the CSDV model results may vary compared to Zorgani et al. (2017) experimental results, although the behavior is similar. So Zorgani et al. (2017) experimental work result proves the validity of the CRV and the CSDV models. Both models, like Zorgani et al. (2017) experimental work, also shows that critical particle transport velocity increases when the flow is turbulent, and then decreases when flow becomes laminar.

4.1.3 Inclination angle effect on CRV and CSDV

Well inclination angle is another parameter needed as an input for critical particle transport velocity calculation. It has a complicated effect on particle transport as not all the well inclination angles with existing flow patterns are investigated for oil and gas production system.

Tomren (1979) reported that a 50 degree inclination angle is a critical point for particle transport, and they are more likely to roll and be suspended when the well inclination is between 0 and 50 degrees. Then, when the inclination angle is higher than 50 degrees, the particles are more likely to accumulate and form particle bed. Peden (1990) believes that the worst sand particle transportation scenario is between 40-60 degrees. Shook and Roco (1991) experiments proved that critical particle transport velocity value increases with the increase of inclination angle. Figure 4.10 shows Roco's (1977) experimental results. He studied critical particle transport velocity change with the change of inclination angle for different sand concentrations. It can be seen that most of the highest critical particle transport velocity values correspond to the inclination angles between 10 and 15 degrees.

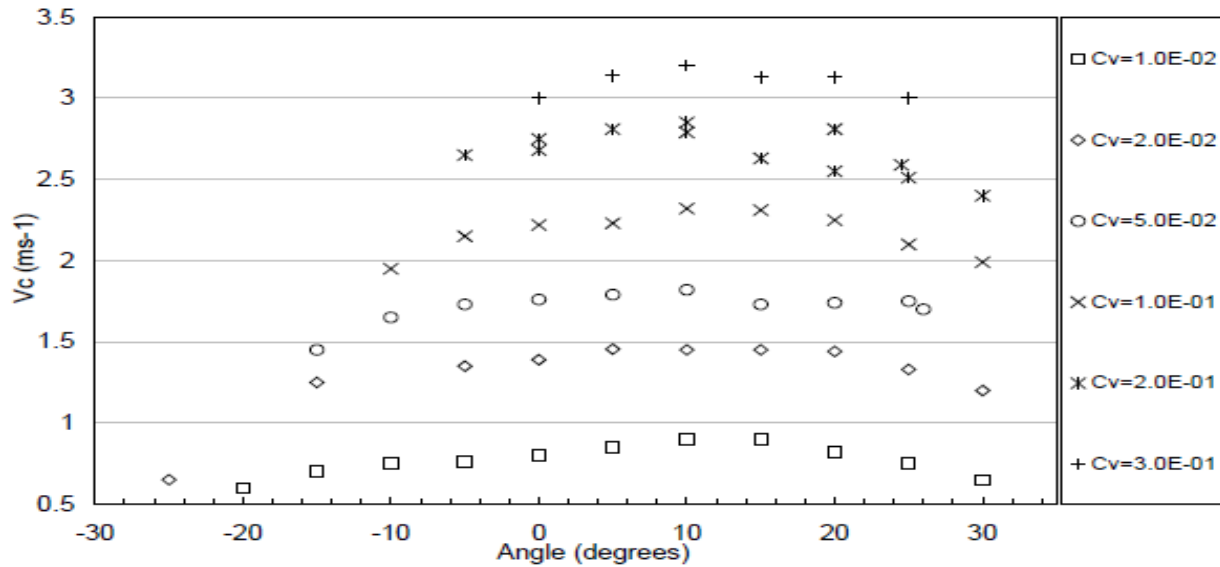


Figure 4.10 Critical Particle Transport Velocity Change with Inclination Angle (Roco, 1977)

Stevenson et al. (2001b, 2002) studied an inclination effect on the isolated sand particles in intermittent flow in a slightly inclined pipeline and stratified flow in a slightly declined pipeline. He noticed particles backward movement in the film section, although he stated that the sand transport velocity is not significantly dependent on the pipe inclination angle that he has investigated (up to 3 degrees). Jimaa (2013) simulated a real well geometry to determine the well inclination angle effect on critical particle transport velocity. The author reported that hole-cleaning issues increase as well inclination angle increases, stating that a higher flow rate is required for highly inclined wells.

Yan (2010) also conducted experimental work on the inclination angle effect. The author summarized that there is no clear difference in critical particle transport velocity comparing horizontal and inclined well sections. Yan (2010) reported that sand concentration used in experimental work was very low, so this may be a reason why there is no difference in critical

particle transport velocity values. Yan (2010) found that sand transportation is strongly dependent on the flow regime.

Sand particle transportation is strongly dependent on flow pattern, because, with the change in inclination angle, the flow pattern changes are very significant, which causes more complexity in sand particle transportation modeling.

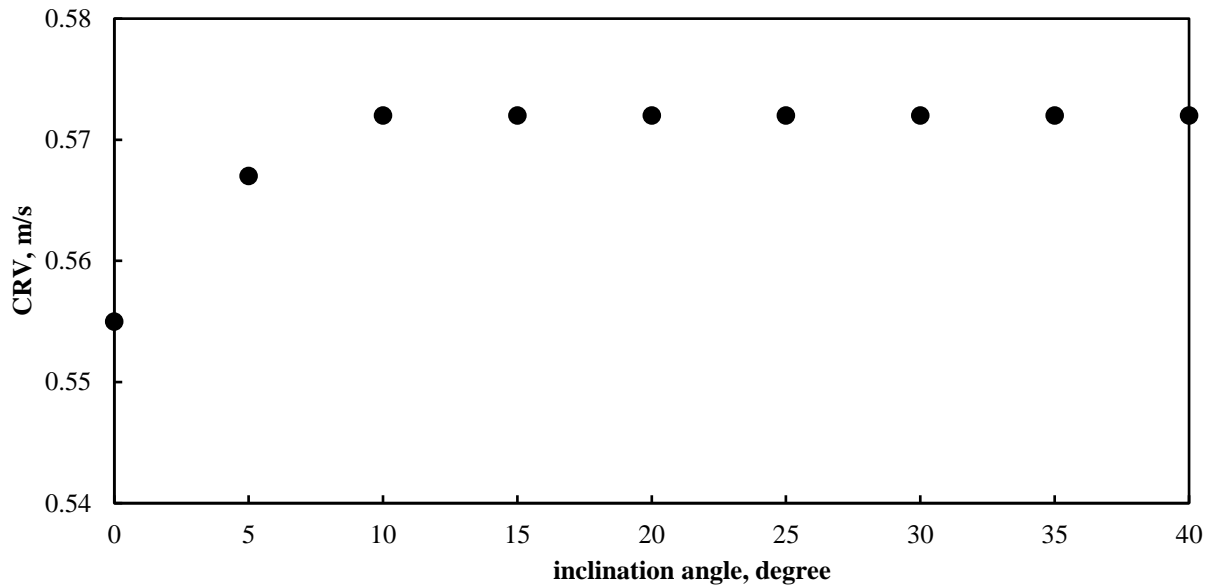


Figure 4.11 CRV versus Inclination Angle

The CRV model is selected for the Dispersed Bubble, Bubbly, and slug section of Slug flow patterns. As shown in Figure 4.11, there is a small increase in CRV value (from 0.555 m/s to 0.572 m/s) with the increase of inclination angle from 0 to 10 degrees, while changes at higher inclination angles are negligible.

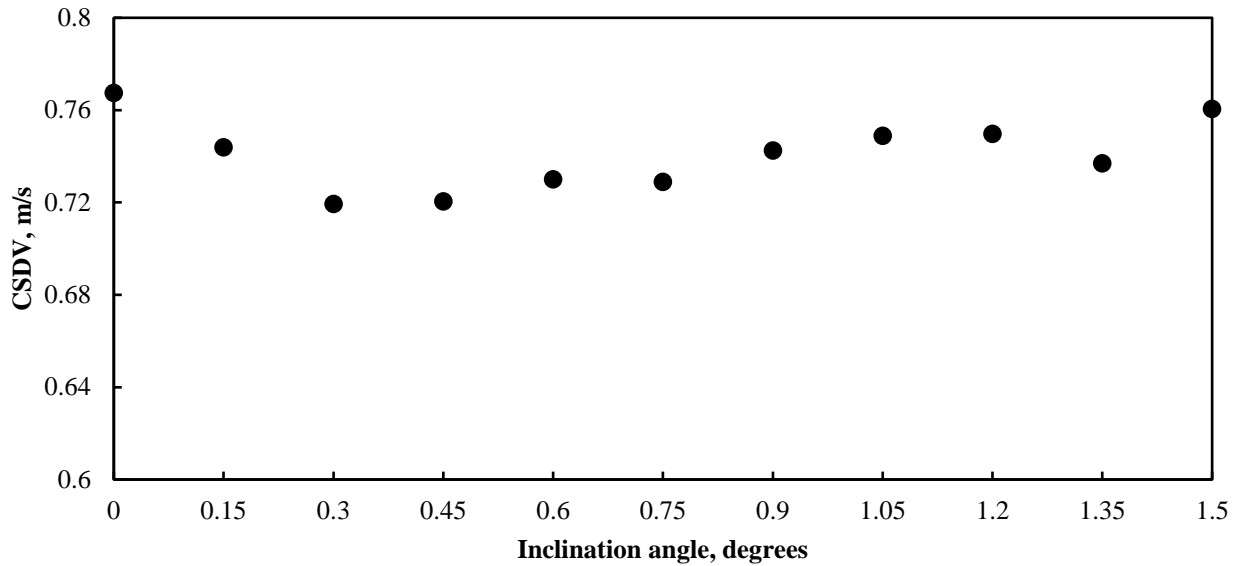


Figure 4.12 CSDV versus Inclination Angle

The CSDV model is only for the Stratified flow and film section of slug flow pattern. So, as it can be seen from Figure 4.12, the inclination angle range is very small. It is small because stratified flow can only exist in horizontal and near-horizontal sections of the well. An impact of inclination angle for the CSDV is not significant, the difference between the highest and lowest CSDV values is only 0.04 m/s.

Comparing the results of the CSDV and the CRV models with the experimental results by other abovementioned researchers, similar phenomena can be observed. Note that the results are only for specific input parameters. With different input parameters, the CRV and the CSDV results may differ.

4.1.4 Sand concentration effect on CSDV

Several investigations have been done to study sand concentration effect on particle transport velocity. Stevenson and Thorpe (1999) found that, generally, the concentration of sand

existing in the petroleum industry is between 5 lb/1000 bbl and 50 lb/1000 bbl. However, the concentration may increase up to 500 lb/1000 bbl during the well shutdown. Yan (2010) reported that critical particle transport velocity increases with the increase of sand concentration in horizontal pipes, claiming that more energy is required to keep sand particles moving with higher particle concentration. Najmi (2014) also experimentally confirmed that critical particle transport velocity tends to increase with the rise of sand concentration.

It is very important to correctly measure sand concentration before running the CSDV model. It is a parameter that may significantly affect the determination of Critical Sand Deposition Velocity. Typically, sand concentration in the production system is much lower than in drilling operation, so lower values are used in the example as an input in the CSDV model.

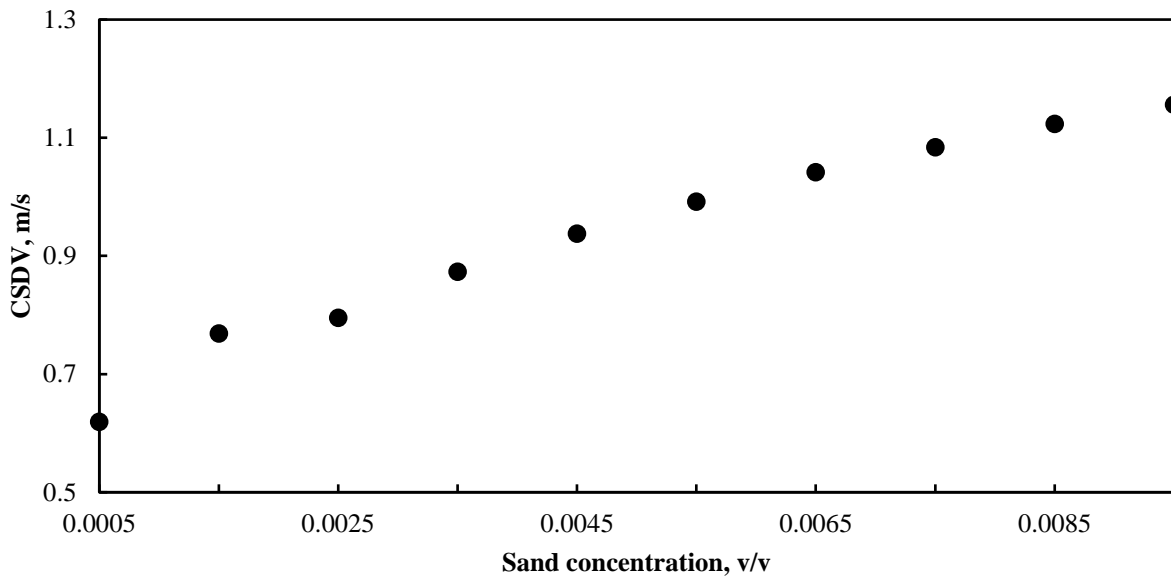


Figure 4.13 CSDV versus Sand Concentration

Figure 4.13 shows the effect of sand concentration on the CSDV. The sand concentration value used in the example is 0.00162 v/v. As can be seen from the figure, it increases

dramatically with the increase in concentration, which confirms that the influence is very significant.

4.1.5 Multiphase flow and gas parameters effect on CSDV

Multiphase flow with gas presence is very common in oil and gas industry. Previously, many researchers developed models to predict critical particle transport velocities in single-phase flow. Recently, many studies considered multiphase flow, but still more investigations are needed to understand the impact of different flow patterns like stratified, slug, bubble, and annular on sand particle transportations.

Gillies et al. (1997) reported that air or gas injection could increase particle transport rate if the liquid flow is turbulent. Angelsen et al. (1989) stated the same and agreed with other researchers that a higher gas flow rate may help in transporting particles. King et al. (2000) investigated particle transport with low and high gas superficial velocities and developed a model, where he concluded that his model works well with low superficial gas flow rates, but does not give accurate results when the flow rate is high. All researchers agree that liquid flow rate is dominant in particle transport, although gas flow rate also has a considerable impact.

Gas parameters as gas viscosity and gas density are also important factors, which need to be taken into consideration. Changing the superficial gas flow rate in the CSDV model will change liquid holdup, which significantly affects CSDV value. In addition to the liquid holdup, an increase or decrease in gas flow rate will change the flow pattern. As a result, different flow behaviors and critical transport velocities will be obtained. Figures 4.14 and 4.15 show the CSDV changes with both gas viscosity and density.

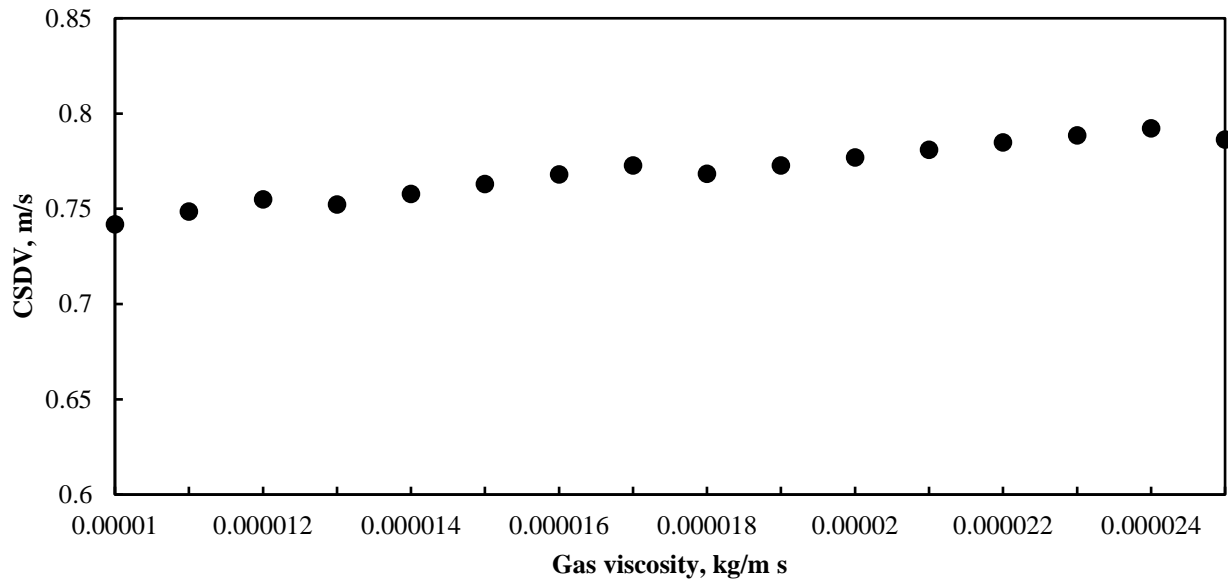


Figure 4.14 CSDV versus Gas Viscosity

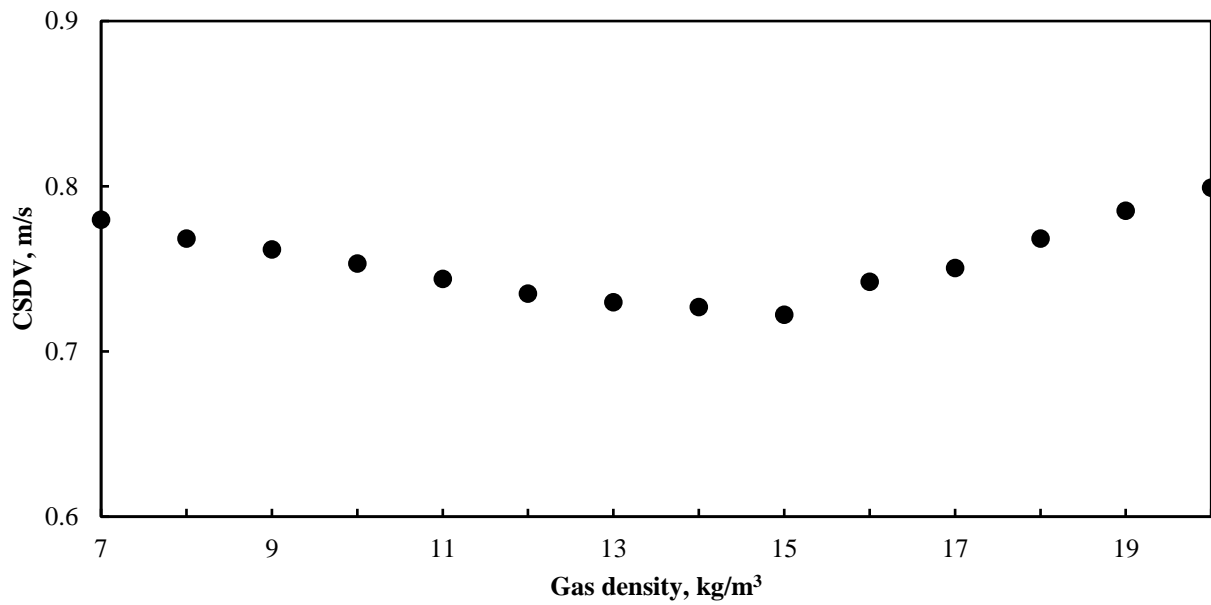


Figure 4.15 CSDV versus Gas Density

4.1.6 Sphericity effect on CRV and CSDV

Having an ideally spherical particle in oil and gas production is almost impossible. The sphericity of the particle has an impact on the drag coefficient. The drag coefficients of spherical and non-spherical particles are different. As it was explained in the previous chapter, the CRV and the CSDV models cover drag coefficient and drag force calculations. Therefore, sphericity influences the CRV and the CSDV calculation. Friction between particles is less for more spherical particles, whereas friction is more for less spherical particles. Figures 4.16 and 4.17 show CRV and CSDV decrease with the increase of sphericity, meaning that it is easier to transport more spherical particles.

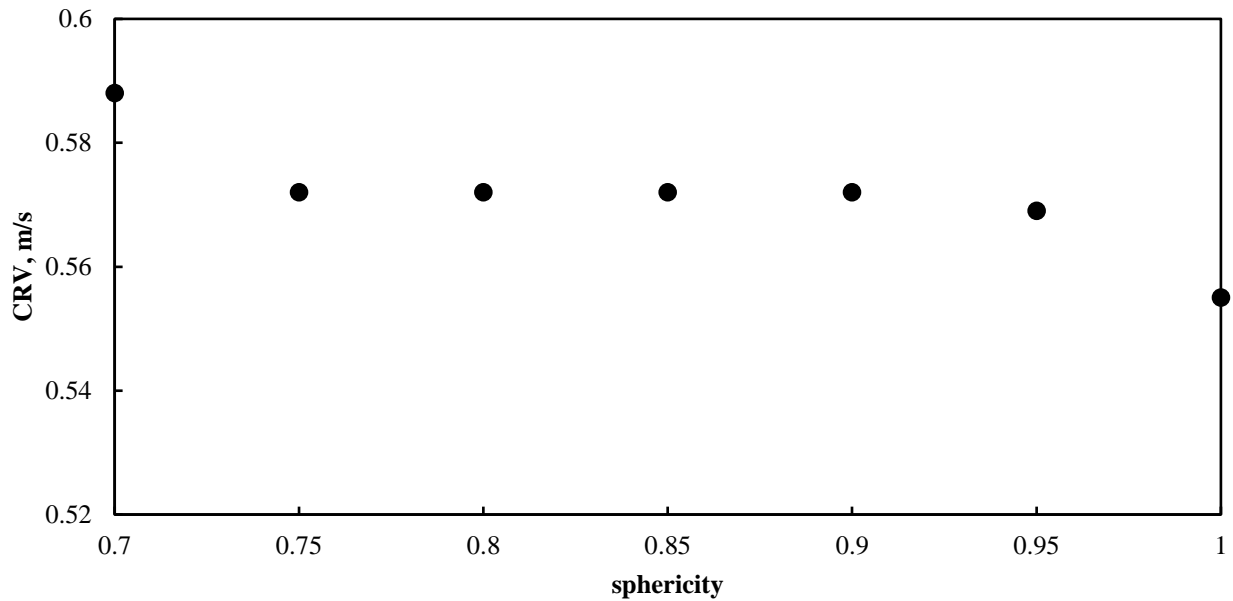


Figure 4.16 CRV versus Sphericity

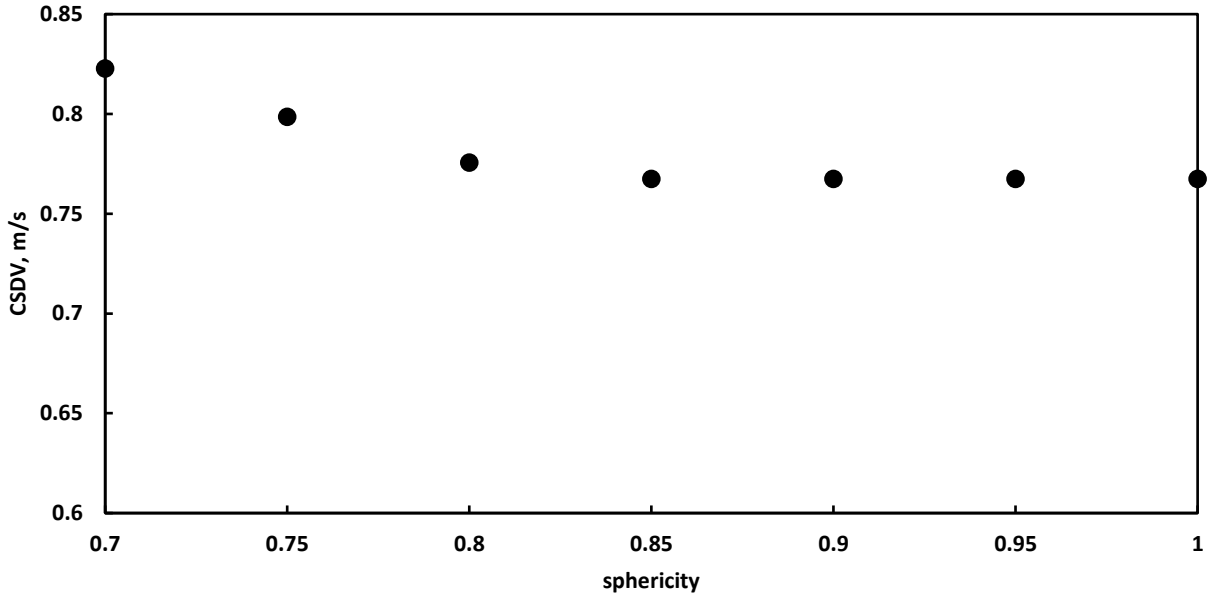


Figure 4.17 CSDV versus Sphericity

4.1.7 Pipe diameter, liquid density, and particle density effect on CRV and CSDV

In literature, it is common to see the statements that critical particle transport velocity increases with the increase in pipe diameter. Durand and Condolios (1953), Spells (1955), Hughmark (1961), and Condolios and Chapus (1963) experimentally confirmed this statement. According to Yan (2010), the shear induced drag and lift force acting on a sand particle is less for the larger pipe at the same liquid velocity. The impact of pipe diameter on CRV can be seen from the Figure 4.18.

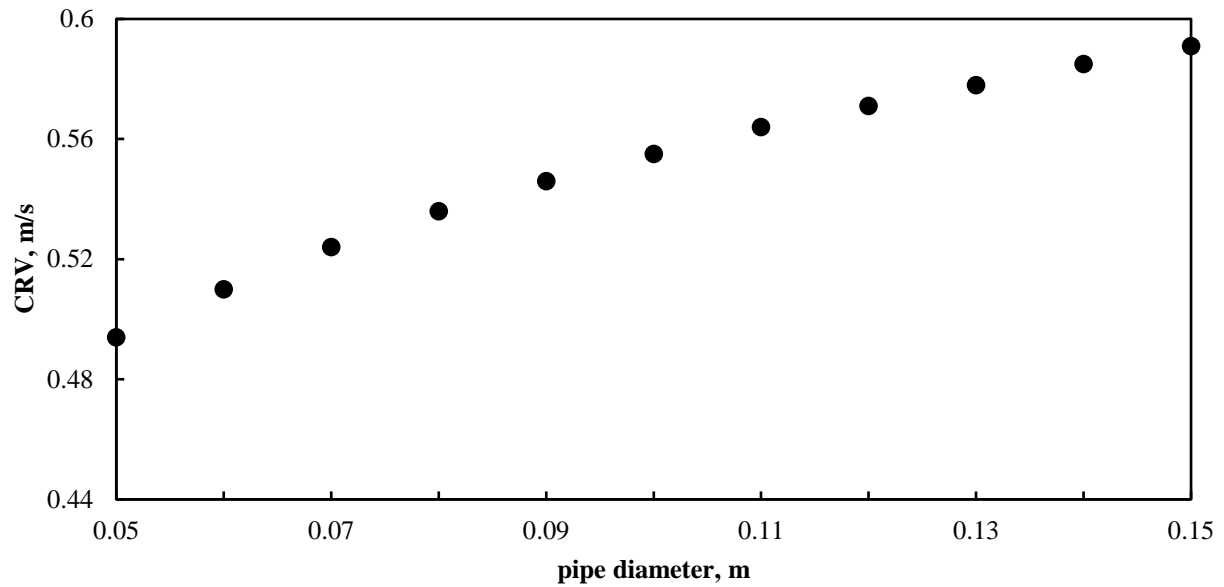


Figure 4.18 CRV versus Pipe Diameter

Another two parameters that impact particle transport are liquid and particle densities. This study presents that with the increase of liquid density, both CRV and CSDV decreases, and with the increase of particle density both CRV and CSDV increase (Figures 4.19, 4.20, and 4.21).

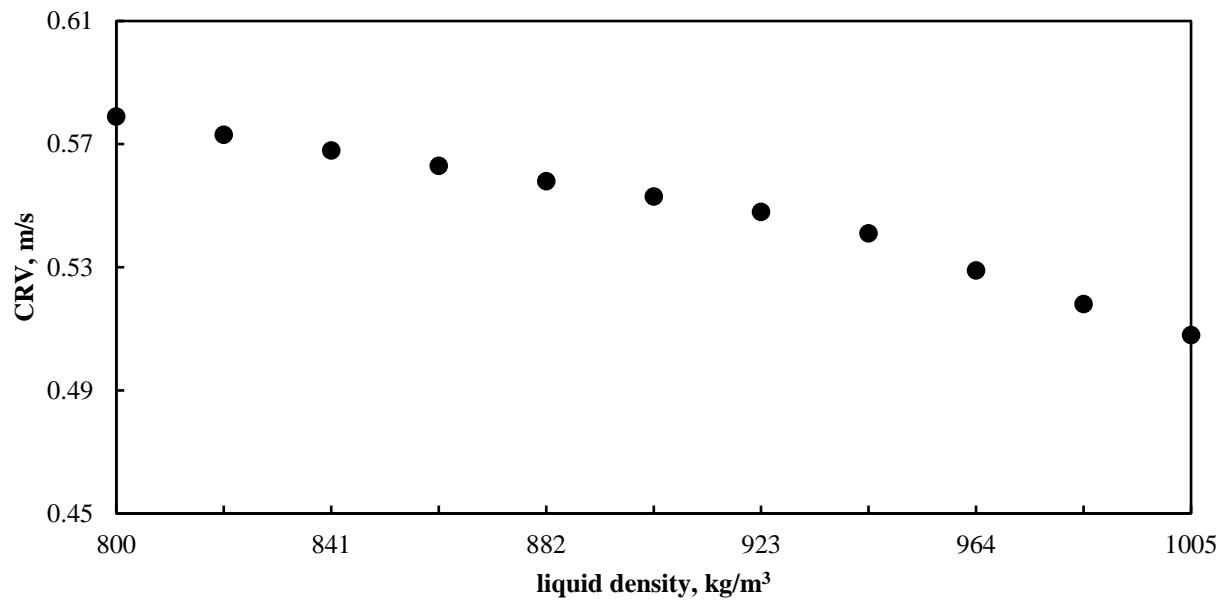


Figure 4.19 CRV versus Liquid Density

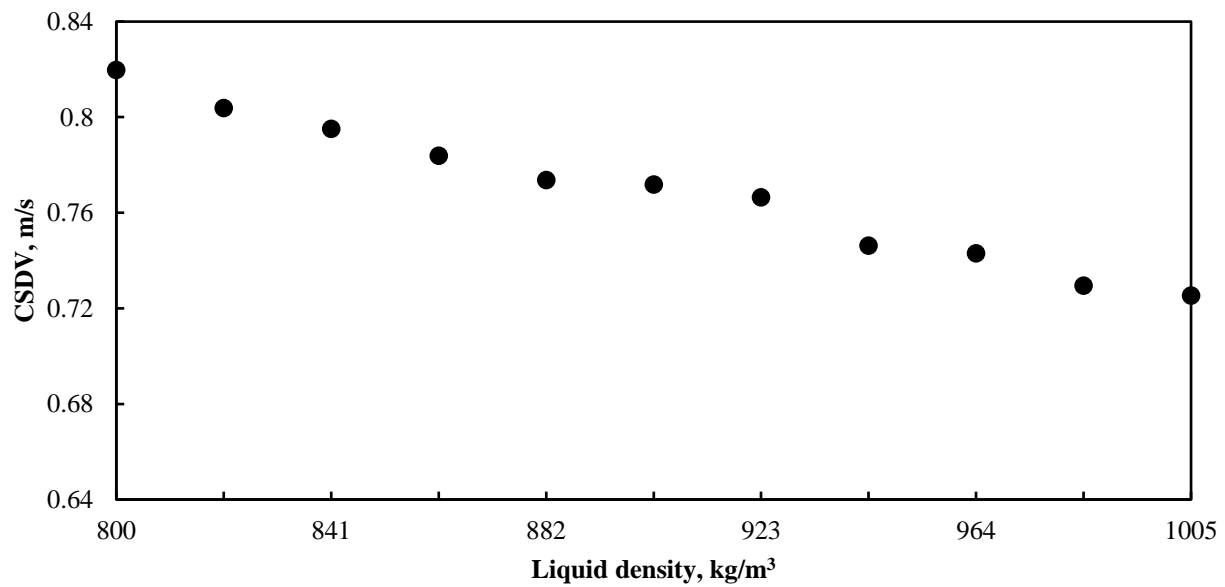


Figure 4.20 CSDV versus Liquid Density

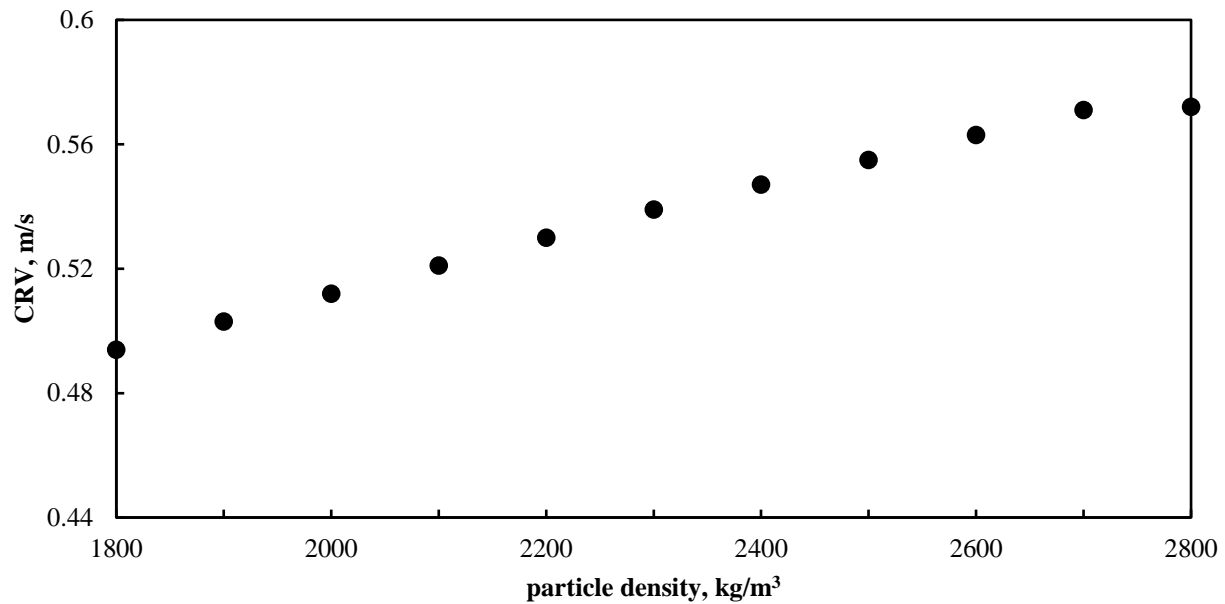


Figure 4.21 CRV versus Particle Density

4.1.8 Conclusions of all variables effect on CRV and CSDV

Looking at Figure 4.22, it can be concluded that sand particle size, angle of repose, and fluid type have the maximum effects on CRV. Inclination angle and sphericity show the lowest effect.

Then, looking at Figure 4.23, it can be concluded that fluid type, sand concentration, and angle of repose have the maximum effects on CSDV, while inclination angle shows the minimum effect.

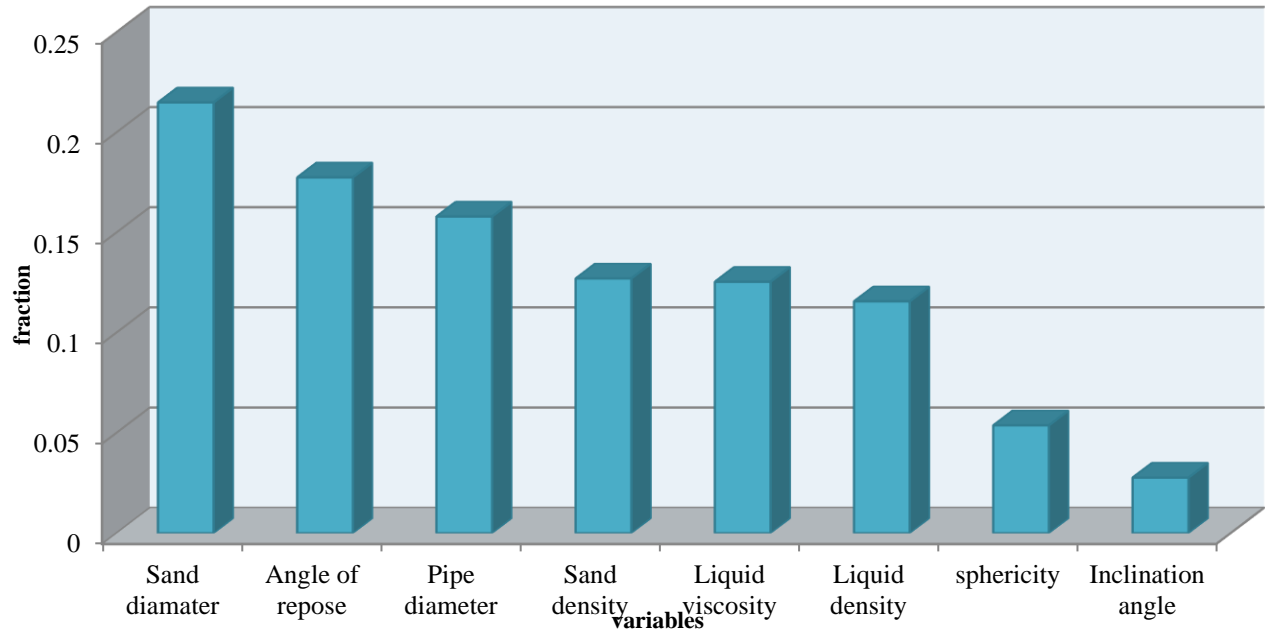


Figure 4.22 Impacts of Different Variables on CRV

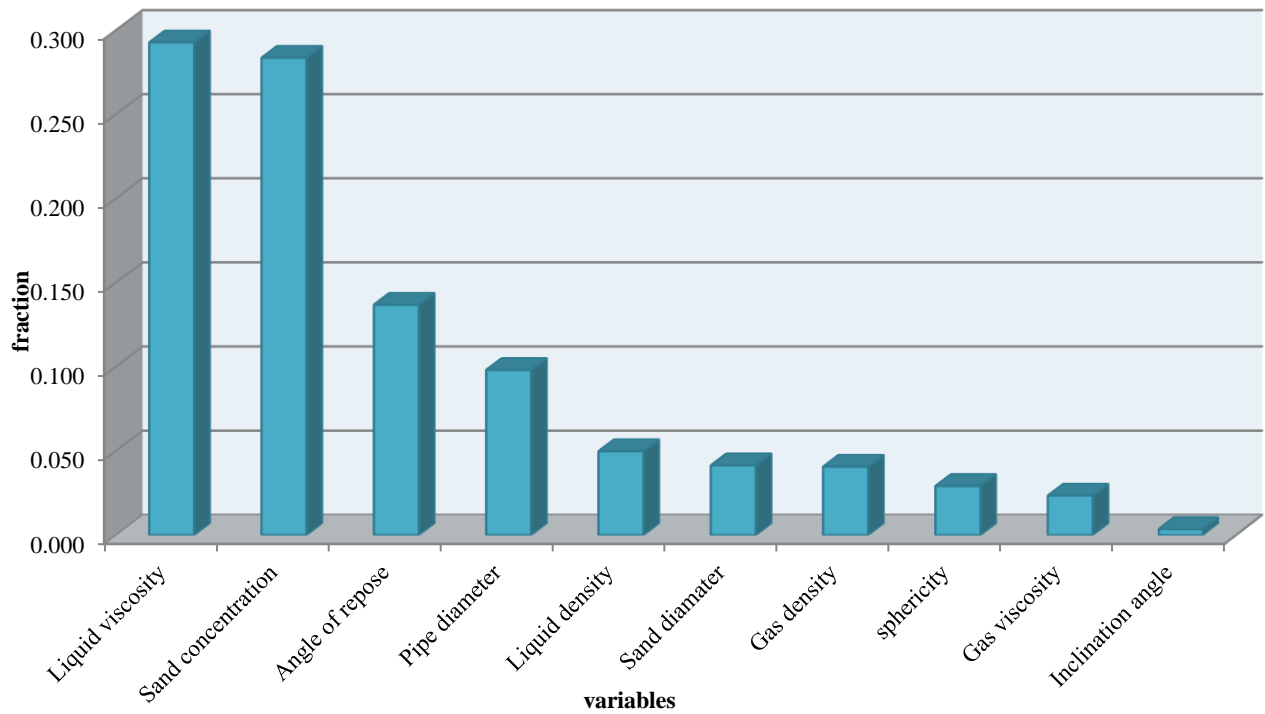


Figure 4.23 Impacts of Different Variables on CSDV

CHAPTER 5

FIELD CASE EXAMPLE

One real well case from an oilfield was taken as an example to check the CSDV model. Due to some unknown data from the oilfield, some assumptions are made for fluid, pipe, and flow pattern parameters. One of the main assumptions is stratified flow pattern and 0 inclination angle, or horizontal well. Particle distribution and types of the given well are shown in Figure 5.1. There is no gravel, very coarse, or coarse sand particles produced from the well with oil and gas. The maximum particle size from the well is 0.00025 m, which is medium-coarse sand, and the minimum particle size is 0.000001 m, which is clay. Particle types like Gravel, Sand, Silt, and Clay with the definitions are shown in Figure 5.2 and Table 5.1.

Table 5.2 presents more specific particle parameters of the well like particle types, particle sizes, and particle frequencies. It can be seen that silt particles occur more than others, with the frequency of 53.7%, then clay with 27.3%. It can be concluded that in this oil and gas production, the particle size range is wide. Much work is needed for researchers to create a mechanistic model for oil and gas production wells, considering all flow patterns, inclination angles, and model validation with experimental results.

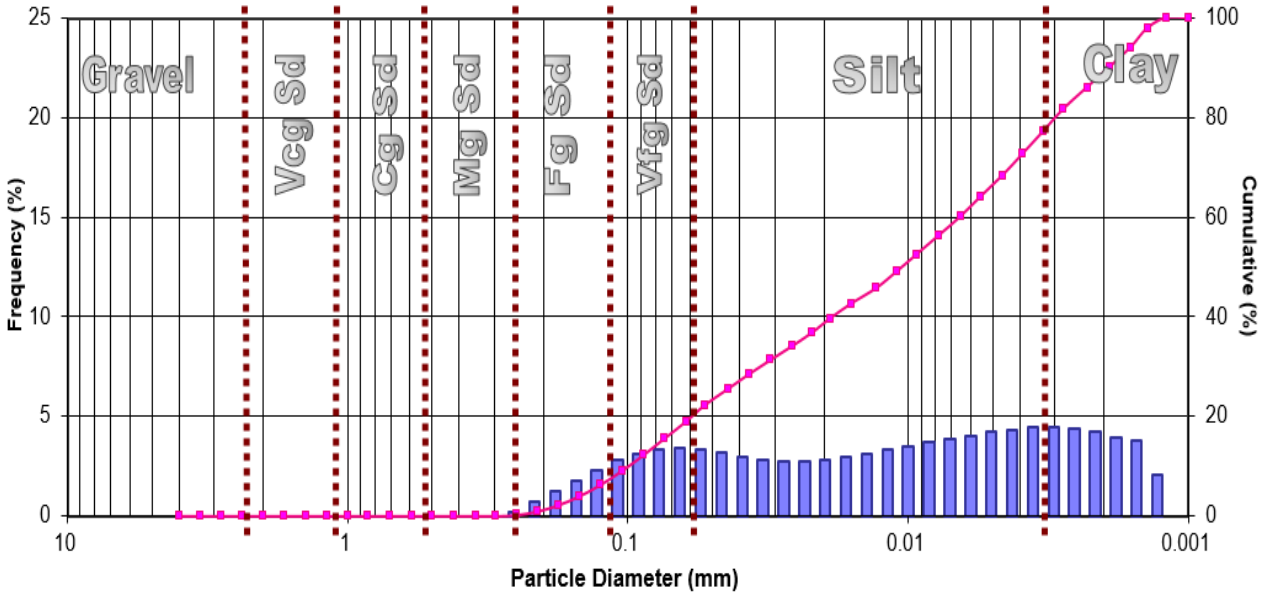


Figure 5.1 Particle Distribution and Types of the Well

Table 5.1 Field Particles Definitions

Field particle name	Field particle definition
Gravel	gravel
VcgSd	very coarse sand
CgSd	coarse sand
MgSd	medium sand
FgSd	fine sand
VfgSd	very fine sand
Silt	coarse silt
	medium silt
	fine silt
	very fine silt
Clay	clay

Table 5.2 Field Example Particle Data

Particle type	Particle size in mm	Particle size in m	Frequency of particles	Frequency of particle types	Cumulative
GRAVEL	4.0000	0.004	0.0	0.0	0.0
	3.3600	0.00336	0.0		0.0

		2.8300	0.00283	0.0		0.0
		2.3800	0.00238	0.0		0.0
		2.0000	0.00200	0.0		0.0
	VCRS SD	1.6800	0.00168	0.0	0.0	0.0
		1.4100	0.00141	0.0		0.0
		1.1900	0.00119	0.0		0.0
		1.0000	0.00100	0.0		0.0
	CRS SD	0.8500	0.00085	0.0	0.0	0.0
		0.7100	0.00071	0.0		0.0
		0.6000	0.00060	0.0		0.0
		0.5000	0.00050	0.0		0.0
	MED	0.4200	0.00042	0.0	0.2	0.0
		0.3500	0.00035	0.0		0.0
		0.2970	0.00030	0.0		0.0
		0.2500	0.00025	0.2		0.2
	FINE	0.2100	0.00021	0.7	6.1	0.9
		0.1770	0.000177	1.3		2.2
		0.1490	0.000149	1.8		4.0
		0.1250	0.000125	2.3		6.3
	VFINE	0.1050	0.000105	2.8	12.7	9.1
		0.0880	0.000088	3.1		12.2
		0.0740	0.000074	3.4		15.6
		0.0620	0.000062	3.4		19.0
Silt	CRS	0.0530	0.000053	3.3	12.3	22.3
		0.0440	0.000044	3.2		25.5
		0.0370	0.000037	3.0		28.5
		0.0310	0.000031	2.8		31.3
	MED	0.0260	0.000026	2.8	11.3	34.1
		0.0220	0.000022	2.8		36.8
		0.0190	0.000019	2.8		39.7
		0.0160	0.000016	3.0		42.6
	FINE	0.0130	0.000013	3.1	13.6	45.7
		0.0110	0.000011	3.3		49.1
		0.0093	0.0000093	3.5		52.6
		0.0078	0.0000078	3.7		56.3
	VFINE	0.0065	0.0000065	3.9	16.5	60.1
		0.0055	0.0000055	4.0		64.2
		0.0046	0.0000046	4.2		68.4
		0.0039	0.0000039	4.3		72.7
CLAY	0.0033	0.0000033	4.4	27.3	77.2	
	0.0028	0.0000028	4.5		81.6	
	0.0023	0.0000023	4.4		86.0	
	0.0019	0.0000019	4.2		90.2	
	0.0016	0.0000016	3.9		94.2	
	0.0014	0.0000014	3.8		97.9	
	0.0012	0.0000012	2.1		100.0	
	0.0010	0.0000010	0.0		100.0	

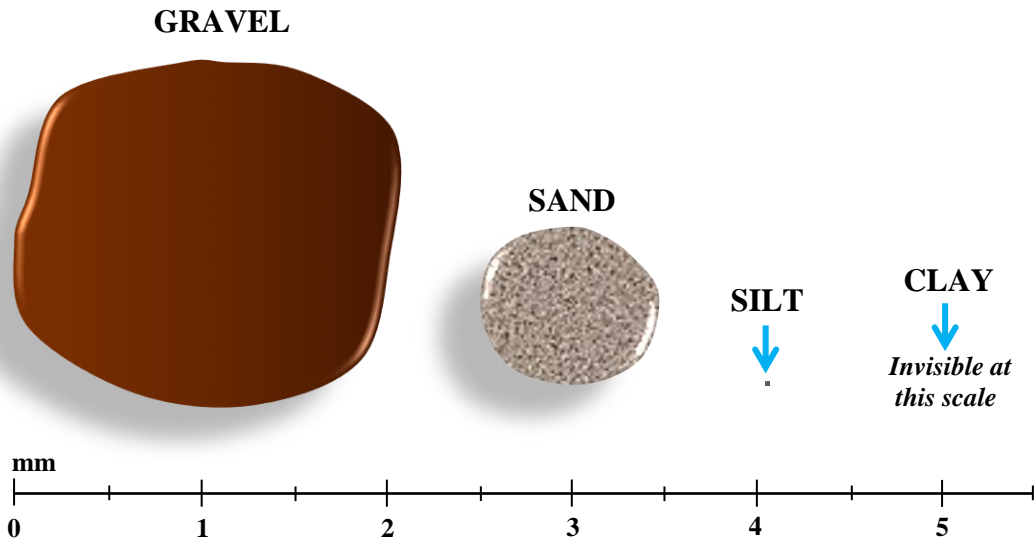


Figure 5.2 Particle Types

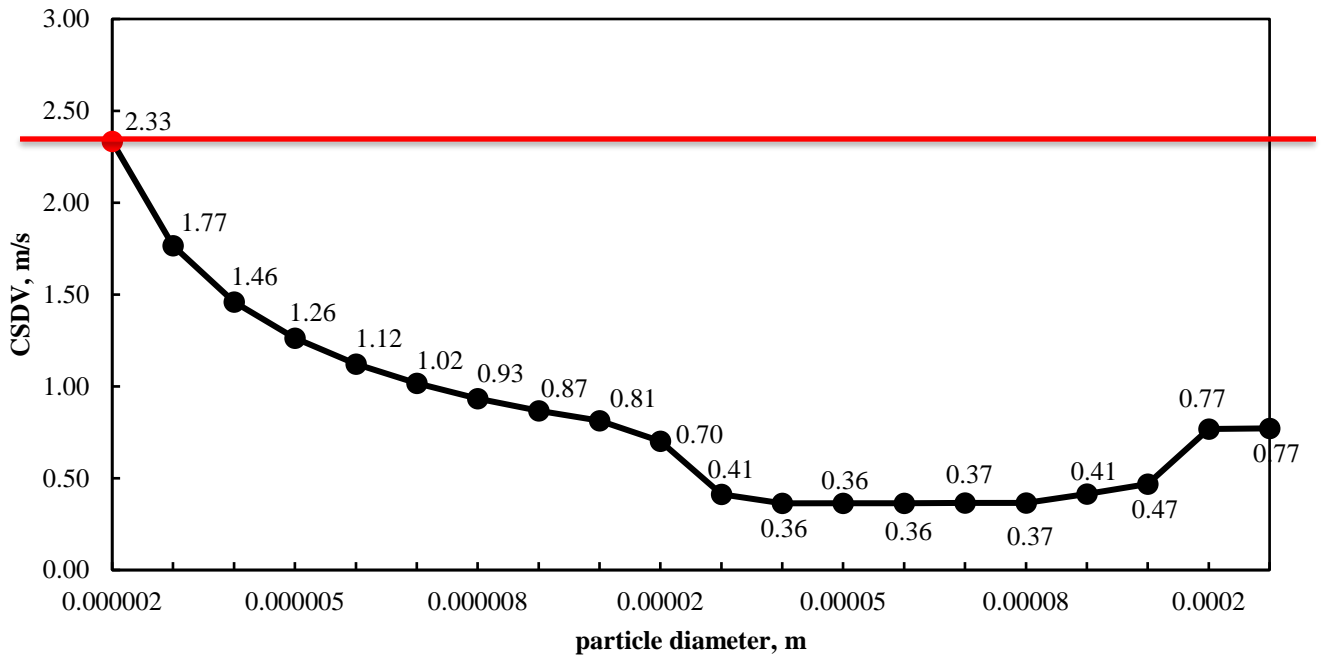


Figure 5.3 CSDV versus Particle Diameter

Figure 5.3 shows the result of the CSDV model. It can be identified that minimum particles require the highest CSDV value to be transported to the surface, while fine, very fine,

and coarse particles require the least CSDV value. Critical Sand Deposition Velocity needed to transport all the particles to the surface is 2.33 m/s. As it was explained before, due to the van der Waals force, the smallest particles require the highest critical particle transportation velocity, because the smallest particles tend to bind together and resist rearrangement, and the volumetric concentration of smaller particles is higher compared to the larger ones. However, it is a very complicated case, because there is almost no work done for the smallest particles, like clay, for the production system including the study of all fluid flow patterns and inclination angles.

CHAPTER 6

CONCLUSIONS AND RECOMMENDATIONS

6.1 Conclusions

The main goal of the study is to find critical sand particle transport fluid velocity in wells under different multiphase flow conditions (different flow patterns and inclination angles) to apply in oil and gas production and transportation systems. Two mechanistic and three empirical models are selected and modified to get improved predictions. To cover all inclination angles, flow patterns, and to get liquid holdup, and all other required variables, Zhang et al. (2003) unified gas-liquid pipe flow model is applied and combined with the abovementioned models.

- 1) The first mechanistic model is the Critical Resuspension Velocity (CRV) model, developed by Duan (2005). Modifications are made to use the model for oil and gas production and transportation systems. The most important variable effect on the CRV model is investigated and compared to the previous models and experiments, and very good matches and behaviors are obtained. It is observed that sand particle size, angle of repose, and fluid type have the maximum effects on CRV, while inclination angle and sphericity show the lowest effect. The CRV model is best for Dispersed Bubble (D-B), Bubbly (BUB), and slug section of Slug flow patterns. The model is applicable for all inclination angles except vertical, near-vertical, and downward sections.
- 2) The second mechanistic model is the Critical Sand Deposition Velocity (CSDV) model, developed by Dabirian (2016). The CSDV model is modified by applying Zhang et al. (2003) unified gas-liquid pipe flow model, mean bed roughness, average bed shear stress,

fluid behavior index, particle sphericity, and by changing near-bed velocity profile, friction factor, particle characteristic area, particle Reynolds number calculation equations. These changes allow users to consider more important variables and acquire more accurate results. The most important variable effect on the CSDV model is investigated and compared with the previous models and experiments. It is observed that fluid type, sand concentration, and angle of repose have the maximum effects on CSDV, while the inclination angle shows the minimum effect. The CSDV model is best for Stratified flow, and the film section of Slug flow. When the flow pattern is Stratified, the model is only applicable for horizontal and near-horizontal sections. However, when the flow pattern is Slug, including horizontal section, the model can also be applicable to even higher inclination angles, with the condition at which Slug flow pattern kept the same as for horizontal section.

- 3) The first empirical model is the Critical Gas Core Velocity model developed by Ibarra (2017). The model is modified by applying Zhang et al. (2003) unified gas-liquid pipe flow model to calculate liquid holdup, flow pattern, and gas core velocity. The model is applicable for the gas core of Annular flow pattern in horizontal and near-horizontal sections.
- 4) The second empirical model is the Minimum Particle Pickup Gas Velocity model, which consists of two different models, one is Cabrejos and Klinzing (1994), and the second is Hayden (2003). Two different models are combined in one to cover more input variables and to extend the range of output data. The model can be applied for gas production wells. Zhang et al. (2003) unified gas-liquid pipe flow model is applied in case of significant liquid phase presence. Otherwise, the liquid holdup is assumed as 0.

- 5) The third empirical model is the Settling Velocity model developed by Chien (1994). The model can be applicable for Dispersed Bubble (D-B) and Bubbly (BUB) flow patterns assuming liquid holdup is 1. The model is only applicable to vertical wells.

A field case example is investigated, proving that the models can be used to determine critical transport particle velocity with the parameters from the field.

6.2 Recommendations

Experimental studies are recommended because the sand particle transport mechanism in all flow patterns and inclination angles is insufficiently investigated. To be specific, only stratified flow pattern have been studied well. The following recommendations may require a facility that allows researchers to investigate all flow patterns, inclination angles, and phases (gas, oil, water, and sand).

- 1) Use more field case examples and experimental data to check the application of two mechanistic and three empirical models presented in Chapter 4.
- 2) Apply Zhang et al. (2006) unified gas-oil-water pipe flow model instead of Zhang et al. (2003) unified gas-liquid pipe flow model. Consider oil and water separately.
- 3) Mechanistic and empirical models are coded in Python programming language. The code in Python can be improved and full computer tool to predict critical particle transport velocity can be developed.
- 4) Conduct an experimental study to check the validity of two mechanistic and three empirical models presented in Chapter 4. Investigate particle transport mechanism of each flow pattern in all inclination angles. If required, modify the models.

- 5) Conduct experimental study and develop a mechanistic model for all flow patterns (Bubbly, Slug, Churn, Annular, Dispersed Bubble) in a vertical well.
- 6) Conduct experimental study to observe the particle transport mechanism in annular flow pattern. Develop a mechanistic or empirical model to find the critical particle transport liquid film velocity of the annular flow pattern in all inclination angles. However, it is important to note that another major issue, which is erosion, may appear. Erosion can be harmful to the facility.
- 7) During experiments, try to apply different fluid (viscosity and density) and sand particle (diameter, concentration, sphericity) parameters.
- 8) CFD simulations can be done for sand particle transport under each flow pattern to predict the critical particle transport velocity.

NOMENCLATURE

g	=	gravitational acceleration	m/s^2
π	=	ratio of the circumference of a circle to its diameter	-
D	=	pipe diameter	m
f_w	=	water fraction	-
μ_w	=	water dynamic viscosity	$\text{Pa}\cdot\text{s}$
μ_o	=	oil dynamic viscosity	$\text{Pa}\cdot\text{s}$
μ_L	=	liquid dynamic viscosity	$\text{Pa}\cdot\text{s}$
μ_g	=	gas dynamic viscosity	$\text{Pa}\cdot\text{s}$
ν	=	liquid kinematic viscosity	m^2/s
K	=	fluid-consistency index	$\text{Pa}\cdot\text{s}^n$
ρ_w	=	water density	kg/m^3
ρ_o	=	oil density	kg/m^3
ρ_L	=	liquid density	kg/m^3
ρ_g	=	gas density	kg/m^3
ρ_p	=	particle density	kg/m^3
n	=	fluid behavior index	-
ε	=	pipe roughness	m
d_p	=	particle diameter	m
y	=	distance from mean bed surface to the particle center	m
φ	=	particle sphericity	-
C_v	=	particle concentration	v/v
α	=	well inclination angle	degrees
β	=	angle of repose	degrees
V	=	average liquid velocity	m/s

V_{LF}	=	liquid film velocity	m/s
V_{SL}	=	superficial liquid velocity	m/s
V_{SG}	=	superficial gas velocity	m/s
V_m	=	mixture velocity	m/s
v_f	=	film velocity	m/s
v_s	=	slug velocity	m/s
ν_{gas}	=	gas kinematic viscosity	m ² /s
h	=	moving bed height	m
R	=	pipe radius	m
S_w	=	wetted perimeter of the well	m
S_b	=	wetted perimeter of a cutting bed	m
A_f	=	fluid flow area above a cutting bed	m ²
D_h	=	hydraulic diameter	m
Re	=	Reynolds number	-
H_L	=	liquid holdup	-
ε_{bed}	=	mean bed roughness	m
f_{bed}	=	bed friction factor	-
τ_{bed}	=	average bed shear stress	Pa
V_f	=	bed friction velocity	m/s
y^+	=	dimensionless distance from the mean bed surface	-
V_{LL}	=	local liquid velocity	m/s
$\frac{dV_{LL}}{dy}$	=	local liquid velocity gradient	-
V_{LL}^+	=	dimensionless local liquid velocity	-
Re_p	=	particle Reynolds number	-
η	=	dimensionless shear rate	-
C_D	=	drag coefficient	-
C_{DU}	=	drag coefficient in a uniform flow	-
C_L	=	lift coefficient	-

F_D	=	drag force	N
F_L	=	lift force	N
A_H	=	Hamaker constant	N·m
s	=	particle-separation distance	m
F_{VDW}	=	van der Waals force	N
F_{VDWR}	=	resultant van der Waals force	N
F_G	=	gravity force	N
F_B	=	buoyancy force	N
Γ	=	momentum rate applied to a particle on a cutting bed	N·m
A	=	pipe cross-sectional area	m ²
A_p	=	characteristic area of the particle	m ²
F_W	=	apparent weight force	N
δ	=	viscous sublayer thickness	m
V_{set}	=	settling velocity	m/s
F_T	=	turbulent force	N
$\frac{y_{MB}}{d_p}$	=	dimensionless moving bed height	-
N	=	dimensionless weight of the analyzed particle and other particles on top of the moving bed layer	-
T	=	torque balance for stationary bed	-
V_{pu}	=	minimum particle pickup gas velocity	m/s
V_G	=	average gas velocity	m/s
$\Delta\rho$	=	difference between particle and liquid density	kg/m ³
V_{MC}	=	critical sand deposition mixture velocity	m/s
N_{Re}	=	modified Reynolds number incorporating gas density effect	-
V_{SGC}	=	critical superficial gas velocity	m/s
V_{gc}	=	critical gas core velocity	m/s
V_{GCV}	=	gas core velocity	m/s
V_D	=	critical deposition velocity	m/s

s_d	=	ratio of solid density to liquid density	-
F_1	=	empirical term accounts for particle size and concentration	-
V_c	=	critical velocity	m/s
u_t	=	particle settling velocity in mixture flow	m/s

BIBLIOGRAPHY

1. Almutahar, F.M. (2006). “Modeling of Critical Deposition Velocity of Sand in Horizontal and Inclined Pipes”. M.S. thesis. The University of Tulsa.
2. Angelsen, S., Kvernfold, O., Lingelem, M., and Olsen, S. (1989). “Long Distance Transport of Unprocessed HC Sand Settling in Multi-Phase Flow Lines”. Proceedings of the 4th International Conference on Multi-Phase Flow, paper D22, BHRA.
3. Barnea, D. (1987). “A Unified Model for Predicting Flow-Pattern Transition for the Whole Range of Pipe Inclinations”. International Journal of Multiphase Flow. Vol. 13, No. 1, pp. 1-12. [https://doi.org/10.1016/0301-9322\(87\)90002-4](https://doi.org/10.1016/0301-9322(87)90002-4).
4. Cabrejos, F.J. and Klinzing, G.E. (1994). “Pickup and Saltation Mechanisms of Solid Particles in Horizontal Pneumatic Transport”. Powder Technology, Vol. 79, No.2, pp. 173-186. [https://doi.org/10.1016/0032-5910\(94\)02815-X](https://doi.org/10.1016/0032-5910(94)02815-X).
5. Chien, S. (1994). “Settling Velocity of Irregularly Shaped Particles”. SPE Drilling and Completion 9 (04): 281-289. SPE-26121-PA. <https://doi.org/10.2118/26121-PA>.
6. Chisholm, D. (1967). “A Theoretical Basis for the Lockhart-Martinelly Correlation for Two-Phase Flow”. International Journal of Heat and Mass Transfer, Vol. 10, No. 12, pp. 1767-1778. [https://doi.org/10.1016/0017-9310\(67\)90047-6](https://doi.org/10.1016/0017-9310(67)90047-6).
7. Condolios, E. and Chapus, E.E. (1963). “Designing Solids Handling Pipelines”. McGraw-Hill, Incorporated. Vol. 70, No. 14, pp. 131-138.
8. Condolios, E. and Chapus, E.E. (1963). “Operating Solids Pipelines”. McGraw-Hill, Incorporated. Vol. 70, No. 15, pp. 145-150.

9. Condolios, E. and Chapus, E.E. (1963). "Transporting Solid Materials in Pipelines". McGraw-Hill, Incorporated. Vol. 70, No. 13, pp. 93-98.
10. Dabirian, R. (2016). "Modeling and Experimental Investigation of Sand in Gas-Liquid Stratified Flow". Ph. D. dissertation. The University of Tulsa.
11. Dabirian, R., Mohan, R.S., and Shoham, O. (2016). "Mechanistic Modeling of Critical Sand Deposition Velocity in Gas-Liquid Stratified Flow". Journal of Petroleum Science and Engineering, Vol. 156, pp. 721-731. <https://doi.org/10.1016/j.petrol.2017.06.006>.
12. Danielson, J. T. (2007). "Sand Transport Modeling in Multiphase Pipelines". Paper presented at the Offshore Technology Conference, Houston, Texas, U.S.A., April. OTC-18691-MS. <https://doi.org/10.4043/18691-MS>.
13. Davies, J.T. (1987). "Calculation of Critical Velocities to Maintain Solids in Suspension in Horizontal Pipes". Chemical Engineering Science, Vol. 42, No. 7, pp. 1667-1670. [https://doi.org/10.1016/0009-2509\(87\)80171-9](https://doi.org/10.1016/0009-2509(87)80171-9).
14. Duan, M. (2005). "An Experimental Study of Small Sand-Sized Cuttings Transport in Horizontal and High Angle Boreholes". M.S. thesis. The University of Tulsa.
15. Duan, M., Miska, S., Yu, M., Takach, N., and Ahmed, R. (2009). "Critical Conditions for Effective Sand-Sized-Solids Transport in Horizontal and High-Angle Wells". SPE Drilling and Completion 24 (02): 229-238. SPE-106707-PA. <https://doi.org/10.2118/106707-PA>.
16. Durand, R. (1953). "Basic Relationships of the Transport of Solids in Pipes Experimental Researches". Proceedings Minnesota International Hydraulics Convention, pp. 89-103.

17. Durand, R. and Condolios, E. (1952). "Experimental Investigation of the Transport of Solids in Pipes". *Deuxieme Journée de lhydraulique, Societé Hydrotechnique de France*. pp. 29-55.
18. Gillies, R.G., Mckibben, M.J., and Shook, C. (1997). "Pipeline Flow of Gas, Liquid, and Sand Mixture at Low Velocity". *Journal of Canadian Petroleum Technology*. PETSOC-97-09-03. <https://doi.org/10.2118/97-09-03>.
19. Gomez, L.E., Shoham, O., Schmidt, Z., Chokshi, R.N., Brown, A., and Northug, T. (1999). "A Unified Mechanistic Model for Steady-State Two-Phase Flow in Wellbores and Pipelines". Paper presented at the SPE Annual Technical Conference and Exhibition, Houston, Texas, October. SPE-56520-MS. <https://doi.org/10.2118/56520-MS>.
20. Graham, D.I. and Jones, T.E.R. (1994). "Settling and Transport of Spherical Particles in Power-Law Fluids at Finite Reynolds Number". *Journal of Non-Newtonian Fluid Mechanics*. Vol. 54, pp. 465-488. [https://doi.org/10.1016/0377-0257\(94\)80037-5](https://doi.org/10.1016/0377-0257(94)80037-5).
21. Hall, D. (1988). "Measurements of the Mean Force on a Particle near a Boundary in Turbulent Flow". *Journal of Fluid Mechanics*, Vol. 187, pp. 451-466. <https://doi.org/10.1017/S0022112088000515>.
22. Hayden, K.S., Park, K., and Curtis, J.S. (2003). "Effect of Particle Characteristics on Particle Pickup Velocity". *Powder Technology*, Vol. 131, No. 1, pp. 7-14. [https://doi.org/10.1016/S0032-5910\(02\)00135-3](https://doi.org/10.1016/S0032-5910(02)00135-3).
23. Hughmark, G.A. (1961). "Aqueous Transport of Settling Slurries". *Industrial and Engineering Chemistry*, Vol. 53, No. 5, pp. 389-390.

24. Ibarra, R., Mohan, and R.S., Shoham, O. (2014). “Critical Sand Deposition Velocity in Horizontal Stratified Flow”. Paper presented at the SPE International Symposium and Exhibition on Formation Damage Control, Lafayette, Louisiana, USA, February. SPE-168209-MS. <https://doi.org/10.2118/168209-MS>.
25. Ibarra, R., Mohan, R.S., and Shoham, O. (2017). “Investigation of Critical Sand-Deposition Velocity in Horizontal Gas/Liquid Stratified Flow”. SPE Production and Operations 32 (03):218-227. SPE-168209-PA. <https://doi.org/10.2118/168209-PA>.
26. Jimaa, G. (2013). “Cutting Transport Models and Parametric Studies in Vertical and Deviated Wells”. M.S. thesis. University of Stavanger.
27. Kallio, G.A. and Reeks, M.W. (1989). “A Numerical Simulation of Particle Deposition in Turbulent Boundary Layers”. International Journal of Multiphase Flow. Vol. 15, No. 3, pp. 433-446. [https://doi.org/10.1016/0301-9322\(89\)90012-8](https://doi.org/10.1016/0301-9322(89)90012-8).
28. Kalman, H., Satran, A., Meir, D., and Rabinovich, E. (2005). “Pickup (critical) Velocity of Particles”. Powder Technology, Vol. 160, pp. 103-113. <https://doi.org/10.1016/j.powtec.2005.08.009>.
29. Kaya, A.S. (1998). “Comprehensive Mechanistic Modeling of Two-Phase Flow in Deviated Wells”. M.S. thesis. The University of Tulsa.
30. King, M.J.S., Farhurst, C.P., and Hill, T.J. (2000). Solids Transport in Multiphase Flows-Application to High-Viscosity Systems”. Journal of Energy Resources Technology, 123(3): 200-204. <https://doi.org/10.1115/1.1385382>.
31. Kökpınar , M.A. and Göğüş, M. (2001). “Critical Flow Velocity in Slurry Transporting Horizontal Pipelines”. Journal of Hydraulic Engineering, Vol. 127, No. 9.

32. Kurose, B. and Komori, S. (1999). "Drag and Lift on a Rotating Sphere in a Linear Shear Flow". *Journal of Fluid Mechanics*, Vol. 384, pp. 183-206. <https://doi.org/10.1017/S0022112099004164>.
33. Najmi, K., McLaury, B.S., and Shirazi, S.A. (2014). "Experimental Study of Low Concentration Sand Transport in Low Liquid Loading Water-Air Flow in Horizontal Pipes". Paper presented at the 9th North American Conference on Multiphase Technology, Banff, Canada, June. BHR-2014-A2.
34. Najmi, K., McLaury, B.S., Shirazi, S.A., Hill, A.L., and Cremaschi, S. (2015). "A Generalized Model to Predict Minimum Particle Transport Velocities in Multiphase Air-Water Horizontal Pipes". *AIChE Journal*, Vol. 61, No. 8, pp. 2634-2646. <https://doi.org/10.1002/aic.14824>.
35. Oroskar, A.R. and Turian, R.M. (1980). "The Critical Velocity in Pipelines Flow of Slurries". *AIChE Journal*, Vol. 26, No. 4, pp. 550-558. <https://doi.org/10.1002/aic.690260405>.
36. Peden, J.M., Ford, J.T., and Oyeneyin, M.B. (1990). "Comprehensive Experimental Investigation of Drilled Cuttings Transport in Inclined Wells Including the Effect of Rotation and Eccentricity". Paper presented at the European Petroleum Conference, The Hague, Netherlands, October. SPE-20925-MS. <https://doi.org/10.2118/20925-MS>.
37. Reed, T.D. and Pilehvari, A.A. (1993). "A New Model for Laminar, Transitional, and Turbulent Flow of Drilling Muds". Paper presented at the SPE Production Operations Symposium, Oklahoma City, Oklahoma, March. SPE-25456-MS. <https://doi.org/10.2118/25456-MS>.

38. Roco, M.C. (1977). "Experimental Investigation of Critical Velocity in Pipelines for Hydrotransport". *St. Cerc. Mec. Appl.* 36: 111–112.
39. Saffman, P.G. (1965). "The Lift on Small Sphere in a Slow Shear Flow". *Journal of Fluid Mechanics*, 22 (2), pp. 385-400. ISSN 0022-1120. <https://doi.org/10.1017/s0022112065000824>.
40. Salama, M.M. (2000). "Sand Production Management". *Journal of Energy Resources Technology*, March, 122(1): 29-33. <https://doi.org/10.1115/1.483158>.
41. Schenkel, J.H. and Kitchener, J.A. (1960). "A Test of the Derjaguin-Verwey-Overbeek Theory with a Colloidal Suspension". *Transaction of the Faraday Society Journal*. Vol. 56. <https://doi.org/10.1039/TF9605600161>.
42. Schlichting, H. (1955). "Boundary Layer Theory". Translated by Kestin, J. McGraw-Hill New York.
43. Shoham, O. (2006). "Mechanistic Modeling of Gas-Liquid Two-Phase Flow in Pipes". Society of Petroleum Engineers. ISBN 978-1-55563-107-9.
44. Shook, C.A. and Roco, M.C. (1991). "Slurry Flow – Principles and Particle". Butterworth-Heinemann series in Chemical Engineering, pp. 116-118.
45. Spells, K.E. (1955). "Correlations for Use in Transport Aqueous Suspensions of Fine Solids through Pipes". *Chemical Engineering Research and Design Journal*, Vol. 33a, pp. 79-84.
46. Stevenson, P. and Thorpe, R.B. (1999). "Towards Understanding Sand Transport in Subsea Flowlines". *Proc. 9th Int. Conf. Multiphase Flow*, Cannes, France.

47. Stevenson, P. and Thorpe, R.B. (2002). "Velocity of Isolated Particles along a Pipe in Stratified Gas-Liquid Flow". *AIChE*, Vol. 48, No. 5, pp. 963-969. <https://doi.org/10.1002/aic.690480506>.
48. Stevenson, P., Thorpe, R.B., Kennedy, J.E., and McDermott, C. (2001b). "The Transport of Particles at Low Loading in Near-Horizontal Pipes by Intermittent Flow". *Chemical Engineering Science*, Vol. 56, No. 6, pp. 2149-2159. [https://doi.org/10.1016/S0009-2509\(00\)00491-7](https://doi.org/10.1016/S0009-2509(00)00491-7).
49. Tomren, P.H. (1979). "The Transport of Drilled Cuttings in an Inclined Eccentric Annulus". M.S. thesis. The University of Tulsa.
50. Turian, R.M., Hsu, F.-L., and Ma, T.-W. (1987). "Estimation of the Critical Velocity in Pipeline Flow of Slurries". *Powder Technology*, Vol. 51, No. 1, pp. 35-47. [https://doi.org/10.1016/0032-5910\(87\)80038-4](https://doi.org/10.1016/0032-5910(87)80038-4).
51. Walker, S. and Li, J. (2000). "The Effect of Particle Size, Fluid Rheology and Pipe Eccentricity on Cuttings Transport". Paper presented at the SPE/ICoTA Coiled Tubing Roundtable, Houston, Texas, April. SPE-60755-MS. <https://doi.org/10.2118/60755-MS>.
52. Wang, Q. and Squired, K.D. (1996). "Large Eddy Simulation of Particle Deposition in a Vertical Turbulent Channel Flow". *International Journal of Multiphase Flow*, Vol. 22, No. 4, pp. 667-683. [https://doi.org/10.1016/0301-9322\(96\)00007-9](https://doi.org/10.1016/0301-9322(96)00007-9).
53. Wicks, M. (1971). "Transport of Solids at Low Concentration in Horizontal Pipes". *Advances in Solid-Liquid Flow in pipes and its Application*. Pp. 101-124. <https://doi.org/10.1016/B978-0-08-015767-2.50010-7>.

54. Xiao, J.J., Shoham, O., and Brill, J.P. (1990). "A Comprehensive Mechanistic Model for Two-Phase Flow in Pipelines". Paper presented at the SPE Annual Technical Conference and Exhibition, New Orleans, Louisiana, September. SPE-20631-MS. <https://doi.org/10.2118/20631-MS>.
55. Yan, W. (2010). "Sand Transport in Multiphase Pipelines". Ph.D. thesis. Cranfield University.
56. Yu, A.B., Feng, C.L., Zou, R.P., and Yang, R.Y. (2003). "On the Relationship between Porosity and Interparticle Forces". Powder Technology, Vol. 130, No. 1-3, pp. 70-76. [https://doi.org/10.1016/S0032-5910\(02\)00228-0](https://doi.org/10.1016/S0032-5910(02)00228-0).
57. Zhang, F. (2015). "Numerical Simulation and Experimental Study of Cuttings Transport in Intermediate Inclined Wells". Ph. D. dissertation. The University of Tulsa.
58. Zhang, H.-Q. and Sarica, C. (2006). "Unified Modeling of Gas/Oil/Water-Pipe Flow- Basic Approaches and Preliminary Validation". Paper presented at the SPE Annual Technical Conference and Exhibition, Dallas, Texas, October. Projects, Facilities, and Construction. SPE-95749-MS. <https://doi.org/10.2118/95749-MS>.
59. Zhang, H.-Q., Wang, Q., Sarica, C., and Brill, J.P. (2003). "A unified Mechanistic Model for Slug Liquid Holdup and Transition between Slug and Dispersed Bubble Flows". International Journal of Multiphase Flow, Vol. 29, No. 1, pp. 97-107. [https://doi.org/10.1016/S0301-9322\(02\)00111-8](https://doi.org/10.1016/S0301-9322(02)00111-8).
60. Zhang, H.-Q., Wang, Q., Sarica, C., and Brill, J.P. (2003). "Unified Model for Gas-Liquid Pipe Flow via Slug Dynamics - Part 1: Model Development". Journal of Energy Resources Technology, 125 (4): 266-273. <https://doi.org/10.1115/1.1615246>.

61. Zhang, H.-Q., Wang, Q., Sarica, C., and Brill, J.P. (2003). “Unified Model for Gas-Liquid Pipe Flow via Slug Dynamics - Part 2: Model Validation”. *Journal of Energy Resources Technology*, 125 (4): pp. 274-283. <https://doi.org/10.1115/1.1615618>.
62. Zorgani, E., Al-Awadi, H., Yan, W., Al-lababid, S., Yeung, H., and Fairhurst, C.P. (2017). “Viscosity Effects on Sand Flow Regimes and Transport Velocity in Horizontal Pipelines”. *Experimental Thermal and Fluid Science*, Vol. 92, pp. 89-96. <https://doi.org/10.1016/j.expthermflusci.2017.08.024>.

APPENDIX A

ANGLE OF REPOSE CALCULATION

As it can be seen from Figures A.1, A.2, A.3, A.4, A.5, and A.6, three types of sand particle samples are taken to see the difference in angle of repose value between them. Figure A.1 and A.2 represent one particle sample, Figures A.3 and A.4 represent the second, and Figure A.5 and A.6 represent the last particle sample.

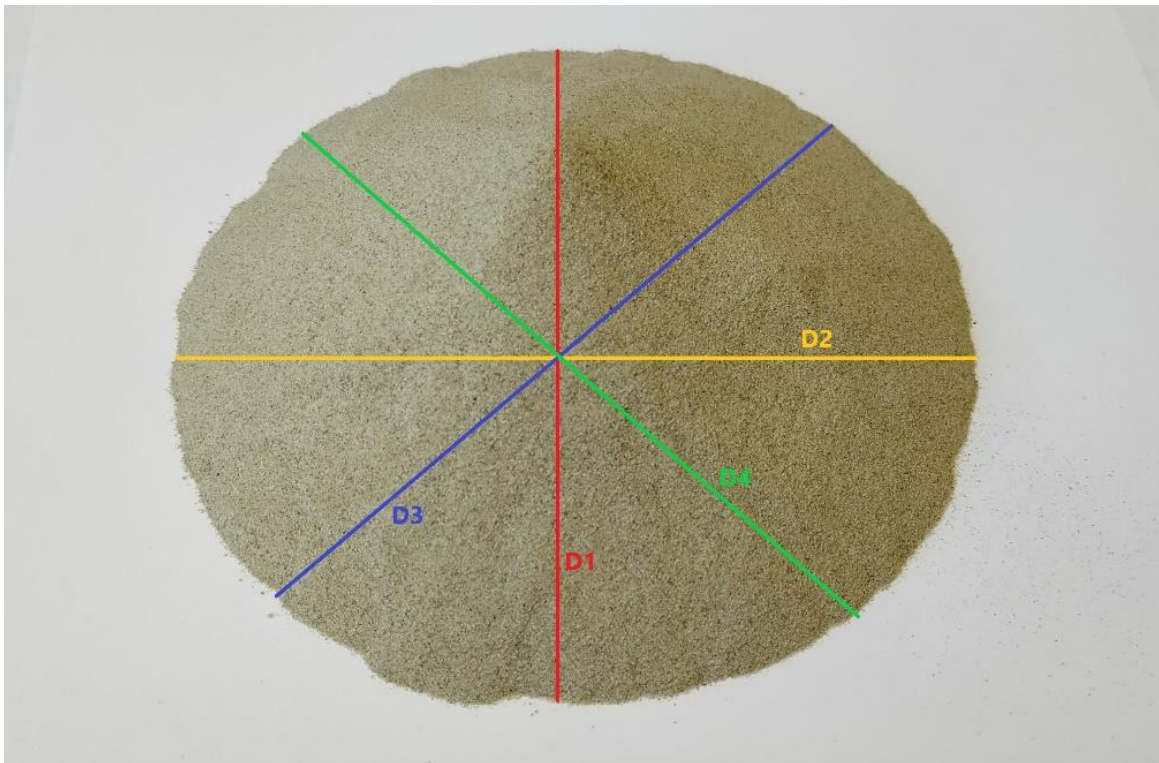


Figure A.1 Sample 1

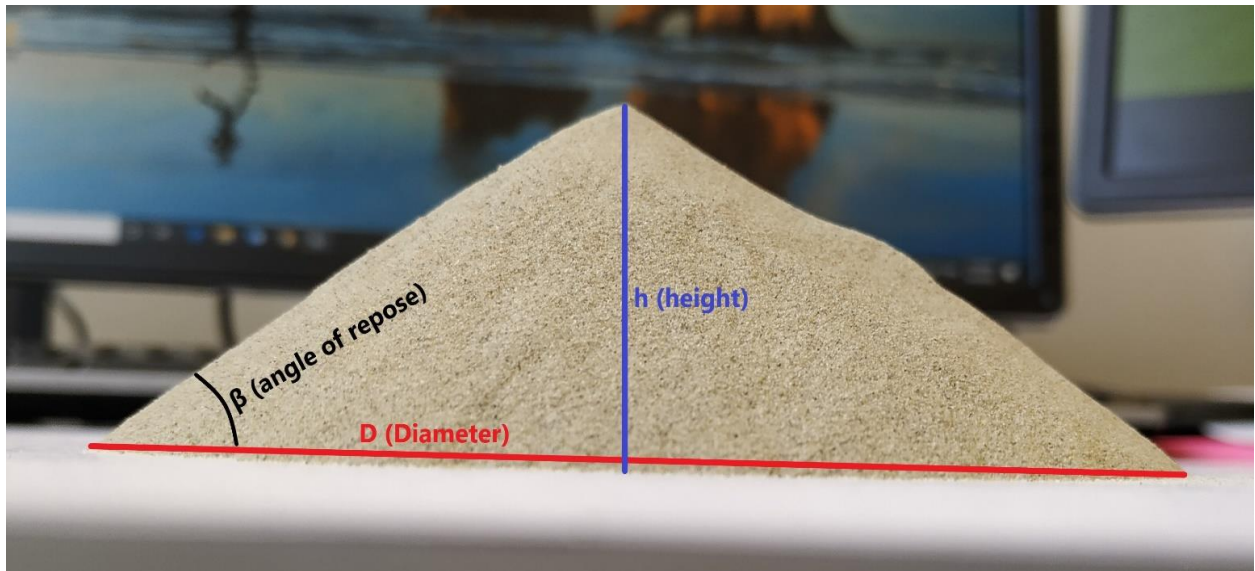


Figure A.2 Sample 1

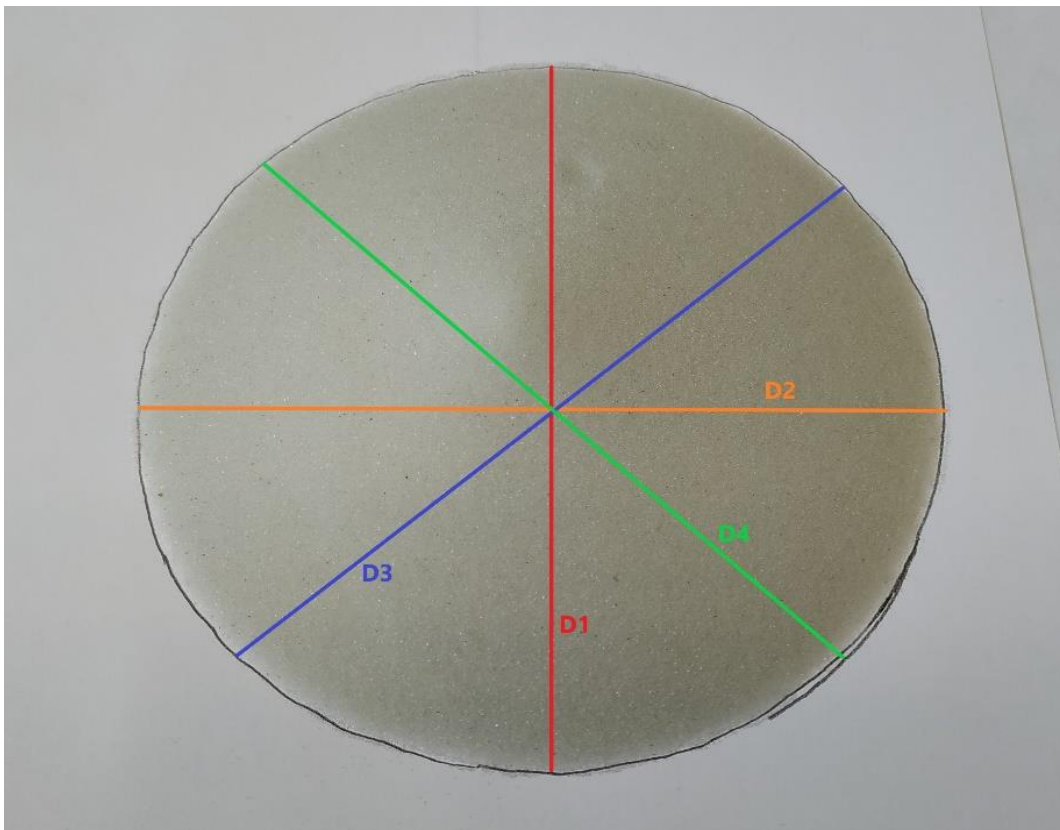


Figure A.3 Sample 2

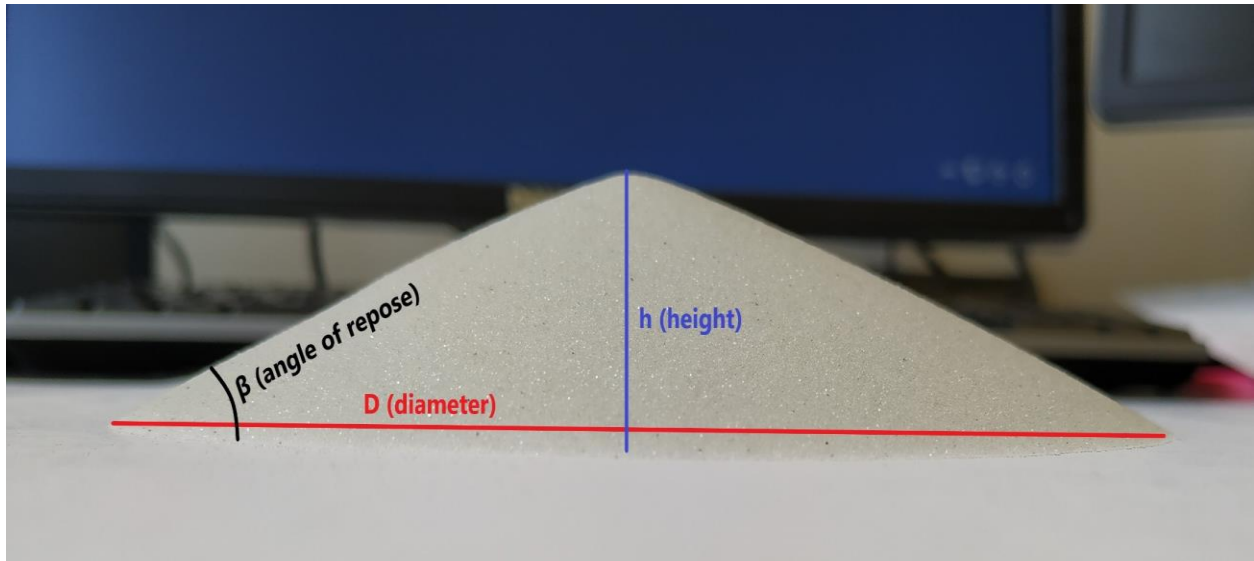


Figure A.4 Sample 2

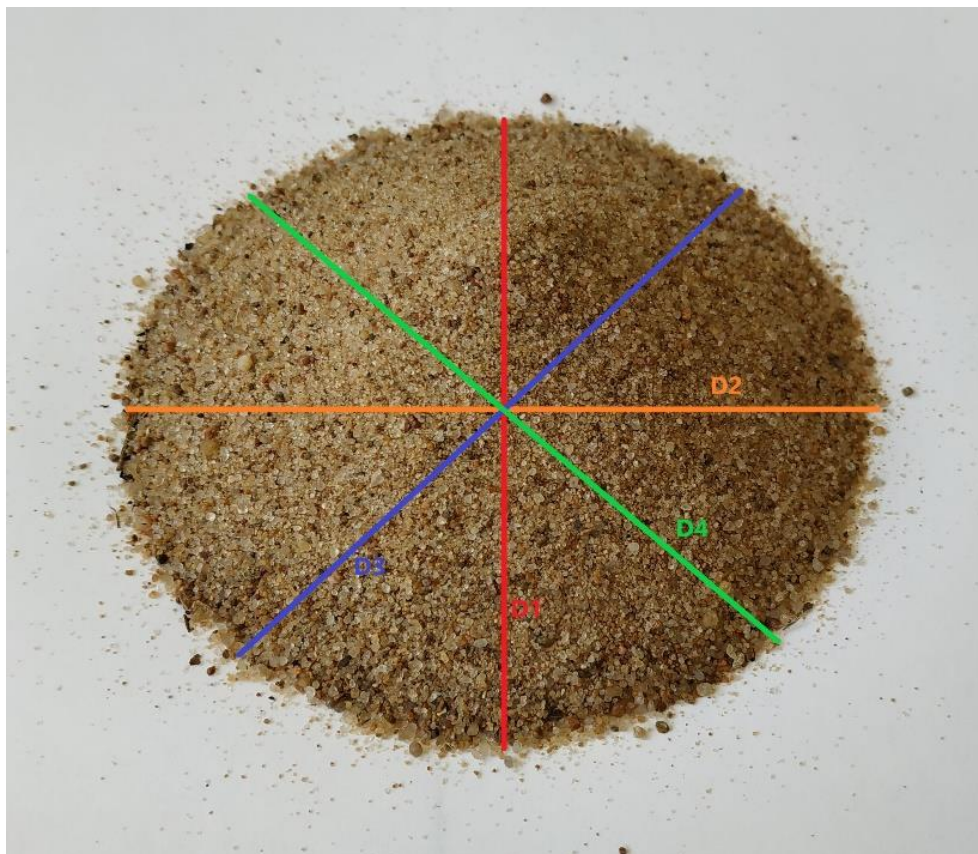


Figure A.5 Sample 3

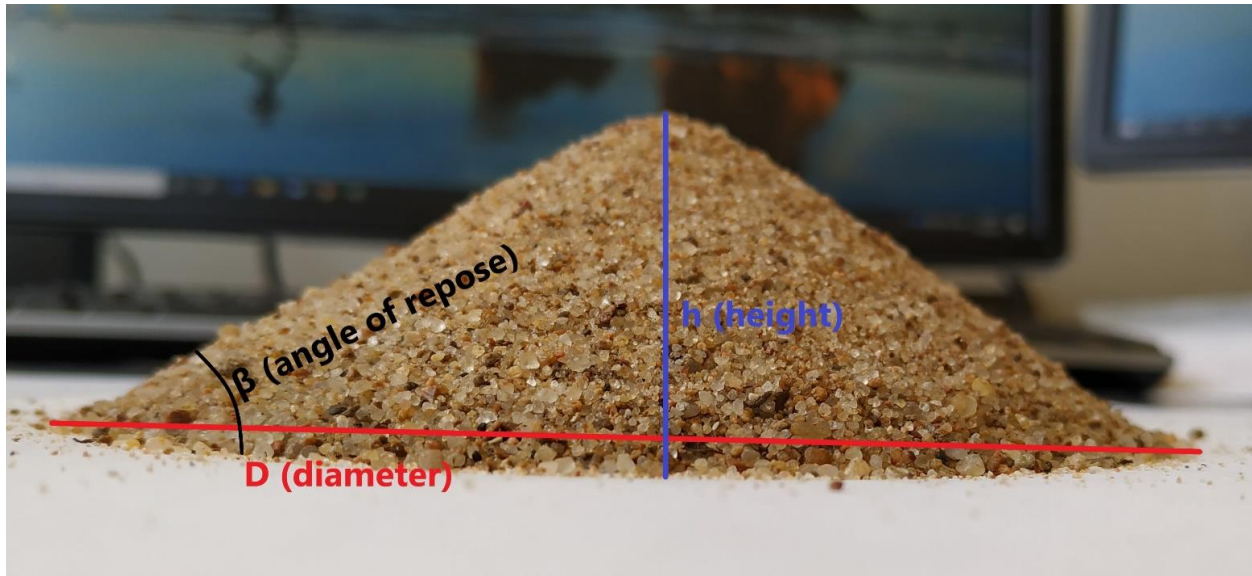


Figure A.6 Sample 3

Each sample has different particle diameters and sphericity. The parameters of each sample are shown in Table A.1.

Table A.1 Sand Particle Parameters

	Sand diameter, mm	Sphericity
Sand sample 1	0.1 - 0.2	less than 1 (non-spherical)
Sand sample 2	0.1 - 0.2	1 (spherical)
Sand sample 3	0.1 - 2 (chaotic size)	less than 1 (non-spherical)

To calculate the angle of repose, sand pile diameters (D_1, D_2, D_3, D_4) and height (h) need to be measured. As it is shown in the figures above, it is more accurate to measure 4 different sand pile diameters. Using the next equations, the angle of repose value can be calculated as

$$R_{ave} = \frac{D_1 + D_2 + D_3 + D_4}{4} \times \frac{1}{2} \quad (A.1)$$

$$\beta = \tan^{-1} \left(\frac{h}{R_{ave}} \right) \quad (A.2)$$

In addition to dry sand particles, the angle of repose of sand in water is also calculated. For the three types of sand particle samples, the angle of repose results are shown in Table A.2.

Table A.2 Angle of Repose Result for Three Sand Particle Samples

	Angle of repose	
	dry sand particles	water filled sand particles
Sand sample 1	30.7	22.8
Sand sample 2	20.6	16.8
Sand sample 3	29.4	24

The results show that the angle of repose of sand in water is 20-25% less than the dry sand angle. In addition, sand sample 2, which is the spherical sample, has the least value. It is because the friction between spherical sand particles is less compared to non-spherical sand particles.